55/2/2023
ISSN 1338-3523
ISSN 0369-2086

Mineralia Slovaca

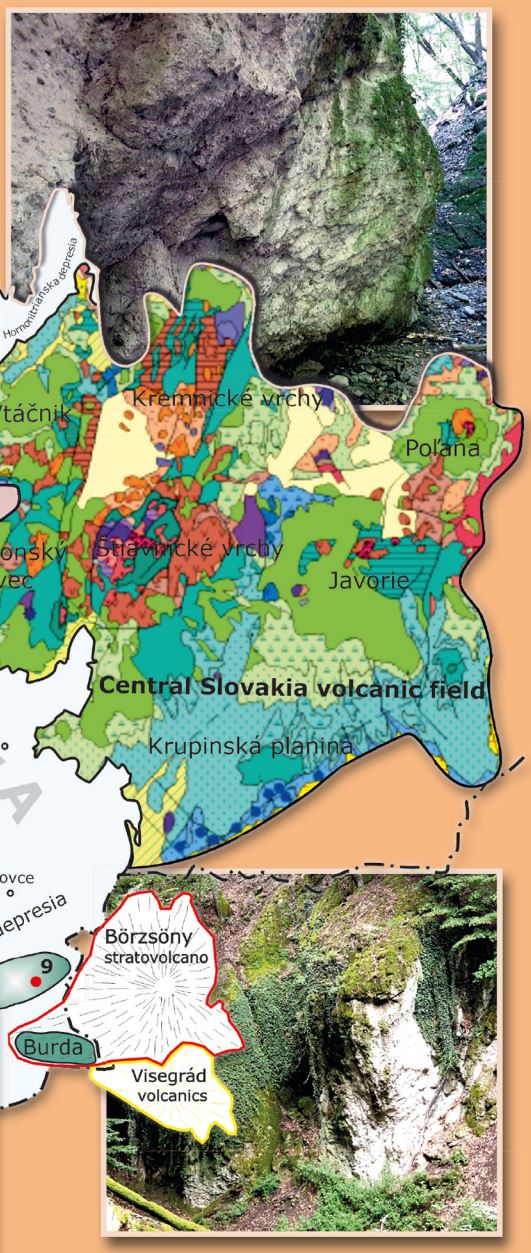

Štátny geologický ústav Dionýza Štúra Bratislava

Mineralia Slovaca

Časopis pre regionálnu a environmentálnu geológiu
a aktivity Slovenskej geologickej spoločnosti a geologických asociácií

Mineralia Slovaca (Web ISSN 1338-3523, ISSN 0369-2086), EV 3534/09, vychádza dvakrát ročne. Vydavateľ a tlač: Štátny geologický ústav Dionýza Štúra, Mlynská dolina 1, 817 04 Bratislava, IČO 31 753 604. Dátum vydania čísla 55/2/2023: december 2023. Predplatné v roku 2023 vrátane DPH, poštovného a balného pre jednotlivcov 22,00 €, pre členov SGS a geologických asociácií 20,90 €, pre organizácie v SR 31,90 €, pre organizácie v ČR 55,00 €. Cena jednotlivého čísla pri osobnom nákupe v predajniach ŠGÚDŠ v Bratislave a v Košiciach je 6,05 € vrátane DPH. Časopis možno objednať v redakcii a v knižnici regionálneho centra v Košiciach. Adresa redakcie: Štátny geologický ústav D. Štúra – RC Košice (Mineralia Slovaca), Jesenského 8, 040 01 Košice. Telefón: 055/625 00 43; fax: 055/625 00 44, e-mail: mineralia.slovaca@geology.sk, e-mail knižnica: secretary.ke@geology.sk

Mineralia Slovaca (Web ISSN 1338-3523, ISSN 0369-2086) is published twice a year by the State Geological Institute of Dionýz Štúr Bratislava, Slovak Republic. The date of issuing of the number 55/2/2023: December 2023.
Subscription for the whole 2023 calendar year (two numbers of the journal): 66.00 € (Europe), 77.00 € (besides Europe), including VAT, postage and packing cost. Claims for nonreceipt of any issue will be filled gratis.
Order of the Editorial Office: Štátny geologický ústav D. Štúra – RC Košice (Library), Jesenského 8, SK-040 01 Košice, Slovak Republic. Phone: +421/55/625 00 43; fax: +421/55/625 00 44, e-mail: mineralia.slovaca@geology.sk, library: secretary.ke@geology.sk

www.geology.sk/mineralia

PÔVODNÉ ČLÁNKY – ORIGINAL PAPERS

COVER: Generalized map in the middle presents covered volcanic centers of the Dunaj volcanics in the Dunaj Basin and outcropped volcanics of the Burda Mts, Börzsöny stratovolcano, as well as volcanics of the areas of Visegrád and Central-Slovakia volcanic field (authorship of the map: L. Šimon). Photograph on the upper left side shows andesite megablock from the breccia of redeposited pyroclastics in the Skalka locality. Photograph on the left down side taken from the apical part of the Burda Mts in the Burdov locality shows the slope of this mountain range, the Danube river and Visegrád volcanics at the background. Right up is displayed the rock cliff of submarine breccia flow present in Kováčov locality and right down the rock cliff of pumice flow in locality of Ipeľské prielohy. Author of all photographs is L. Šimon. The topic of volcanic activity in the Burda Mts is treated in this issue in article by Šimon et al. on pp. 117–132.

OBÁLKA: Generalizovaná mapa v strede znázorňuje zakryté vulkanické centrá dunajských vulkanitov v Dunajskej panve a odkryté vulkanity pohoria Burda, stratovulkánu Börzsöny, vyšehradských vulkanitov a stredoslovenských vulkanitov (autor mapy je L. Šimon). Vľavo hore na fotografii je megablok andezitu z brekcie redeponovaných pyroklastík na lokalite Skalka. Vľavo dole je fotografia z vrcholovej časti pohoria Burda na lokalite Burdov znázorňujúca pohľad na svah tohto pohoria, rieku Dunaj a na vyšehradské vulkanity v pozadí. Vpravo hore na fotografii je skalné bralo submarinného brekciovitého prúdu na lokalite Kováčov. Vpravo dole je skalné bralo pemzového pyroklastického prúdu na lokalite Ipeľské prielohy (autor fotografií je L. Šimon). Problematikou neogénneho vulkanizmu pohoria Burda sa zaoberá článok autorov Šimon et al. v tomto čísle časopisu na s. 117 – 132.

Mineralia Slovaca, Web ISSN 1338-3523, ISSN 0369-2086, https://doi.org/10.56623/ms.2023.55.2.1
55, 2 (2023), 103 – 116, © Authors 2023. CC BY 4.0

Neo-Alpine uplift and subsidence zones in the Western Carpathians: Product of kinematic activity on Cenozoic AnD3 (NW-SE and NE-SW) and AnD4 (E-W – subequatorial and N-S – submeridian) regional faults

ZOLTÁN NÉMETH[1], JURAJ MAGLAY[1], ĽUBOMÍR PETRO[1], MARIÁN STERCZ[1], DANIEL GREGA[1], ONDREJ PELECH[1] and ĽUDOVÍT GAÁL[2]

[1]State Geological Institute of Dionýz Štúr, Mlynská dolina 1, SK-817 04 Bratislava, Slovak Republic; zoltan.nemeth@geology.sk
[2]State Nature Conservancy of the Slovak Republic, Slovak Caves Administration, Hodžova 11, SK-031 01 Liptovský Mikuláš, Slovakia

Abstract: Article presents the role of disjunctive (brittle and brittle-ductile) regional faults of two Cenozoic Neo-Alpine orogenic phases in the Western Carpathians: The AnD3 phase, producing conjugate systems of NW-SE (dominantly dextral shearing) as well as NE-SW (dominantly sinistral shearing), and younger AnD4 phase manifested with regional faults of subequatorial (E-W) and submeridian (N-S) courses (with dominantly uplift and subsidence kinematics). The disintegration of upper crust by kinematic activity on both (AnD3 and AnD4) fault systems produces the origin of block-shaped setting with lateral offsets, eventual rotation (in AnD3), as well as mutual uplifts or subsidences (in AnD4) of individual blocks. This tectonic setting represents the most striking morphological feature at the end of Cenozoic Neo-Alpine orogenic cycle, frequently overprinting or re-activating older tectonic structures.
Article provides an interpretation that parallel with the applied global stress field, the AnD4 subequatorial (E-W) and submeridian (N-S) coursing faults can originate also by merging of individual segments of synthetic (oriented N-S) and antithetic (oriented E-W) megashears between parallel AnD3 shear faults of both systems (NW-SE or NE-SW). Merging of individual segments of antithetic shears arranged naturally in one line creates a predisposition for the origin of equatorial (E-W) trending faults, while merging of synthetic segments produces meridian (N-S) trending faults, both being principal in later AnD4 phase.

Key words: XD labelling, AnD3 shear zones trending NW-SE and NE-SW, AnD4 regional faults of E-W (equatorial) and N-S (meridian) trend, overprinting relations, structural research, dilatometric research, Western Carpathians

Graphical abstract

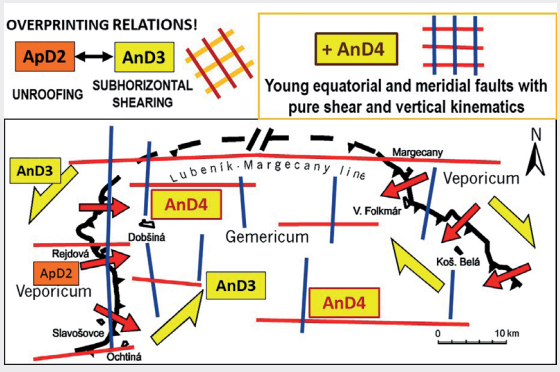

Highlights

- Combined effect of activity on simple shear NW-SE and NE-SW trending faults (shear zones) of Cenozoic AnD3 phase and regional faults of subequatorial (E-W) and submeridian (N-S) courses of AnD4 phase produces the block-shaped disintegration of the territory of W. Carpathians with lateral offsets / uplift / subsidence of individual rock blocks, being reflected in morphology;
- There is indicated the role of equatorial and meridian trending faults in XD4 terminating phase of any orogenic cycle (expressed by the XD labelling method) for the new riftogenesis in $X^{+1}D0$ phase of new orogenic cycle.

Introduction

The youngest faults in the Western Carpathians, being the topic of this treatise, have dominant subequatorial and submeridian directions. Some cases demonstrate that they are (A) coeval with faults of conjugate NW-SE and NE-SW oriented fault systems, in other cases (B) the overprinting relations demonstrate that faults of diagonal conjugate systems are moderately older. Nevertheless, observer must still have in mind that besides geodynamic reasons for establishing / development / location of new fault(s) an important role is played also by structural predisposition – existence of older generation faults, thrust planes, old fold limbs, bedding planes, etc.

To simplify the designation of relative time succession of origin of geological structures, but especially the origin

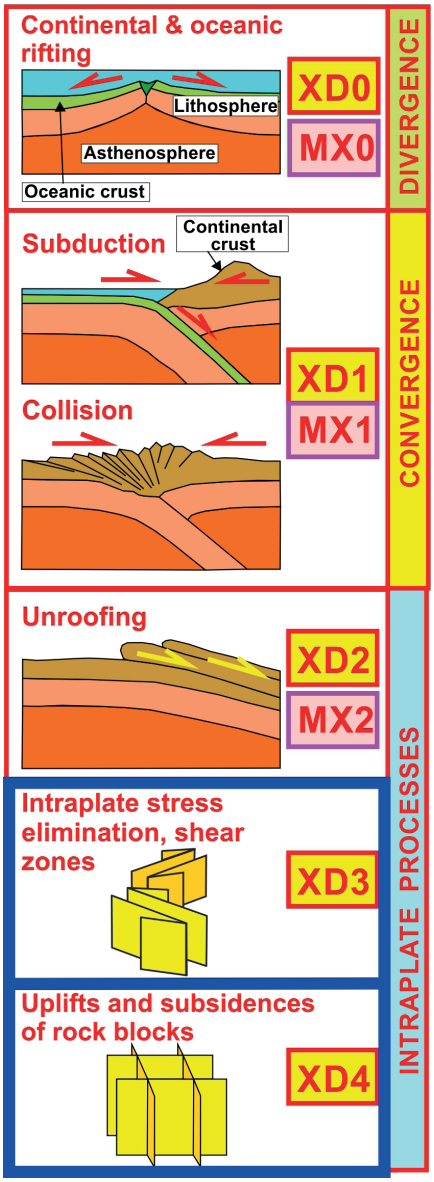

Fig. 1. The XD labeled sequence of orogenic phases within an orogenic cycle in upside down ordering. Blue rectangles highlight the youngest – Neo-Alpine AnD3 and AnD4 orogenic phases / geodynamic events with related lithotectonic units and generated structures in the Western Carpathins. Scheme is taken from Németh (2021; reproduced with permission).

of lithotectonic units, as the elements for any geological-geodynamic thoughts, a new concept of XD labelling was presently defined (Németh, 2021). This concept is based fully on plate tectonic principles of orogenic cycles and their orogenic phases (Fig. 1).

The methodology of XD labelling has universal application for present, but also past orogenic cycles world-wide. Each orogenic (Wilson) cycle – in the W. Carpathians they are dominantly Variscan (letter X is replaced by abbreviaton V), Paleo-Alpine (Ap) and Neo-Alpine (An) cycles, consisting of the same sequence of orogenic phases: XD0 – rifting (divergence), XD1 – convergence consisting of subduction (a), obduction (b), collision (c); XD2 – post-collisional overheating, active metamorphic core complex origin, uplift of collisional zone and related unroofing, XD3 – subhorizontal shearing and XD4 – subequatorial and submeridional faulting. The XD3 and XD4 phases represent the post-collisional stress adaptation / absorption within the crust. The genesis of XD3 and XD4 structures, their kinematics and products are the topic of this case study from the territory of Western Carpathians. In Fig. 1 they are highlighted by blue rectangles. The concept of XD labelling (l.c.) was defined in the Western Carpathians, representing symmetric moderately concave bended segment of the Alpine-Carpathian-Himalayan belt. Individual phases of three orogenic cycles are clearly visible here and were scientifically proved.

Within lithospheric plates, old cratonized regions, but also those regions, where the particular orogenic (Wilson) cycle is just terminated by levelling (peneplenization) of morphology, are built of fault bounded blocks, consisting of rock sequences / lithotectonic units. Owing to still acting stress field, the mutual displacement of individual blocks is represented either by lateral offsets and eventual rotation (dominantly in XD3), uplift or subsidence (dominantly in XD4) or their combination. Our present treatise aims to describe in time sequence the role of horizontal and vertical displacement along faults in the Western Carpathians as an example of polyorogenic belt within the Alpine-Carpathian-Himalayan zone. Despite, the primary driving forces for these displacements – the mantle convection currents and mantle plumes – are mentioned in this treatise only marginally, being a topic of our further publication (Németh, in print).

In polyorogenic terranes, consisting of a sequence of several orogenic (Wilson) cycles and their orogenic phases, the observer must give a special attention on ductile, brittle-ductile and brittle structural signs, indicating the evolution from higher grade to low grade tectonometamorphic overprints of relevant lithology, or generating these overprints / structures in still shallower crustal levels. Because present study deals with Neo-Alpine (Cenozoic) AnD3 and AnD4 shearing and faulting, it describes relatively "colder" structures, originating at brittle and brittle-ductile conditions and in relatively shallow crustal levels.

From the historical retrospective, the scientific dispute on the dominance of subvertical vs. subhorizontal movements in geodynamic processes has a long time tradition, in individual periods preferring either first or second alternative. The dominantly vertical kinematics was preferred by Neptunists with the main protagonist of A. G. Werner

(1749–1817) and parallel with Plutonists with A. L. Moro (1687–1764), but mainly J. Hutton (1726–1797) as the first protagonists. Later the geosynclinal concept of orogenesis based on isostatic uplift was compiled by James Hall (1811-1898) and James Dwight Dana (1813-1895). Vertical movements at mountain building and sedimentary basins development were principal in this first period of orogenic considerations. Nearly two centuries later, the global geodynamics started to account the subhorizontal displacements at mountain building, based on concept of continental drift, popularized by A. L. Wegener (1880–1930), though not generally accepted until the 1950s. The Wegener's concept of centrifugal forces as driving ones for the displacement of continents on the Earth's surface has failed, revealing their insufficiency for this (e.g. by P. S. Epstein, 1883–1966). The research during later period, based mainly on paleomagnetic results has contributed greatly to postulating a new concept of plate tectonics. Among tens of leading researchers, the important recognition deserves J. T. Wilson (1908–1993), contributing to concept of orogenic cycles, presently successfully explaining majority of geodynamic processes on the Earth. This short retrospective aims to highlight that the concept of each protagonist has its own justification and logic, based on that time available knowledge, observation results and data. Also the research of Western Carpathians has experienced a period with dominating vertical movements in interpretation of mountain building (orogenesis; XD4 in present day expression) and period with dominating nappe displacement kinematics (presently XD1bc). Despite, none of them has counted the role of subhorizontal displacements along shear zones (presently XD3). Hence – available parts of mosaic are building a time relevant concept, which still better describes the processes and their products in the real nature.

Used research methodology and state of present knowledge

Research consisted of (1) field geological mapping and study of affiliation of rock sequences / lithotectonic units to individual phases of orogenic cycles based on evolutionary criteria in the Western Carpathians. This article deals with the youngest – AnD3 and AnD4 phases of Cenozoic Neo-Alpine orogenic cycle, characteristic with brittle to brittle-ductile deformation, so the structural inventory of earlier Variscan and Paleo-Alpine cycles, as well as Neo-Alpine AnD12 phases are treated here only partially.

The research was accompanied with (2) structural / tectonic research, revealing the overprinting relations and displacement kinematics of individual rock sequences, rock blocks and *sensu lato* lithotectonic units. Regional scale geological mapping and tectonic research have benefitted also from (3) earlier regional geologic, tectonic and petrologic studies from the W. Carpathians published by numerous other referred researchers.

Registering overprinting relations at outcrop scale represents the most important part of structural research, aiming to clearly decipher the succession of the origin of individual structures (folds, reverse or normal faults, strike slip faults, etc.). Revealing and understanding this succession provides the principal information about geological / tectonic evolution of the region.

In this paper, the results of **recent** 3D **micromovements monitoring on neotectonic AnD34 faults** using the TM-71 devices (Fig. 2; cf. Petro et al., 2004) are presented from two measuring sites – the Hodruša-Hámre (the All Saints' mine adit) and Ipeľ (Izabela adit; Fig. 8). The idea of creating a network of measuring stations on tectonic faults in Europe or in a global scale was created on the basis of the international project COST 625 *3-D monitoring of active tectonic structures* established at the beginning of 2000. Altogether 29 monitoring stations with 3D monitoring devices TM-71 were built on the territory of the Slovak Republic. They are currently under the scope of the EU TecNet project (Briestenský et al., 2018, a.o.), and 6 locations of them are managed by the State Geological Institute of Dionýz Štúr within the project Partial monitoring system of geological factors of the environment, Subsystem 02: Tectonic and seismic activity of the territory (Petro et al., 2022). Measurements have been carried out at some of these locations for more than two decades, which makes it possible to characterize dynamic phenomena on these monitored tectonic discontinuities with relatively high relevance.

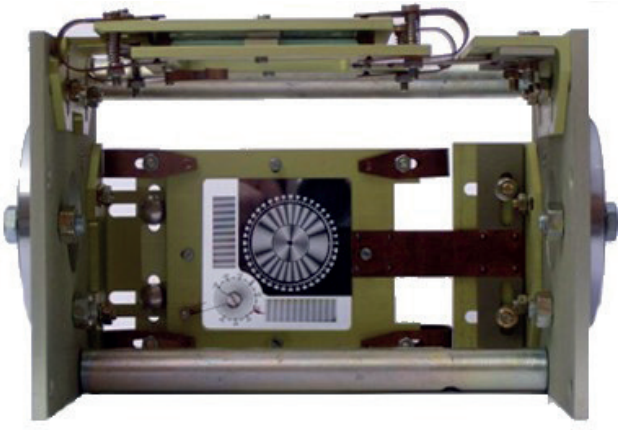

Fig. 2. Mechanical-optical dilatometer of TM-71 type.

The principle of the TM-71 dilatometer (Fig. 2) is based on optical-mechanical interference, i.e. the creation of moiré structures, visible between two glass tables with a special optical grid (Košťák, 1969). The shape of the moiré pattern has the character of a group of radially arranged stripes, the number and geometry of which

corresponds to the mutual eccentric displacement of the plates with the optical gratings. The measured values are usually read manually (with the help of a digital camera), but currently, devices with an additional equipment for automatic scanning of optical grids, including a control unit and a data logger, are installed at several locations around the world.

The device can measure very slow displacements, i.e. ≤ 0.01 mm and rotation 0.01 gr. The measurements are carried out in two planes perpendicular to each other, so that the mutual spatial movement (3D) of both monitored blocks can be detected by calculations.

Brief description of geological and tectonic setting of the Western Carpathians

Arcued elongated orogenic belt of the Western Carpathians is a segment of Alpine-Carpathian-Himalayan zone. W. Carpathians are characteristic with dominant northern vergency of Alpine (Paleo-Alpine ApD and Neo-Alpine AnD) tectonic imbrication and nappe stacking (cf. Plašienka et al., 1997; Putiš et al., 2009, 2021, 2023), despite having incorporated also southern vergency tectonic structures of earlier Variscan (VD) evolution.

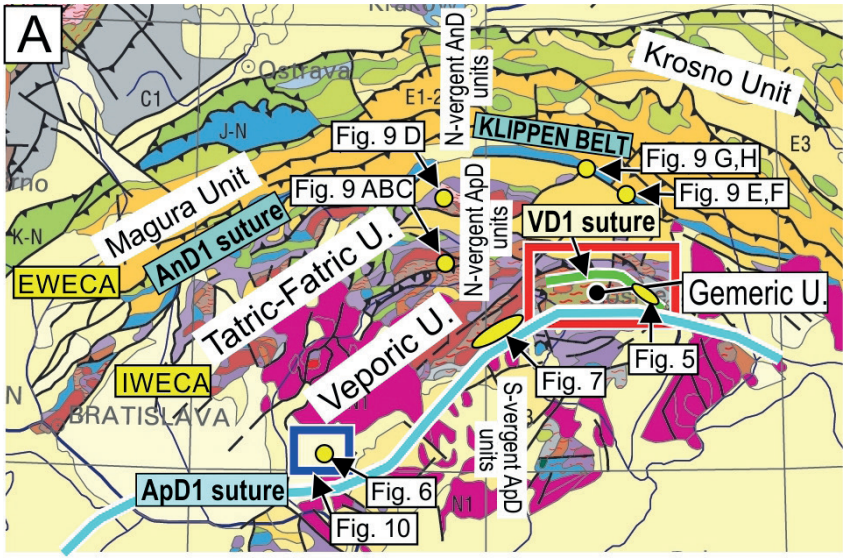

Fig. 3. General tectonic structure of Western Carpathians: A – emphasizing the role of three orogenic (Wilson) cycles producing a.o. three suture zones (Variscan – VD1 – marked light green, Paleo-Alpine – ApD1 – light blue and Neo-Alpine – AnD1 – dark blue), and B – extreme number of disjunctive structures contributing to present block setting with several levels of uplifts and subsidences. Part B highlights only the AnD34 structures – AnD3 NW-SE trending dominantly dextral faults (visualized with dark brown colour), NE-SW dominantly sinistral faults (orange colour) and the youngest AnD4 E-W trending faults (red colour). and N-S trending faults (blue colour). AnD4 faults manifest mainly pure shear kinematics and contribute to uplifts and subsidences in combination with earlier AnD3 faults, contributing by simple shear type transpression and transtension. The way how conjugate NW-SE and NE-SW faults can contribute to origin of E-W and N-S faults, in numerous cases representing joint segments of synthetic and antitethic segments of faults of conjugate system, are explained in the text and pale yellow rectangle in Figs. 7 and 10. Basemap of A: Asch (ed., 2007) – IGME 5000, magnified segment of W. Carpahtians is reproduced with permission), basemap of B: Bezák (ed., 2004) – Tectonic map of Slovak Republic (slightly modified with highlighted AnD23 faults).

The division of the Western Carpathians to Outer, Central and Inner W. Carpathians, dominantly used in the past (e.g. Maheľ, 1986), is presently simplified by division to Outer (External – EWECA) and Inner (Internal – IWECA) W. Carpathians (cf. Hók et al., 2019), better distinguishing units with dominant Neo-Alpine (Cenozoic) vs. dominant Paleo-Alpine / Variscan (Mesozoic / Paleozoic) evolution. The dividing line between External and Internal W. Carpathians is formed by the Klippen Belt.

Internal Western Carpathian (IWECA) belt

The Paleo-Alpine setting consists of following main lithotectonic units with northern general vergency of thrusting and nappe displacement: *Tatric-Fatric*, *Veporic* and *Gemeric units* (all three represent so-called basement nappes), *Meliatic (Bôrka nappe)*, *Turnaic (Tornaic)* and *Silicic units* (representing the superficial nappes; cf. Fig. 3A). From the space between Tatric and Veporic units the *Fatric Unit (Krížna nappe) wa*s derived and from the space between *Veporic* and *Gemeric units* it was the *Hronic Unit (Choč nappe)*.

The Tatric Unit (*Tatricum*; probable equivalent of Lower Austroalpine Unit of the Eastern Alps) – crops out in the W. Carpathian core mountains and consists of Variscan medium to high-grade metamorphic rocks (schistose gneisses with sporadic HP metamorphics and granitoids). The primary cover of Tatricum starts with Upper Paleozoic / Lower Triassic clastics, being followed by Middle Triassic carbonates. The *Tatricum* represents the lowermost unit of Internal Carpathians. In the present north-vergent ApD tectonic setting the Tatric tectonic underlier is unknown, and tectonic flat-lying nappe overlier is represented by *Fatricum,* containing sedimentary sequences corresponding with that of Tatric cover.

The Veporic Unit (Veporicum), similarly like Tatric Unit, comprises of Variscan crystalline basement and Upper Paleozoic / Mesozoic cover. The Alpine evolution zone between Veporic and Gemeric units is interpreted to be the homeland of *Hronic Unit (Hronicum)* consisting of Carboniferous-Permian volcanosedimentary formations.

The *Gemeric Unit (Gemericum)* as the uppermost Paleo-Alpine ApD basement nappe, has well preserved Lower Paleozoic volcano-sedimentary sequences of Variscan VD0 riftogenous phase (cf. Grecula, 1982; Radvanec et al., 2017), as well as – in Northern-Gemeric rim – well preserved VD1 suture zone, including also HP and UHP blocks subducted and exhumed from Variscan subduction zone and VD1b exhumed / obducted southward on Variscan passive margin sequences (Radvanec & Németh, 2018). The Gemeric Upper Paleozoic / Mesozoic cover sequences are bearing superficial nappes of *Meliatic Unit (Meliaticum; Bôrka nappe)*, *Turnaic and Silicic units*.

External Western Carpathian (EWECA) belt

This belt is a product of Upper Cretaceous-Cenozoic Neo-Alpine AnD evolution. External Carpathian Flysch belt consists of Cenozoic rootless nappes thrust over the North-European platform. The flysch-like Mesozoic and Paleogene formations predominate. The *Magura group of nappes (Unit)* consists mainly of Paleogene flysch formations with prevailing sandstones. These are AnD1 thrust northward over the *Krosno Unit of Flysch Belt*, built of prevailing variegated claystones.

The Klippen Belt (Oravic Unit; cf. Hók et al., 2019, p. 39 ibid.; Fig. 3A). represented in Neo-Alpine AnD0 evolution the Czorsztyn ridge – hypothetical continental ribbon, separated from the European Platform on the north by oceanic domain of the Northern Penninicum (Magura Ocean) and from the Internal Western Carpathians by the oceanic domain of the Southern Penninicum (Plašienka, 2012; Plašienka & Soták, 2015).

Above described multiple nappe and thrust setting was overprinted by AnD34 shearing and faulting, being described in more details in present treatise.

Origin and role of AnD3 and AnD4 phases in present morphology of W. Carpathians

In the Western Carpathians, the existence and role of conjugate system of shear zones of generally NE-SW "Western Carpathian direction" and NW-SE "Eastern Carpathian direction" (AnD3 in our present classification) was firstly discovered by Grecula et al. (1990; Fig. 4), owing to extended regional research in the Gemeric Unit (red colour rectangle in Fig. 3A). Referred research has implemented generally N-S trending profiles in mutual distance of 1 km with application of detail geophysical profiling and soil metallometry, including detail (scale 1 : 10 000) field geological mapping, so the offsets and partial rotation of individual rock strips, but also e.g. ore veins courses, were clearly observable. Even then it was clear mainly from morphology and map view that the youngest structures, usually segmenting the course of shear zones, are represented by N-S and E-W trending (AnD4) faults.

Detail of relations of Cenozoic Neo-Alpine AnD3 and AnD4 faults, overprinting older Variscan, or even Paleo-Alpne setting are shown in Fig. 5, being focused on Eastern Gemeric course of Variscan suture zone in the area of Košická Belá and Nižný Klátov municipalities. It is generally valid that NW-SE trending AnD3 faults are preferable developed on older VD12 and ApD12 discontinuities (former reverse and normal faults). The NE-SW trending AnD3 faults are characterized by the kinematics of transform faults, originating during the arc-bending, transforming the original zonal setting. Both AnD3 systems are further cut by AnD4 submeridian and subequatorial faults.

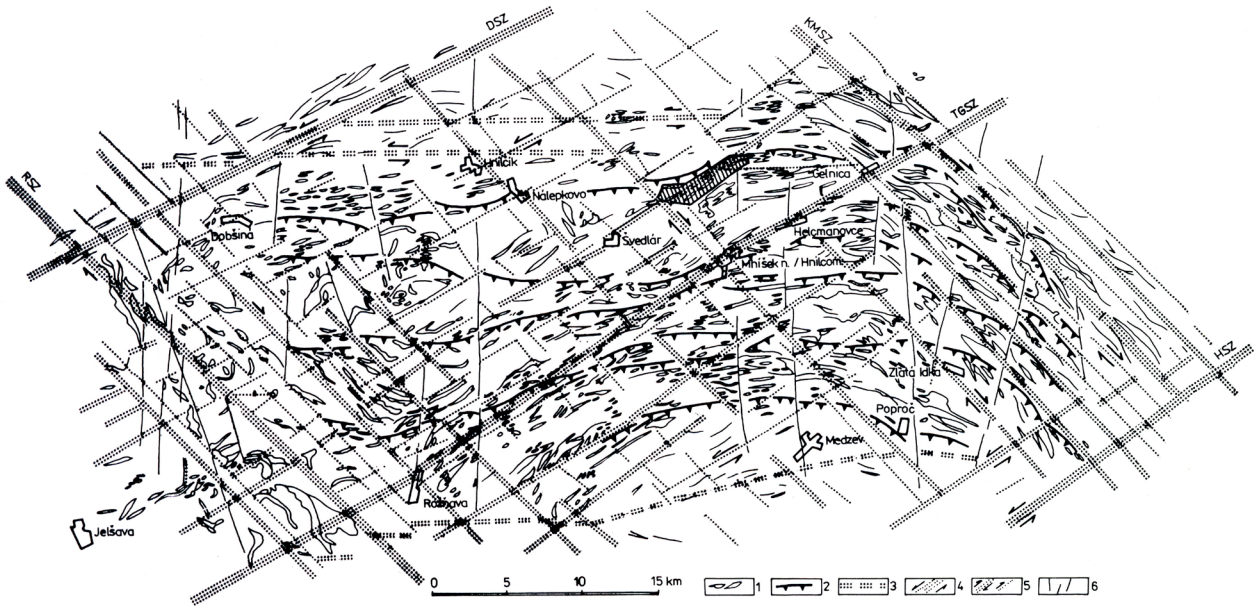

Fig. 4. Schematic visualization of shear zones of Gemericum (Grecula et al., 1990; published with permission), representing the milestone in understanding of the role of Cenozoic Alpine faulting in the territory of the Internal Western Carpathians. RSZ – the Rejdová shear zone, DSZ – the Dobšiná shear zone, KMSZ – the Košice-Margecany shear zone, TGSZ – the Transgemeric shear zone, HSZ – the Hodkovce shear zone; 1 – course of lithological units, 2 – nappes, 3 – Alpine rejuvenated older generation shear zanes, 4 – principal Alpine shear zones, 5 – shear zones of lower order, 6 – faults with a pure shear character (the youngest ones).

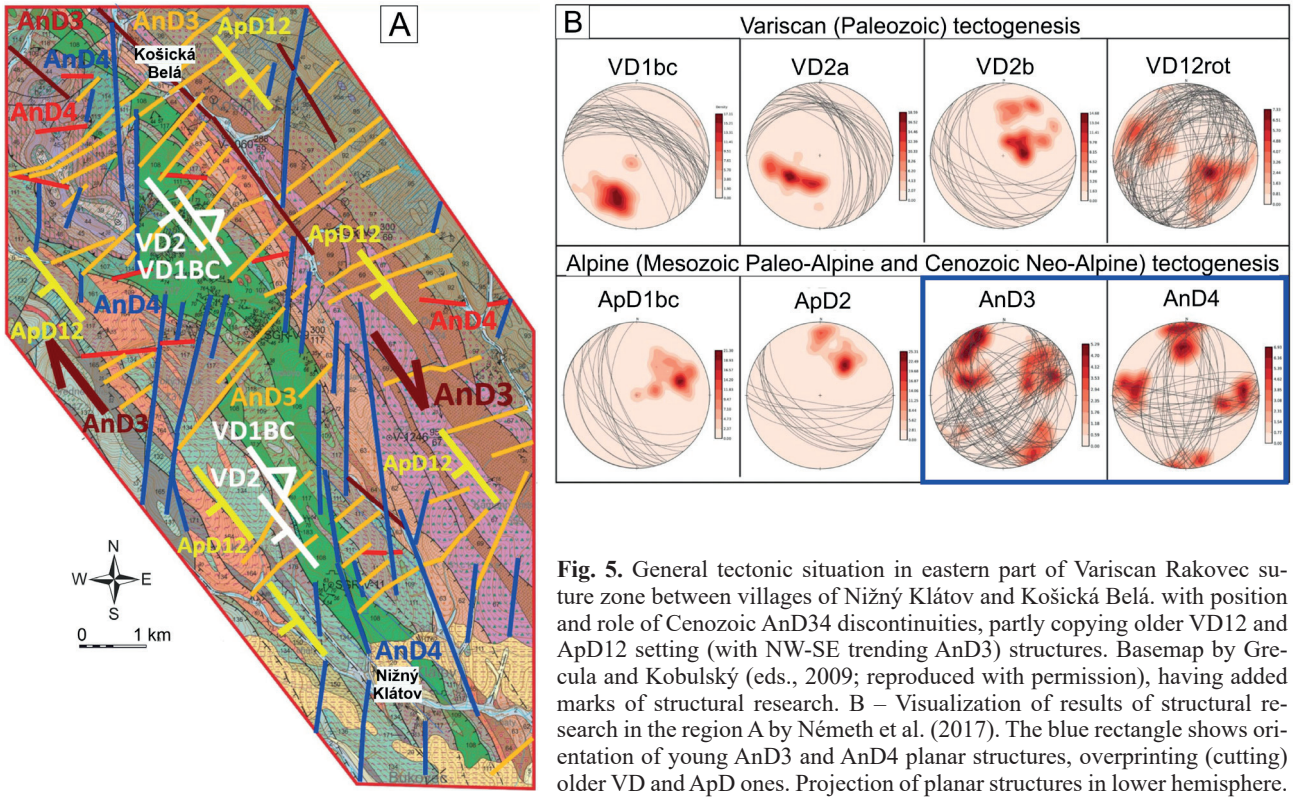

Fig. 5. General tectonic situation in eastern part of Variscan Rakovec suture zone between villages of Nižný Klátov and Košická Belá. with position and role of Cenozoic AnD34 discontinuities, partly copying older VD12 and ApD12 setting (with NW-SE trending AnD3) structures. Basemap by Grecula and Kobulský (eds., 2009; reproduced with permission), having added marks of structural research. B – Visualization of results of structural research in the region A by Németh et al. (2017). The blue rectangle shows orientation of young AnD3 and AnD4 planar structures, overprinting (cutting) older VD and ApD ones. Projection of planar structures in lower hemisphere.

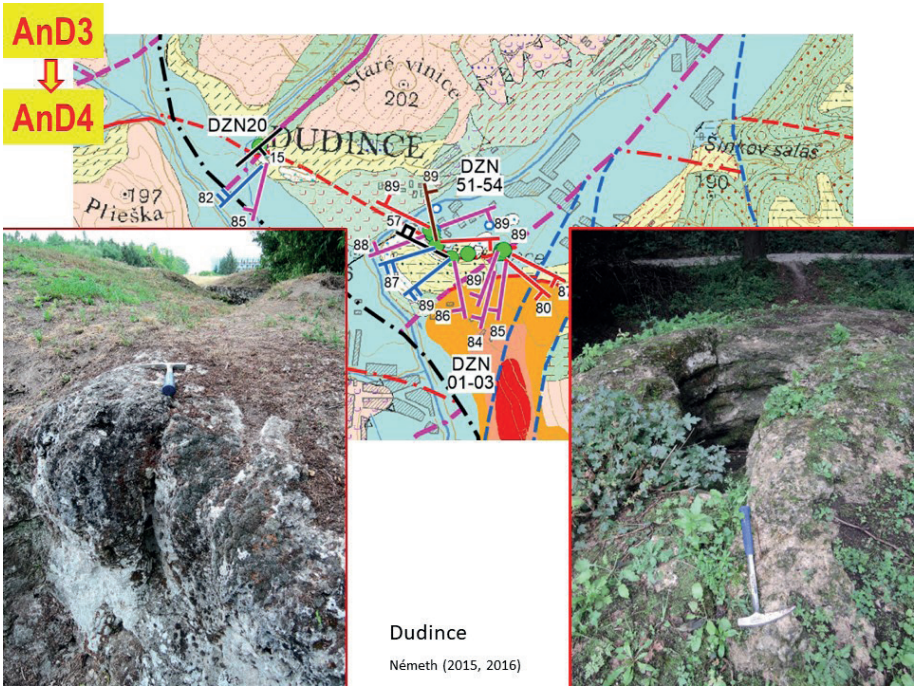

Fig. 6. Revealed course and dip of AnD3 cleavage and joints (blue and red structural marks) and AnD4 joints (velvet marks, incl. young E-W trending fracturing in travertine mounds), distinguished by their overprinting relations in outcrops at Dudince municipality, but also other localities in wider region around Dudince represent indications of importance of synthetic and antithetic mega-shears between simple shear faults of both – NW-SE and NE-SW directions – for the origin of E-W and N-S trending faults. These faults originate by merging of individual segments at their linear arrangement.

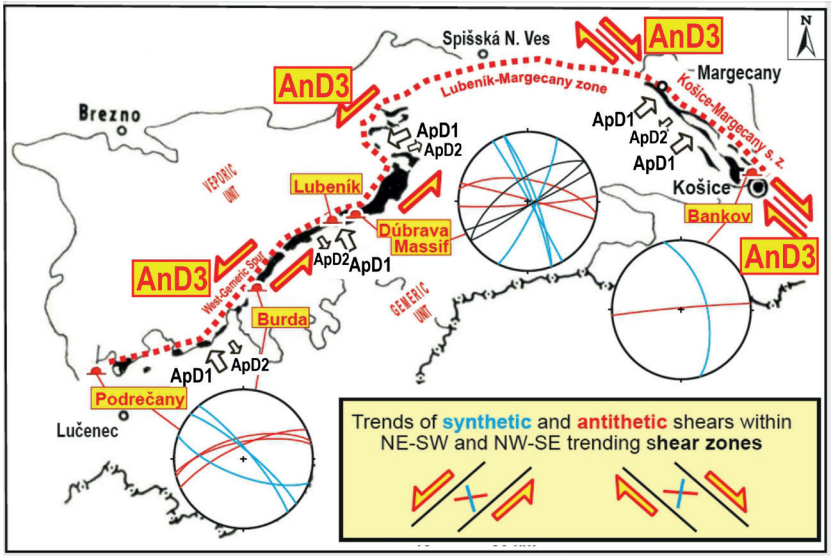

Fig. 7. Interpretation of the origin of AnD4 adits in caves present in magnesite bodies during late Alpine evolution (Németh in Gaál et al., 2017; reproduced with permission).

The role of synthetic and antithetic megashears between NW-SE and NE-SW trending shear faults for the origin of N-S and E-W trending faults in the territory of W. Carpatians was confirmed by Németh (2015, 2016 in Bačová et al., 2017),) performing geological mapping and structural research at the contact of eastern margin of Danube basin with Neogene volcanic area (Figs. 6 and 10; for location see dark blue rectangle in Fig. 3A). This kinematics was later confirmed by structural research attempting to explain the origin of caves in Upper Paleozoic magnesite bodies present along the contact zone of Gemeric and Veporic lithotectonic units and representing relatively rare phenomenon (Fig. 7).

Displacement along selected faults revealed by dilatometry

The comprehensive summary of results from all dilatometric monitoring sites, including the interpretation of results, is a topic of another paper (in preparation), so here we present dilatometric results from two sites only, located in southern part of Internal W. Carpathians (Fig. 8).

Izabela adit, Ipeľ (N 48°34'2.98"; N 19°42'59.76") – the place of installation of the device is in the Stolické vrchy Mts locality in the cadastral territory of the Ipeľský Potok village. The surrounding of monitored fault is built of Paleozoic metamorphic and igneous rocks, belonging

The role of Cenozoic AnD23 faults in uplifts and subsidences in fault delimited blocks

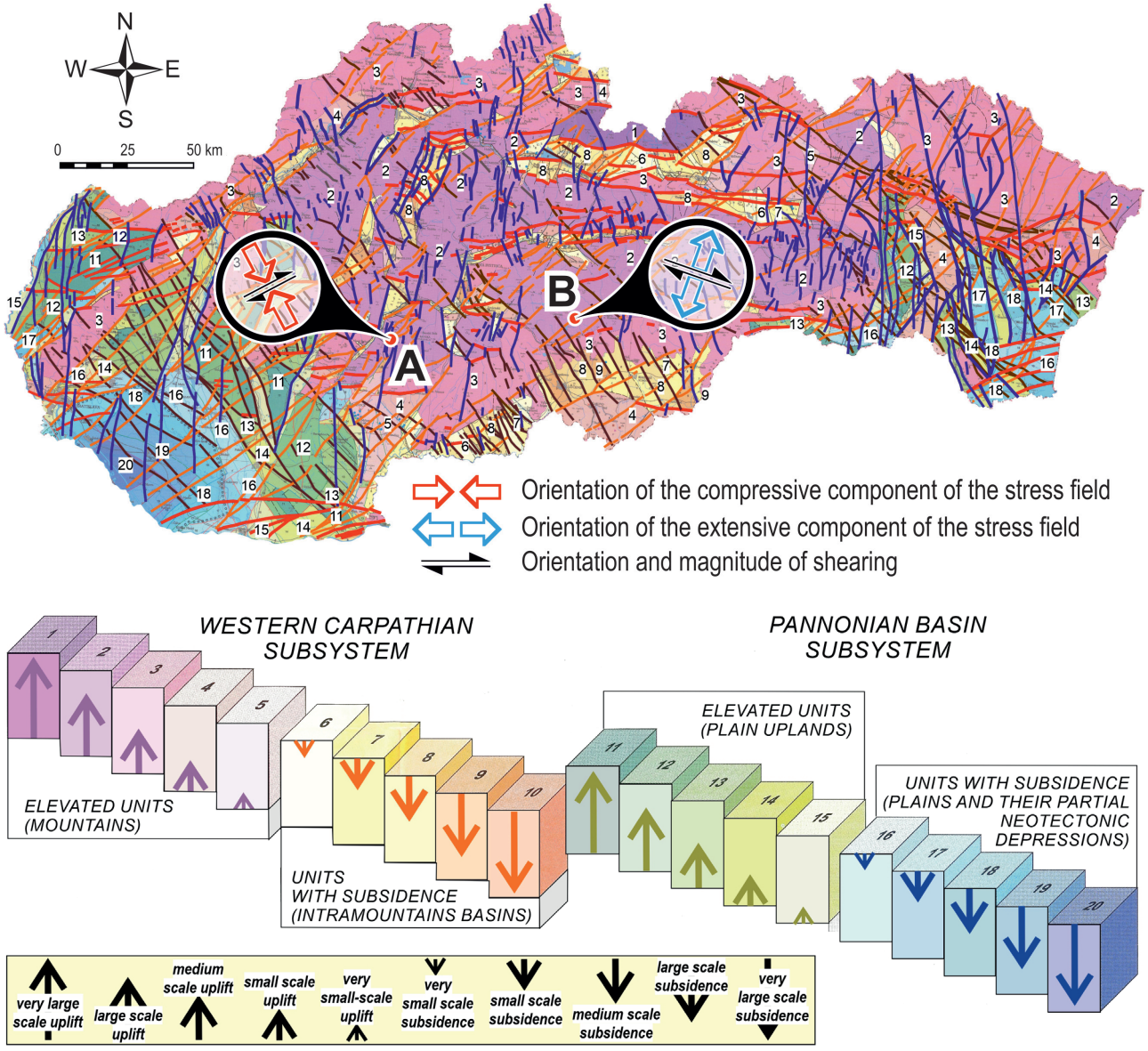

Fig. 8. Display of trends of long-term movements on tectonic faults in selected locations: A – the Hodruša-Hámre (the All Saints' mine adit), B – Ipeľ (Izabela adit) in the Western Carpathians with TM-71 installation. Base map indicates uplifts and subsidences of individual blocks during AnD34 phases, being visualized in diagram below the map. Both, Neotectonic map with slightly modified diagram are taken after Maglay (ed., 1999; reproduced with permission). Map highlights the courses of NW-SE, NE-SW, E-W and N-S trending faults (correspondingly with Fig. 3B).

Fig. 9. Morphological examples of AnD4 N-S and E-W trending structures (several of many thousand). A–C – The Nízke Tatry (Low Tatra) Mts: A – Main ridge on both sides of the Chopok peak (2024 m a.s.l.); B – Subsidiary mountain ridges of Prašivá (1667) and Baňa (1859) peaks branching off from the main (Figs. 6 and 10; and the Litvorova dolina valley between them; C – Rock cliffs of Pusté (1501) parallel with the main ridge; D – The Vysoké Tatry (High Tatra) Mts – Parallel N-S trending ridges of Klin (2176), Bystrá (2248) and Kriváň (2494) peaks; E–H – The East Slovakian segment of Klippen Belt represents prominent AnD3 reactivated NW-SE trending tectonic zone, being cut by numerous E-W trending faults forming elongated cliffs of this direction: E–F – "The Sleeping Monk" cliffs south of Kyjov village. Its general E-W course contradicts to NW-SE trending general course of Beskydok (730) ridge as a part of the Klippen Belt; G – Haligovské skaly cliffs and H – Aksamitova skala partial ridge; G–H – located to N and ENE of Haligovce village with tectonic situation corresponding to that described at photographs E–F. (Author of all photographs: Z. Németh.)


Chopok peak
W
E
A
N
S
N
S
N
S
B
W
E
C
Klin peak
N
S
Bystrá peak
N
S
Kriváň peak
N
S
D
NW
SE
E
W
E
E
W
F
W
E
G
E
W
H

to Veporic lithotectonic unit (LTU). The only device, installed on this site in 2002, is monitoring one of the most important fault systems of the Western Carpathians running through the Ipeľ river valley – the Muráň-Maľcovce system (Pospíšil et al., 1986; Dvořák et al., 2005) with its southern part – the Muráň-Divín system, consisting of several parallel NE-SW faults (Pospíšil et al., 1989). In the monitoring period, the vertical component predominates (89 %) having decreasing character. The direction of the extensional component of the stress field is NE–SW. The minor horizontal component, representing only about 11 % of the total movement, has a dextral character, both altogether representing the steep dextral subsidence of north-eastern block.

Hodruša-Hámre (N 48°27'59.58"; N 18°49'26.49") – the TM-71 device was installed in 2005 in the All Saints mine adit, located in Štiavnické vrchy Mts within the Hodruša-Hámre village cadaster. The monitored tectonic structure penetrates the quartz-diorite porphyry of the middle part of stratovolcano. Even if the resulting long-

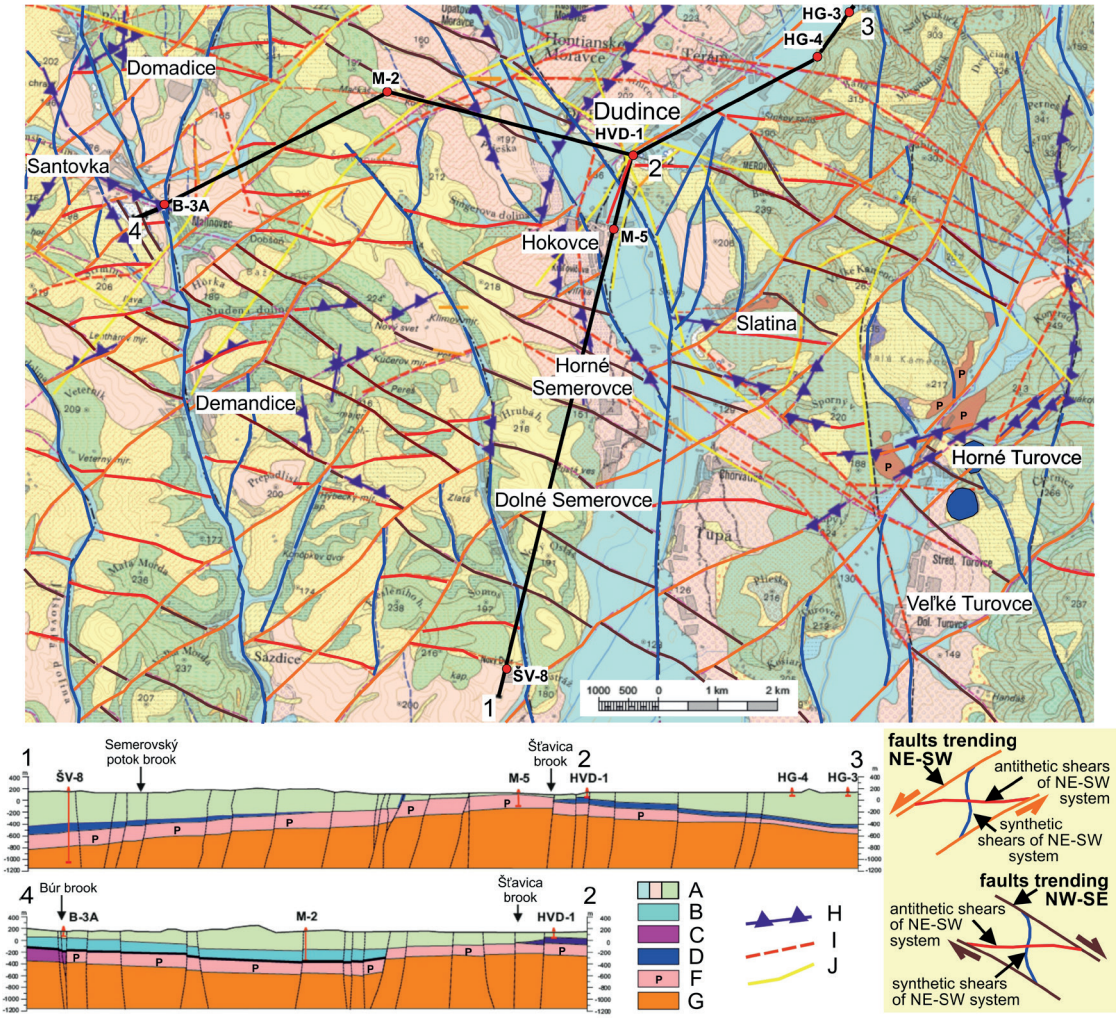

Fig. 10. Distribution of AnD3 and related AnD4 faults in the wider surrounding of Dudince municipality located in the southern part of Central Slovakia Neogene Volcanic Field. Base map by Konečný, ed., et al. (1998). Lithology: A – Quaternary and Neogene sequences undivided; Dominantly in cross-sections: B – Limestones and sediments of the Choč nappe undivided; C – Permian and Triassic cover of the Northern Veporicum; D – Quartzites and other rocks of Föderata Group undivided; E – Permian sequences of Revúca Group; D–E – cover of Southern Veporic zone; F – Lower Paleozoic basement rocks of Southern Veporicum undivided. Based on geological mapping, reambulation and structural research (Németh, 2017) there was revealed an extended net of faults of generally four directions: AnD3 faults with simple shear kinematics – system trending NE–SW (mainly sinistral shearing; coloured orange) and NW–SE (dextral; dark brown). Both systems have developed their own antithetic shears (generally E–W – subequatorial direction; red) and synthetic shears (generally N–S direction; blue) interconnecting individual faults. At linear position of several antithetic or synthetic fault segments and appropriate regional stress field, individual E–W or N–S segments can join, forming new (AnD4) regional faults trending E–W or N–S (visualization is in yellow rectangle right down). Course of individual fault systems was proved also by earlier geophysical research by Linsser method (H), weight boudaries (I) and gB geoelectrical methods (J; Šefara, 1976; Tkáčová, 1978 in Melioris et al., 1986).

term movement is only a tenth of millimeter, indicating minor dextral horizontal component of ENE-SWW direction. The vertical component is a moderate uplift at the NW-SE oriented compressional component of the stress field.

Discusion

The research of Cenozoic (Neo-Alpine) regional faults and shear zones in the Western Carpathians has more than forty years tradition. In the beginning, their kinematics and overprinting relations were not fully clear. Owing to high degree of symmetricity of concave arc bending of the W. Carpathian belt, this region represented an ideal study area to find answers to the above-mentioned ambiguities.

Among first visualizations of a dense net of AnD3 and AnD4 faults in the W. Carpathians (expressed in present XD nomenclature) belong map of photolineations (Pospíšil et al., 1986; Fig. 1 ibid.) and sketch of conjugate system of shear zones trending generally NW–SE and NE–SW in the Gemeric region of Internal W. Carpathians by Grecula et al. (1990; Fig. 3 – copied in this paper). After these pioneering works, numerous high quality structural and tectonic researches have been focused on prominent W. Carpathian NE–SW trending shear faults of Alpine age, e.g.: Muráň fault (cf. Pospíšil et al., 1989; Marko, 1993; Gerátová et al., 2022), Pohorelá line (Hók & Vojtko, 2011), Carpathian Shear Corridor (Marko et al., 2017), but also regional faults trending NW–SE – Mýto-Tisovec fault (penetrating crystalline basement and Muráň plain; Marko & Vojtko, 2006), Pravno fault (in the Žiar Mts; Fekete & Vojtko, 2013).

The AnD4 uplift was documented mainly in zones trending subequatorial, e.g.: Vikartovce zone (Marko et al., 2010; Vojtko et al., 2011a, b), Kozie chrbty Mts and the western part of Hornád Depression (Sůkalová, 2011), Spišská Magura and Eastern Tatra Mts (Vojtko et al., 2010) and the Tatra Mts (Králiková et al., 2014).

Comprehensive studies about Cenozoic deformation and stress field, reflected also in genesis of AnD3 and AnD4 faults, were published by Kováč (2000), Kováč & Plašienka (2002) and Kováč et al. (2002), but also from the Orava region (Pešková et al., 2009) and the northern Laborec drainage basin (Vojtko et al., 2012).

Presently the topic of subequatorial and submeridian trending lineaments based on products of Neogene volcanism was highlighted by Bacsó (2023). It is long time accepted that faults trending N–S and E–W in prevailing cases cut older AnD3 faults (and all older structures as well) and therefore represent the youngest discontinuities, being by us classified as AnD4 generation of faults. Our present paper highlights again a special genetic concept explaining the origin of these faults in continental conditions (earlier presented in Gaál et al., 2017, and Bačová et al., 2017), interpreting that faults trending N–S and E–W can originate at appropriate nearly linear arrangements of fault segments oriented N–S and E–W – synthetic and antithetic shears among faults of AnD3 faults trending NW–SE and NE–SW, so faults of both genetic types are closely interconnected. Merging of fault segments of the same spatial orientation at an appropriate linear arrangement requires also appropriate orientation of the stress field. This topic is included in following treatise.

Within the orogenic cycles, the close interconnection of XD3 and XD4 intra-plate processes (as shown in the W. Carpathians – owing to genetic relations of AnD4 faults with AnD3 strike-slip faults), similarly as close interconnection of earlier XD0, XD1 and XD2 orogenic phases (rifting – subduction – collision – post-collisional unroofing, presented by XD labelling methodology in our other treatises, e.g. Németh, 2021, 2024 – in print) show meaningfulness of the use of the principle of orogenic (Wilson) cycles at study and description of geologic (geodynamic, tectonic, metallogenic, etc.) processes.

Conclusion

This article deals with the youngest – AnD3 and AnD4 phases of Cenozoic Neo-Alpine orogenic cycle. The principles stated in this study are valid also for other orogenic cycles and other territories besides Western Carpathians, or even besides European continent.

Their role in terminating phase of orogenic cycle (XD4) and in originating new one ($X^{+1}D0$ phase) is indicated. The role and young ages of systems of N-S / E-W directed faults with dominating pure shear kinematics are explained owing to the high level of knowledge concerning the Cenozoic evolution of the Western Carpathians, encompassing the results of geological mapping, structural research, but also dilatometric registration of present faults microkinematics.

Acknowledgements

Authors express his thanks to Ministry of Environment of the Slovak Republic for funding numerous scientifically contributing regional geological and metallogenetic projects, as well as on international project COST 625 *3-D monitoring of active tectonic structures* (2000–2006) and other research possibilities on EC Horizon 2020, Horizon Europe and UNESCO/IUGS IGCP bases. Comments of two reviewers contributed much to improvement of primary manuscript. This paper is also a contribution of the State Geological Institute of Dionýz Štúr (SGUDS), Slovakia, for the EC – CINEA HORIZON-CL5-2021-D3-D2 project 101075609 Geological Service for Europe (GSEU) within WP6 – Geological framework for the European geological data & information system.

References

Asch, K. (ed.), 2005: International Geological Map of Europe and adjacent areas at the scale of 1 : 5 000 000 (IGME 5000). *Hannover, BGR.*

Bacsó, Z., 2023: The Brehov volcanogenic and stratabound base metal and gold deposit (Eastern Slovakia): Position and genetic relations in the Internal Carpathian-Alpine Cenozoic metallogenetic belt. *Mineralia Slovaca, 55, 1, 27–52.*

Bačová, N., Bajtoš, P., Németh, Z., Michalko, J., Repčiak, M. & Fedorová, Ľ., 2017: Vyhľadávací hydrogeologický prieskum štruktúry minerálnych vôd Dudince – Santovka. Final report. *Manuscript. Bratislava, archive of State Geological Institute of Dionýz Štúr, 2–225* (in Slovak).

Beták, J. & Vojtko, R., 2009: Implementácia nástrojov tektonickej geomorfológie v neotektonickom výskume (na príklade pohoria Považský Inovec). *Geografický časopis / Geographical Journal, 61, 1, 29–47* (in Slovak).

Bezák, V. (ed.), Broska, I., Ivanička, J., Reichwalder, P., Vozár, J., Polák, M., Havrila, J., Mello, J., Biely, A., Plašienka, D., Potfaj, M., Konečný, V., Lexa, J., Kaličiak, M., Žec, B., Vass, D., Elečko, M., Janočko, J., Pereszlényi, M., Marko, F., Maglay, J. & Pristaš, J., 2004: Tectonic map of Slovak Republic. *Bratislava, State Geological Institute of Dionýz Štúr – Ministry of Environment of the Slovak Republic.*

Briestenský, M., Hochmuth, Z., Littva, J., Hók, J., Dobrovič, R., Stemberk J., Petro, Ľ. & Bella, P., 2018: Present-day stress orientation and tectonic pulses registered in the caves of the Slovenský kras Mts. (south-eastern Slovakia). *Acta Geodyn. Geomater., 15, 2 (190), 93–103.*

Dvořák, P., Pospíšil, L., Hotovcová, J., Mojzeš, M. & Papčo, J., 2005: Geo-analýza horizontálních pohybových tendencí na východním Slovensku. *Exploration Geophysics, Remote Sensing and Environment, 12, 9–22* (in Czech with English Abstract).

Fekete, K. & Vojtko, R., 2013: Neotectonic activity of the Pravno fault in the area of the Žiar Mts. *Acta Geologica Slovaca, 5, 2, 117–127.*

Gaál, Ľ., Németh, Z., Bella, P. & Koděra, P., 2017: Caves in magnesite – a rare phenomenon of karstification: The case study from Slovakia. *Mineralia Slovaca, 49, 2, 157–168.*

Gerátová, S., Vojtko, R., Lačný, A. & Kriváňová, K., 2022: The structural pattern and tectonic evolution of the Muráň fault revealed by geological data, fault-slip analysis, and paleostress reconstruction (Western Carpathians). *Geologica Carpathica*, *73, 1, 43–62.*

Grecula, P., 1982: Gemerikum – segment riftogénneho bazénu Paleotetýdy. *Bratislava, Alfa, 1–263* (in Slovak with extended English resumé).

Grecula, P., Návesňák, D., Bartalský, B., Gazdačko, Ľ., Németh, Z., Ištván, J. & Vrbatovič, P., 1990: Shear zones and arc structure of Gemericum, the Western Carpathians. *Mineralia Slovaca, 22, 2, 97–110.*

Grecula, P. (ed.), Kobulský, J., Gazdačko, Ľ., Németh, Z., Hraško, Ľ., Novotný, L. & Maglay, J., 2009: Geological map of the Spiš-Gemer Ore Mts. *Bratislava, State Geological Institute of Dionýz Štúr – Ministry of Environment of the Slovak Republic.*

Hók, J. & Vojtko, R., 2011: Interpretácia pohorelskej línie v podloží stredoslovenských neovulkanitov (Západné Karpaty). *Acta Geologica Slovaca, 3, 1, 13–19.*

Hók, J., Pelech, O., Teťák, F., Németh, Z. & Nagy, A., 2019: Outline of the geology of Slovakia (W. Carpathians). *Mineralia Slovaca, 51, 2, 31–60.*

Konečný, V. (ed.), Lexa, J., Halouzka, R., Dublan, L., Šimon, L., Stolár, M., Nagy, A., Polák, J., Vozár, J., Havrila, M. & Pristaš, J., 1998: Geological map of Štiavnické vrchy Mts and Pohronský Inovec Mts, scale 1 : 50 000. *Bratislava, Geological Survey of Slovak Republic – Ministry of Environment of Slovak Republic*.

Kováč, M., 2000: Geodynamický, paleogeografický a štruktúrny vývoj karpatsko-panónskeho regiónu v miocéne: nový pohľad na neogénne panvy Slovenska. *Bratislava*, *VEDA, 1–202* (in Slovak).

Kováč, M. & Plašienka, D., 2002: Geological structure of the Alpine-Carpathian-Pannonian junction and neighbouring slopes of the Bohemian Massif. *Bratislava*, *Comenius Univ., 1–45.*

Kováč, M., Bielik, M., Hók, J., Kováč, P., Kronome, B., Labák, P., Moczo, P., Plašienka, D., Šefara, J. & Šujan, M., 2002: Seismic activity and neotectonic evolution of the Western Carpathians (Slovakia). *EGU Stephan Mueller Special Publication Series 3*, *167–184.*

Košťák, B., 1969: A new device for in-situ movement detection and measurement. *Easton, Experimental Mechanics, 9, 8, 374–379.*

Králiková, S., Vojtko, R., Sliva, Ľ., Minár, J., Fügenschuh, B., Kováč, M. & Hók, J., 2014: Cretaceous-Quaternary tectonic evolution of the Tatra Mts (Western Carpathians): constraints from structural, sedimentary, geomorphological, and fission track data. *Geologica Carpathica*, *65, 4, 307–326.*

Maglay, J. (ed.), Halouzka, J., Baňacký, V., Pristaš, J. & Janočko, J., 1999: Neotectonic map of Slovakia, 1 : 500 000. Bratislava, Geological Survey of Slovak Republic – Ministry of Environment of Slovak Republic.

Marko, F., 1993: Kinematics of Muráň fault between Hrabušice and Tuhár village. In: Rakús, M. & Vozár, J. (eds.): Geodynamický model a hlbinná stavba Západných Karpát. *Konferencie – Sympóziá – Semináre. Bratislava, Geologický Ústav Dionýza* Štúra, 253–*261.*

Marko, F. & Vojtko, R., 2006: Structural record and tectonic history of the Mýto-Tisovec fault (Central Western Carpathians). *Geologica Carpathica, 57, 3, 211–221.*

Marko, F., Preusser, F., Vojtko, R., Madarás, J. & Kováčová, M., 2010: A contribution to dating Quaternary faults (Vikartovce fault, Western Carpathians). In: Kohút, M. (ed.): Proceedings to the Conference Dating 2010. *Bratislava*, *State Geological Institute of Dionýz Štúr*.

Marko, F., Andriessen, P. A. M., Tomek, Č., Bezák, V., Fojtíková, L., Bosanský, M., Piovarči, M. & Reichwalder, P., 2017: Carpathian Shear Corridor – A strike-slip boundary of an extruded crustal segment. *Tectonophysics, 703–704, 119–134.*

Melioris, L., Hyánková, K., Pospíšil, P., Böhm, V., Čech, F., Mucha, I., Fendeková, M., Némethy, P., Paulíková, E. & Ženišová, Z., 1986: Dudince – Santovka – Slatina. Final report of hydrogeological exploration. *Manuscript.*

Bratislava, archive of State Geological Institute of Dionýz Štúr, 1–100.

Németh, Z., Radvanec, M. & Gazdačko, Ľ., 2017: Výskum geologickej stavby a zostavenie geologických máp v problematických územiach Slovenskej republiky. Téma: A – 03/14 Spresnenie geologickej mapy a tektogenézy rulovo-amfibolitového komplexu a metamafických hornín severogemerickej zóny a centrálnej časti gemerika (oblasť Dobšiná – Mlynky, Nálepkovo – Závadka, Košická Belá – Nižný Klátov, severné okolie Medzeva a Gemerskej Polomy; SGR). Final report. *Manuscript. Bratislava, archive of State Geological Institute of Dionýz Štúr, 95–159*.

Németh, Z., 2021: Lithotectonic units of the Western Carpathians: Suggestion of simple methodology for lithotectonic units defining, applicable for orogenic belts world-wide. *Mineralia Slovaca, 53, 2, 81–90.*

Németh, Z., 2024: Multiple continental breakup produced by geodynamics of polyorogenic zones parallel with equator: Case study from the Western Carpathians.*Contribution in AGU Monograph, Wiley, in print.*

Pešková, I., Vojtko, R., Starek, D. & Sliva, Ľ, 2009: Late Eocene to Quaternary deformation and stress field evolution of the Orava region (Western Carpathians). *Acta Geologica Polonica, 59, 1, 73–91.*

Petro, Ľ., Vlčko, J., Ondrášik, R. & Polaščinová, E., 2004: Recent tectonics and slope failures in the Western Carpathians. *Engineering Geology, 74, 203–212.*

Petro, Ľ., Stercz, M., Grega, D., Vizi, L., Papčo, J., Cipciar, A., Csicsay, K., Littva, J., Staník, P. & Briestenský, M., 2022: Čiastkový monitorovací systém – Geologické faktory, podsystém 02: Tektonická a seizmická aktivita územia. Správa za rok 2021 (in Slovak). *Manuscript. Bratislava, archive of State Geological Institute of Dionýz Štúr.*

Plašienka, D., Grecula, P., Putiš, M., Kováč, M. & Hovorka, D., 1997: Evolution and structure of the Western Carpathians: An overview. In: Grecula, P., Hovorka, D., Putiš, M. (eds.): Geological evolution of the Western Carpathians. Monograph. *Bratislava, Geocomplex, 1–24i.*

Plašienka, D., 2012: Jurassic syn-rift and Cretaceous syn-orogenic, coarse-grained deposits related to opening and closure of the Váhic (South Penninic) Ocean in the Western Carpathians – an overview. *Geological Quaterly, 56, 4, 601–628.*

Plašienka, D. & Soták, J., 2015: Evolution of Late Cretaceous--palaeogene synorogenic basins in the Pieniny Klippen Belt and adjacent zones (Western Carpathians, Slovakia): Tectonic controls over a growing orogenic wedge. *Annales Societatis Geologorum Poloniae, 85, 43–76.*

Pospíšil, L., Nemčok, J., Graniczny, M. & Doktór, S., 1986: Příspěvek metod dálkového průzkumu k identifikaci zlomů s horizontálním posunem v oblasti Západních Karpat. *Mineralia Slovaca, 18, 385–402* (in Czech).

Pospíšil, L., Bezák, V., Nemčok, J., Feranec, J., Vass, D. & Obernauer, D., 1989: Muránsky tektonický systém – významný príklad horizontálnych posunov v Západných Karpatoch. *Mineralia Slovaca, 21, 305–322* (in Slovak).

Putiš, M., Frank, W., Plašienka, D., Siman, P., Sulák, M. & Biron, A., 2009: Progradation of the Alpidic Central Western Carpathians orogenic wedge related to two subductions: Constrained by $^{40}Ar/^{39}Ar$ ages of white micas. *Geodin. Acta, 22, 31–56.*

Putiš, M., Nemec, O., Danišík, M., Jourdan, F., Soták, J., Tomek, Č., Ružička, P. & Molnárová, A., 2021: Formation of a composite Albian-Eocene Orogenic Wedge in the Inner Western Carpathians: P-T estimates and $^{40}Ar/^{39}Ar$ geochronology from structural units. *Minerals, 11, 988.*

Putiš, M., Scherer, E. E., Nemec, O., Ackerman, L. & Ružička, P., 2023: Geochemistry, Lu-Hf garnet ages, and P-T conditions of blueschists from the Meliatic and Fatric nappes, Western Carpathians: Indicators of Neotethyan subduction. *Geosystems and Geoenvironment, 2, 100150.*

Sůkalová, Ľ., Vojtko, R. & Pešková, I., 2011: Cenozoic deformation and stress field evolution of the Kozie chrbty Mountains and the western part of Hornád Depression (Central Western Carpathians). *Acta Geologica Slovaca, 4, 1, 53–64.*

Šefara, J., 1976: Geofyzikálny výskum podložia stredoslovenských neovulkanitov. Final report of the project No. 5514: Geofyzikálny výskum podložia neovulkanitov a megaštruktúr neovulkanitov stredného Slovenska. *Manuscript. Bratislava, archive of State Geological Institute of Dionýz Štúr*, *1–241* (in Slovak).

Tkáčová, H., 1978: Dudince – Slatina – geofyzikálny prieskum Levickej žriedelnej línie. Manuscript. *Bratislava, archive of State Geological Institute of Dionýz Štúr, 1–19* (in Slovak).

Vojtko, R., Tokárová, E., Sliva, Ľ. & Pešková, I., 2010: Reconstructon of Cenozoic paleostress fields and revised tectonic history in the northern part of the Central Western Carpathians (the Spišská Magura and Východné Tatry Mountains). *Geological Carpathica, 61, 3, 311–225.*

Vojtko, R., Marko, F., Preusser, F., Madarás, J. & Kováčová, M., 2011a: Late Quaternary fault activity in the Western Carpathians: evidence from the Vikartovce Fault (Slovakia). *Geologica Carpathica, 62, 6, 563–574.*

Vojtko, R., Beták, J., Hók, J., Marko, F., Gajdoš, V., Rozimant, K. & Jozseš, A., 2011b: Pliocene to Quaternary tectonics in the Horná Nitra Depression (Western Carpatians). *Geologica Carpathica, 62, 4, 381–393.*

Vojtko, R., Petro, Ľ., Benová, A., Bóna, J. & Hók, J., 2012: Neotectonic evolution of the northern Laborec drainage basin (northeastern part of Slovakia). *Geomorphology, 138, 276–294.*

Neoalpínske zóny výzdvihu a poklesu v Západných Karpatoch: produkt kinematickej aktivity na kenozoických regionálnych zlomoch smeru SZ – JV a SV – JZ v orogenetickej fáze AnD3 a mladších subekvatoriálnych (V – Z) a submeridiánnych (N – S) zlomoch v orogenetickej fáze AnD4

Článok opisuje vertikálne pohyby blokov hornín v dôsledku kinematickej aktivity na regionálnych zlomoch dvoch kenozoických neoalpínskych orogenetických fáz v Západných Karpatoch, AnD3 a AnD4 (v zmysle novej geodynamickej klasifikácie litotektonických jednotiek a tektonických štruktúr, tzv. XD indexovania; Németh, 2021; obr. 1). Počas orogenetickej fázy AnD3 boli generované hlavne zlomy párového systému strižných zón, a to dominantne pravostranné horizontálne posuvné zlomy smeru SZ – JV a ľavostranné horizontálne posuvné zlomy smeru SV – JZ. Následná orogenetická fáza AnD4, ktorá je v Západných Karpatoch najmladšia, sa prejavovala vznikom regionálnych zlomov subekvatoriálneho (V – Z) a submeridiánneho (S – J) smeru s dominantnou vertikálnou zložkou pohybu. Dezintegrácia vrchnej kôry kinematickou aktivitou uvedených (AnD3 a AnD4) zlomov vytvorila v západokarpatskej orogénnej zóne blokovú stavbu v závere neoalpínskeho orogenetického cyklu a jednotlivé bloky zaznamenali vzájomný výzdvihovo-poklesový charakter pohybu. Blokový výzdvih či pokles sa prejavil v morfológii územia a bol ďalej zvýrazňovaný vonkajšími geologickými činiteľmi [napr. ďalším zvýrazňovaním priebehu horských hrebeňov (obr. 9) či prehlbovaním údolí].

Článok interpretuje možný prvopočiatok genézy zlomov s priebehom v smere S – J a V – Z, charakteristických pre orogenetickú fázu AnD4. Kinematickou aktivitou strižných zón smeru SV – JZ a SZ – JV už počas orogenetickej fázy AnD3 sa posunmi v rámci týchto diagonálnych strižných zón začali generovať tzv. syntetické a antitetické strihy medzi paralelnými zlomami. V oboch prípadoch – v prípade systému smeru SV – JZ aj smeru SZ – JV – mali syntetické strihy generálnu orientáciu v smere S – J a antitetické strihy generálnu orientáciu v smere V – Z. V prípade tektonicky veľmi exponovaného územia vznikala v orogenetickej fáze AnD3 vysoká hustota syntetických a antitetických strihov – segmentov budúcich zlomov. Ak sa takého segmenty vytvorili v línii, reprezentovali oslabenú zónu, z ktorej sa následne v orogenetickej fáze AnD4 vygenerovali kontinuálne zlomy s priebehom v smere S – J alebo V – Z. Vzájomné priestorové vzťahy zlomov párového systému AnD3 a orientácie súvisiacich syntetických a antitetických strihov zobrazujú diagramy v pravej dolnej časti obr. 7 a 10.

Doručené / Received: 8. 12. 2023
Prijaté na publikovanie / Accepted: 21. 12. 2023

Mineralia Slovaca, Web ISSN 1338-3523, ISSN 0369-2086, https://doi.org/10.56623/ms.2023.55.2.2
55, 2 (2023), 117 – 132, © Authors 2023. CC BY 4.0

Neogene volcanics of the Burda mountain range nearby Štúrovo, Slovakia

LADISLAV ŠIMON, VIERA KOLLÁROVÁ and MONIKA KOVÁČIKOVÁ

State Geological Institute of Dionýz Štúr, Mlynská dolina 1, SK-814 07 Bratislava, Slovakia;
ladislav.simon@geology.sk

Abstract: The Neogene volcanic products of the Burda mountain range nearby Štúrovo belong to Burda Formation. At the base of the Burda Formation a succession of epiclastic volcanic rocks and pyroclastic rocks of andesites has developed. In the central part of the formation, the volcanic products associated with the activity of submarine volcanism of the Badenian age developed. Submarine extrusive volcanic domes of andesites are typical. In the upper part of the Burda Formation, pyroclastic and epiclastic facies of andesites were formed. Deposits of pyroclastic flows and redeposited pyroclastics are characterized by the presence of relics of petrified tree trunks, indicating transport from emergent forest-covered slopes from the higher levels of the volcanic edifice of the Börzsöny Mountains in today's Hungary. This part of the Burda volcanics represents a transitional volcanic zone with the Börzsöny stratovolcano.

Key words: volcanics, pyroclastic rocks, epiclastic rocks, andesite extrusive dome, Burda Formation

Graphical abstract

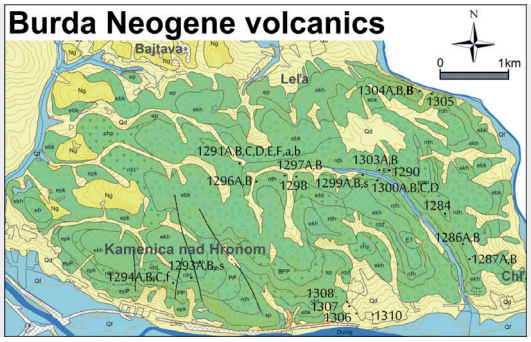

Highlights

- Article presents a new map of Neogene volcanic products in Burda volcanic mountain range, neighbouring with Börzsöny and Visegrád volcanic mountains;
- Detail field study has contributed to compiling of new lithostratigraphy of volcanic products included into new lithostratigraphic column;
- Petrified tree trunks in pyroclastic flows indicate transport from higher levels of the volcanic edifice of Börzsöny stratovolcano.

Introduction

The Burda volcanic mountain range (Mts) near Štúrovo is the smallest geomorphological volcanic group in Slovakia. It is located in southwestern Slovakia, at the state border with Hungary. Westward Burda Mts border with the Danube Upland. The southern border is formed by the bed of the Danube river, which in the Vyšehrad (Visegrád) Gate separates Burda Mts from the Hungarian Pilis Mts. The eastern border is formed by the Ipeľ river bed, which separates Burda Mts from Hungarian Börzsöny Mts. The northwestern part of the mountain range is bounded by the Bajtava Gate. The maximum length of the mountain range is 7.5 km and the maximum width is only 3.5 km. Its highest peak is Plešivec 395 m a.s.l. in the central part of the Burda Mts. Volcanic rocks of the Burda Mts are encompassed to Burda Formation (Bezák et al., 2009). The products of the Burda Formation occur within the Burda peat block. The heather block is tilted to the northwest. The flow of the Danube follows the east-west direction of the fault zone at the southern edge of the lowland. The rocks of Burda Formation of Badenian age pass W- to NW-ward to contemporary Bajtava Formation. The assemblage contains a rich marine fauna of the Dagenid zone and the nannoplankton community of the NN-5 zone, corresponding to the Lower Badenian (Nagy et al., 1998). The uranium (Fe) fission track method (Repčok, 1978) revealed 15.7 ± 1.4 Ma age of andesite fragment near Kamenica nad Hronom and K/Ar method 15.2 ± 1.2 Ma age of andesite body (Vass et al., 1979).

Methods

The volcanic rocks of the Burda Mts near Štúrovo were mapped by modern methods of volcanological analysis applying the Garmin GPS map St 62 device, recording the graphic, audio and photographic field documentation diary into the Samsung Galaxy N9 device. The field documentation consisted of more than 150 points, applying the LocusPro program, which enabled us to perform accurate online mapping of volcanic products with digital geolocation. We took 43 samples (Fig. 1) for further detailed research in the ŠGÚDŠ laboratories in Bratislava, encompassing volcanic, lithological, petrographic, mineralogical and geochemical analyses (samples Nos. 1284, 1296A, B, 1287A, B, 1290, 1291A,

B, C, D, E, Fa, b, 1293A, B, s, 1294A, B, C, f, 1296A, B, 1297A, B, 1298, 1299A, B, s, 1300A, B, C, D, 1303A, B, 1304B, 1305, 1306,1307, 1308, 1310). Thin sections of the samples were studied by the JENAPOL optical microscope and photographic documentation of the samples was done by the Olympus Camedia C5060 digital camera in the ŠGÚDŠ in Bratislava. Rock-forming minerals were analyzed by CAMECA SX 100 electron-probe microanalyzer (EPMA) in the ŠGÚDŠ laboratory in Bratislava using 15 kV accelerating voltage, 20 nA beam current and predominantly 5 μm beam diameter. Analyzed elements, their measured spectral lines and used standards: Si Kα – wollastonite, orthoclase; Ti Kα – TiO_2; Al Kα – Al_2O_3; Cr Kα – Cr; Fe Kα – fayalite; Mg Kα – rhodonite; Mg Kα – forsterite, MgO; Ca Kα – wollastonite; Ni Kα – Ni; Sr Lα – $SrTiO_3$; Ba Lα– barite; Na Kα – albite; K Kα – orthoclase, F Kα – CaF_2, Cl Kα – NaCl. Whole-rock major and trace element compositions were obtained in the ŠGÚDŠ Geoanalytical laboratories in Spišská Nová Ves (samples 1291A, 1291B, 1293S, 1294F, 1299S, 1304B).

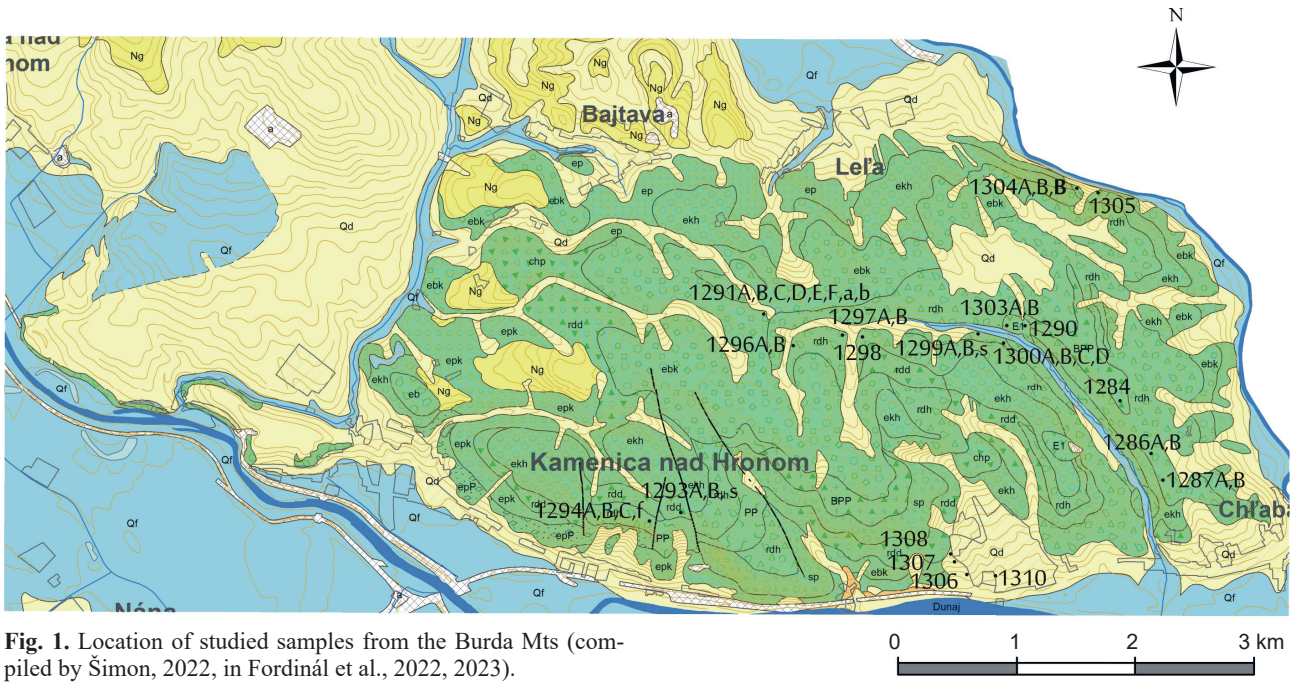

Fig. 1. Location of studied samples from the Burda Mts (compiled by Šimon, 2022, in Fordinál et al., 2022, 2023).

Characteristics of the volcanic rocks of the Burda Mts

Volcanics of the Burda Mts are represented by the Burda Formation (Fig. 2). At the base of formation, a succession of andesite epiclastics and pyroclastics are developed. Rocks in the central part of the formation are products of Badenian submarine volcanism. Submarine andesite extrusive domes are typical, having elliptical to isometric cross-sections with size of up to 220 m. They consist of massive andesite with an irregular blocky separation with a transition to brecciated andesite and up to breccia with a chaotic orientation of fragments. As a result of gradual destruction of these volcanic domes, debris-like material was formed and deposited even outside of its volcanic center further into space by mass breccia flows, debris flows and deposition of coarse to blocky breccias. In upper part of the Burda Fm, facies of pyroclastics and epiclastics of andesites were formed. Deposits of pyroclastic flows and lahars are characterized by the presence of relics of petrified tree trunks, indicating transport from the emergent forest-covered slopes of the higher levels of the Börzsöny volcanic edifice located in nowadays Hungary. These parts of the Burda volcanics represent the transitional volcanic zone of the Börzsöny stratovolcano.

At the base of Burda Fm, a succession of andesite epiclastics and pyroclastics is developed. Upwards there occurs a succession of facies of epiclastics, pyroclastics and products of submarine extrusive domes. The Burda Fm is made up of following facies: epiclastic and pyroclastic horizons, epiclastic volcanic sandstones with pumice, epiclastic volcanic sandstones and conglomerates, epiclastic volcanic sandstones, fine-grained epiclastic volcanic conglomerates, coarse-grained epiclastic volcanic conglomerates, epiclastic volcanic breccias and conglomerates, epiclastic volcanic breccias, fine- and coarse-grained redeposited pyroclastics, block ash pyroclastic flows, subaqueous breccia flows, chaotic breccias of redeposited pyroclastics, extrusive breccias of am-

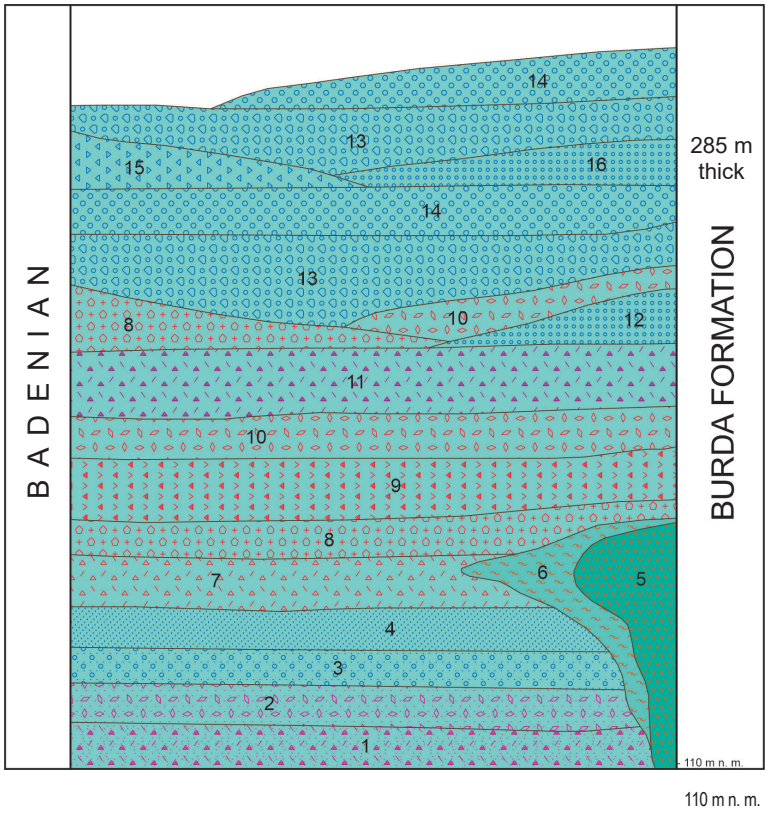

Fig. 2. Lithostratigraphic table of the Burda Formation (compiled by Šimon, 2023): 1 – epiclastic and pyroclastic horizon; 2 – epiclastic volcanic sandstones with pumice; 3 – epiclastic volcanic sandstones and conglomerates; 4 – epiclastic volcanic sandstones; 5 – extrusive domes of amphibole-pyroxene andesites; 6 – extrusive breccias of amphibole-pyroxene andesite domes; 7 – subaquatic breccia flows; 8 – block-ash pyroclastic flows; 9 – chaotic breccias of redeposited pyroclastics; 10 – ash-pumice streams; 11 – redeposited coarse-grained pyroclastics; 12 – redeposited fine-grained pyroclastics; 13 – epiclastic volcanic breccias and conglomerates; 14 – epiclastic coarse-grained volcanic conglomerates; 15 – epiclastic volcanic breccias; 16 – epiclastic fine-grained volcanic conglomerates.

phibole-pyroxene andesite domes and extrusive domes of andesites. The horizon of epiclastics and pyroclastics (Fig. 3A, B, C) represents a succession of volcanoclastic rocks of volcanosedimentary origin with rare positions of autochthonous pyroclastic rocks. This material was accumulated in the intervolcanic period, and partly also in the syneruptive period, when pyroclastic flows and pumice tuffs were formed. Intervolcanic period is represented by positions of epiclastic volcanic breccias, conglomerates, sandstones, but also occasional flows, rapid flushes (hyperconcentrated currents), lahars and mudflows, debris flows and debris avalanches. These epiclastic lithofacies occur in the transitional to marginal volcanic zone. From the petrographic point of view, the volcaniclastic material consists mainly of andesites, but pyroxene andesites are also present, and we have also rarely observed rocks of non-volcanic material and relics of a petrified wood from the original Badenian forest vegetation. Epiclastic volcanic sandstones of andesites are characterized by the presence of autochthonous light porous pumice of angular to spherical shape. Epiclastic volcanic sandstones occur mainly in the lower and marginal parts of the Burda Fm near Kamenica nad Hronom, where epiclastic volcanic conglomerates are deposited in their immediate vicinity. Epiclastic volcanic sandstones are predominantly coarse-grained, fairly well sorted, and occasionally show signs of stratification. There are also small or minor andesite sheets or lenticular positions of fine-grained epiclastic volcanic conglomerates with isolated blocks of andesites. Light porous pumice can be observed, intergrowing into individual beds. The material of epiclastic volcanic sandstones is represented by andesites of dark grey, grey and reddish brown colors, which was proved petrographically. Porous pumice stone, predominantly light grey in colour, has an acidic dacite composition. Epiclastic volcanic sandstones with conglomerates of amphibole-pyroxene andesites occur together with sandstones especially in the marginal parts of the Burda Fm near Kamenica nad Hronom municipality.

Epiclastic volcanic conglomerates consist of small fragments of dark brown, dark or light grey oval or perfectly oval shaped andesites. Epiclastic volcanic sandstones are coarse-grained with fragments of light-coloured andesites that alternate with each other in irregular and occasionally lenticular positions of relatively well sorted conglomerates and sandstones of andesite clasts. Epiclastic volcanic sandstones of andesites occur mainly in the lower and marginal parts of the Burda Fm in the vicinity of Kamenica nad Hronom, Bajtava and Leľa. Epiclastic volcanic sandstones are predominantly coarse-grained, moderately to well sorted and occasionally quite well laminated. Very rarely, andesite sheets and fragments are present, which can form simple thread-like beds of small epiclastic volcanic conglomerates in epiclastic volcanic sandstones. Epiclastic volcanic sandstones consist of dark and light grey, as well as dark brown andesites. Small epiclastic volcanic conglomerates of andesites appear mainly in the upper and marginal parts of the volcaniclastic complex of the Burda Fm in the vicinity of the Chľaba site in Veľká dolina valley. Epiclastic volcanic conglomerates of andesites form positions up to 25 meters thick (Fig. 3D).

Epiclastic volcanic conglomerates (Fig. 3E) contain andesite fragments having up to 35 cm in size, but also andesite sheets up to 50 cm in size are rarely present.

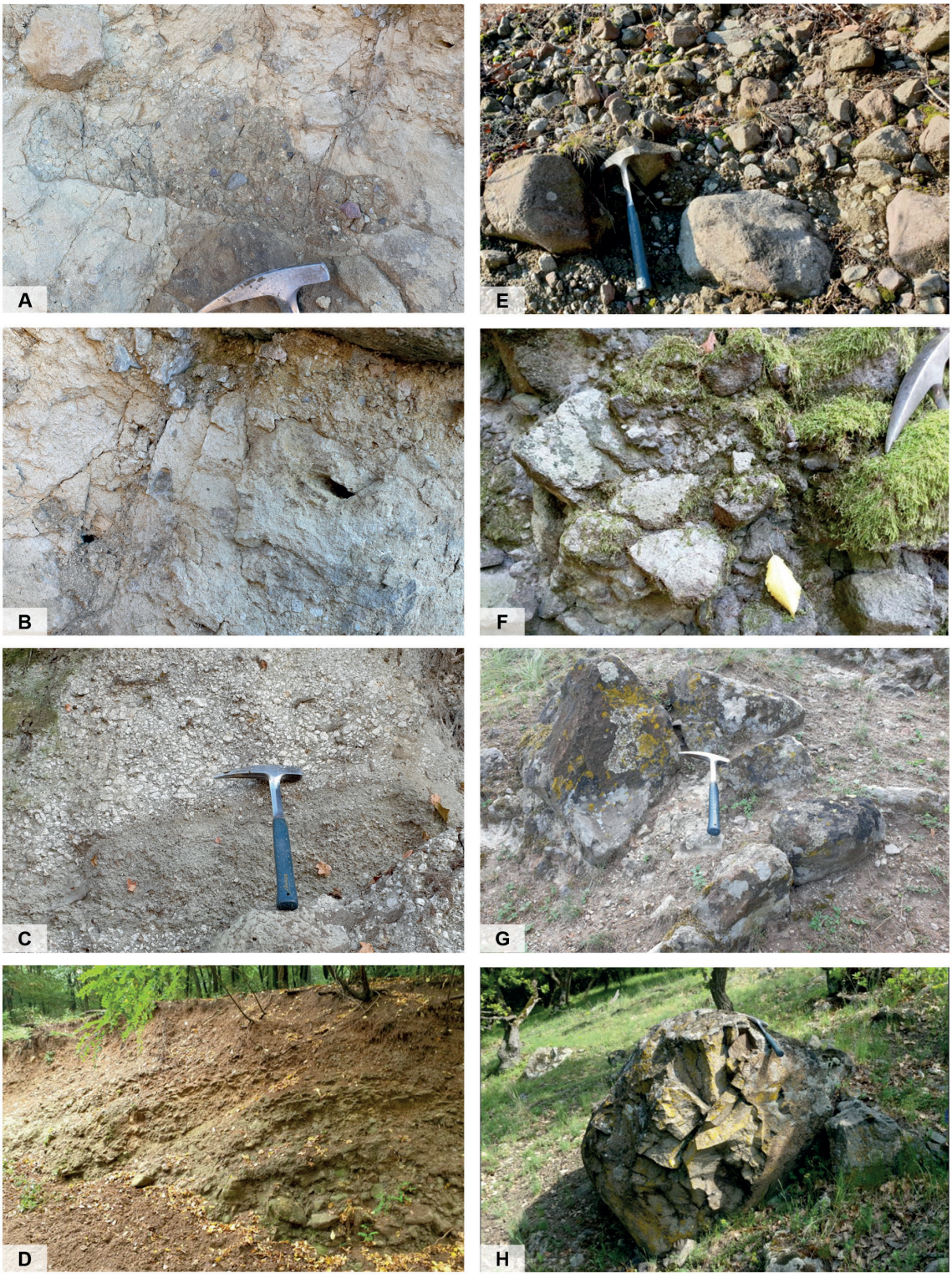

Fig. 3. Morphostructures of volcanogenic rocks in the Burda Mts. A – Submarine debris avalanche. In the rubble avalanche, there is a bounded layer of autochthonous pyroclastics (above the hammer), which was torn down, deformed and transported after a sudden volcanic collapse; B – Submarine debris avalanche. Holes are after petrified wood in the debris avalanche. A–B – Kamenica nad Hronom locality; C – Alternation of submarine pumice and ash flows, Nad Hrdličkou locality; D – Epiclastic volcanic small-boulder conglomerates, Leliansky les locality; E – Epiclastic volcanic boulder-type conglomerates. Čierna hora locality; F – Epiclastic volcanic breccias, Leliansky les locality; G – Breccias of redeposited pyroclastics, Kráľova hora locality; H – Megablock of andesite in breccias of redeposited pyroclastics, Skalka locality.

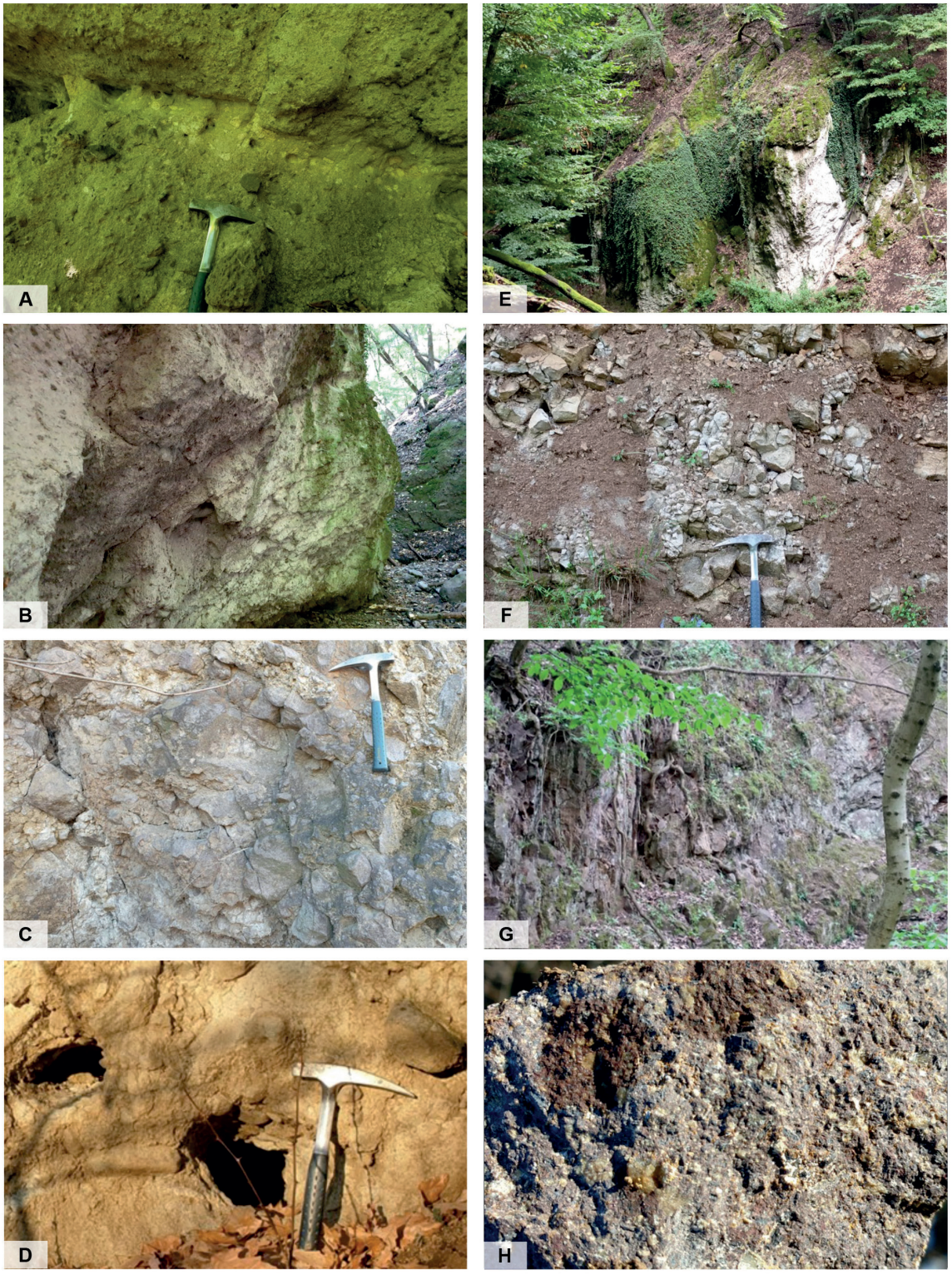

Fig. 4. Morphostructures of volcanogenic rocks in the Burda Mts. A – Block-ash pyroclastic flows, Burdov locality; B – Submarine breccia flows, Kováčov locality; C – Chaotic breccia of deposits of submarine breccia currents, Nosta, Burda locality; D – Holes after petrified trees in volcanic clastics, Višnové locality; E – Pumice pyroclastic flow, Ipeľské prielohy locality; F – Tuff beds, Pod horou locality; G – Andesite of vertical detachment from an extrusive dome, Chľaba locality (near Ipeľ river); H – Fragment of coarse-grained amphibole-pyroxene andesite with brownish-grey garnet affected by weak argillization and silicification, Čierny vrch locality.

The andesites have a suboval to perfectly oval shape. They are dark- and light-grey, grey, dark brown in colour. Beds of epiclastic volcanic conglomerates are poorly or moderately well sorted. Observed was inconspicuous or moderate layering. In some locations, the ungradedness of the andesite beds can be observed within thick bench-like beds, representing the deposits of debris flows. The matrix in epiclastic volcanic conglomerates is medium to coarse-grained sandy, light grey or greenish grey in colour. Epiclastic volcanic conglomerates consist of andesites, but sometimes amphibole-pyroxene andesites with garnet are also present. Coarse-grained to blocky epiclastic volcanic conglomerates of andesites occur mainly in the upper part of the Burda Fm in the vicinity of Kamenica nad Hronom, Bajtava, Leľa and Chľaba localities. Epiclastic volcanic conglomerates form beds up to 20 m thick. They form successions with interbeds of fine-grained epiclastic volcanic conglomerates and epiclastic volcanic sandstones. The size of the andesite fragments is on average up to 55 cm. Positions of conglomerates, containing andesite boulders up to 95 cm in size, also rarely appear. The conglomerate matrix is medium to coarse sandy. In the matrix there are beds of andesites with a solid texture, but sometimes also with a porous texture, dark grey, grey, dark brown or reddish in colour.

Epiclastic volcanic breccias to conglomerates of amphibole-pyroxene andesites (Fig. 3F) occur in the middle and upper part of the Burda Fm in the vicinity of the Leľa, Bajtava and Chľaba localities. They form beds thick up to 15 m. Within the beds, the fragments and sheets of andesites with a diameter of 1 to 25 cm occur. Rarely, there occur also interbeds of coarser or finer epiclastic volcanic breccias and epiclastic volcanic conglomerates, which are poorly sorted and partly layered. Their matrix is unsorted, medium to coarse sandy with small fragments of andesites. Fragments of amphibole-pyroxene andesites have subangular or even oval shape. Andesites have a cohesive and porous texture and are from dark- to light-grey, brown, or reddish-brown in colour. Epiclastic volcanic breccias of amphibole-pyroxene andesites occur in the middle part of the Burda Fm in the vicinity of Kamenica nad Hronom and Leliansky les localities (Fig. 3F).

Epiclastic volcanic breccias form beds up to 20 m thick. Fragments of andesites up to 75 cm in size are present in epiclastic volcanic breccias. Andesites are mostly angular and subangular in shape, but occasionally suboval andesites are also present. Andesites are grey, dark grey, brown or brown-red in colour. Epiclastic volcanic breccias are poorly sorted and poorly bedded. The matrix in them is unsorted, coarsely sandy with small fragments of integral grey andesites. Petrographic study confirms andesite composition of epiclastic volcanic breccias. Small redeposited pyroclastics (Fig. 3G) appear in the complex of volcanic clastics of the Burda Fm in the vicinity of the Chľaba, Bajtava and Kamenica nad Hronom localities.

Redeposited pyroclastics create positions up to 15 m thick, being formed by dark grey or brownish angular and subangular fragments of andesites up to 20 cm in size. The matrix is sandy-tuffitic and unsorted with small fragments of petrographically proved andesites. Coarse-grained re-deposited pyroclastics occur in the volcaniclastic complex of the Burda Fm in the vicinity of the Chľaba, Leľa and Kováčov localities, where they form positions up to 20 m thick. They are formed by fragments of andesites up to 60 cm in size, but megablocks up to 200 cm in size are sporadically present, too (Fig. 3H).

Fragments of andesites have an angular and subangular shape and their colour is dark grey or brownish. The matrix is sandy-tuffitic and unsorted with small fragments of petrographically proved andesites. Block-ash pyroclastic flows (Fig. 4A) of andesites emerge in the upper part of the Burda Fm around the Kováčov and Chľaba localities. Block-ash pyroclastic flows create positions up to 20 m thick, consisting of chaotic breccias, which are formed by angular and spherical fragments of andesites of size up to 60 cm in the amount of up to 60 %. Fragments of andesites have a porous texture and some have the character of annealed lighter fragments that were deposited in an unsorted, poorly sintered detrital matrix. The matrix consist of tuff and contains light pumice.

Submarine breccia flows (Fig. 4B, C) of andesites emerge in the middle part of the Burda Fm around the Kováčov locality. Subaqueous breccia currents create positions up to 50 m thick. They are formed by coarse chaotic breccias that associate with the source extrusive bodies.

Chaotic breccias contain fragments of andesites ranging in size from 1 cm to 200 cm. Their colour is dark grey, having an integral texture and angular shape. Brownish colour andesites with porous texture, angular and spherical shape are also present (Fig. 4D). Fragments of andesites are stored in a matrix, representing up to 70 % of rock material. The matrix is ungraded tuff with small clasts of andesites. The occasional redness of the matrix can be observed with a higher degree of homogenization and compaction. From a petrographic point of view, subaqueous breccia flows are formed by porphyritic andesites. Chaotic breccias of redeposited pyroclastics occur in the upper part of the Burda Fm in the vicinity of the Kováčov locality. Chaotic and unsorted breccias of redeposited pyroclastics are up to 25 m thick, they are slightly strengthened by matrix alteration. They are formed of fragments of andesites of dark grey, brown and reddish colours, solid or porous texture. Fragments have an angular and subangular shape. The size of andesite fragments is up to 100 cm, and there

are rare fragments up to 150 cm in size. Fragments are stored in a matrix with a content of up to 50 %. The matrix is tuff-sandy with small fragments of grey andesites and light pumice. Holes after petrified trees are occasionally observed (Fig. 4D).

The pumice pyroclastic flow (Fig. 4E) of andesites forms a more continuous horizon of tuffs (Fig. 4F), which are mostly unsorted, chaotic, indistinctly layered in a bench-like form in the lower part of the Burda Fm in the vicinity of the Chľaba and Kováčov localities.

Within the beds, the matrix is predominant, which is tuff, it also contains grey-white pumice, and various fragments of petrographically proved andesites of angular and spherical shape, porous and glassy texture and dark grey to black-grey colors are also present. Sometimes we also record fragments of non-volcanic material in the tuffs. Intrusive-extrusive breccias of amphibole-pyroxene andesites occur in the lower part of the Burda Fm in the vicinity of the Kováčov and Chľaba localities. Breccias represent marginal parts of intrusive-extrusive bodies. On the one hand, they are connected by a transition to their own body, on the other hand, they eventually pass into the breccias of subaqueous breccia flows. The brecciation zones are up to tens of meters thick. Extrusive breccias appear in facies with massive solid texture andesites of a light grey colour with facies built of angular fragments of grey non-porous andesite in a crushed lava matrix. Extrusive breccias are unsorted, chaotic, with a maximum fragment size of up to 100 cm. Fragments of andesites in extrusive breccias are present in amounts up to 80 %. Occasionally there occur weakly oxidized red-brown andesite and spherical fragments of brown andesite both with porous texture. The matrix is formed by crushed andesites of light grey colour and porous texture, being petrographically proved. Extrusive domes of andesites in the lower part of the Burda Fm occur in the vicinity of the Kováčov and Chľaba localities (near Ipli) (Fig. 4G, H). Extrusive domes are isometric shape, occasionally slightly elliptical bodies with dimensions up to 200 m, formed of massive andesite with vertical, blocky and roughly blocky separation. Indistinct fluid textures were observed in the bodies. The textures have a typical vertical to fan-like course. Zones of extrusive breccias developed at the edges of extrusive domes. The bodies are made of light grey to greenish porphyritic andesite with phenocrysts of plagioclase, hypersthene, augite and amphibole in the ground mass, which is microlithic in the middle part of the bodies and microlithic to microlithic-hyalopilitic at the edges of the bodies.

Geochemistry of volcanic rocks of the Burda Formation

These rocks were analysed for whole-rock major and trace element contents: 1291A, B – amphibolic andesite with biotite and orthopyroxene, 1293S – biotitic-amphibolic andesite with orthopyroxene, 1294F – biotitic-amphibolic andesite with orthopyroxene, 1299S – biotitic-amphibolic andesite with orthopyroxene, 1304B – amphibolic andesite with biotite and orthopyroxene. According to the classification TAS diagram (Le Bas et al., 1986; Fig. 5), the analysed samples represent andesite and the sample 1291A corresponds to dacite. Samples 1291B, 1293S, 1299S and 1304B have a relatively similar composition. Sample 1294F can be considered as acid andesite. All andesites correspond to high-potassium andesite and belong to the high-potassium calc-alkaline series (high-K CA) according to the diagram of SiO_2 vs. K_2O (Peccerrillo & Taylor, 1976; Fig. 6). The trace element contents of the studied rocks can be presented

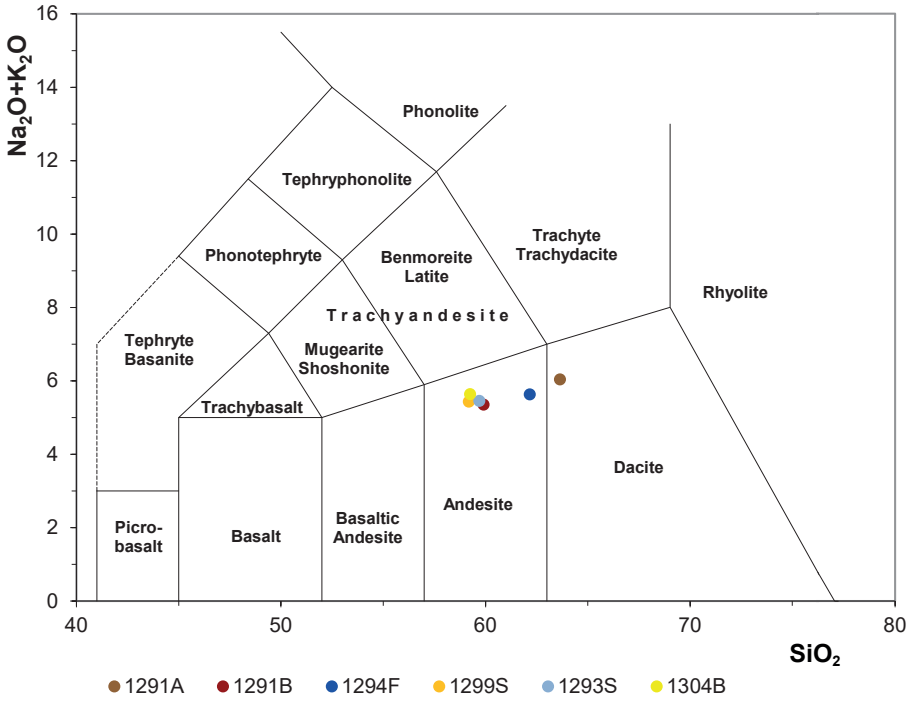

Fig. 5. Position of studied samples in classification TAS (total alkali – silica) diagram (sensu Le Bas et al., 1986).

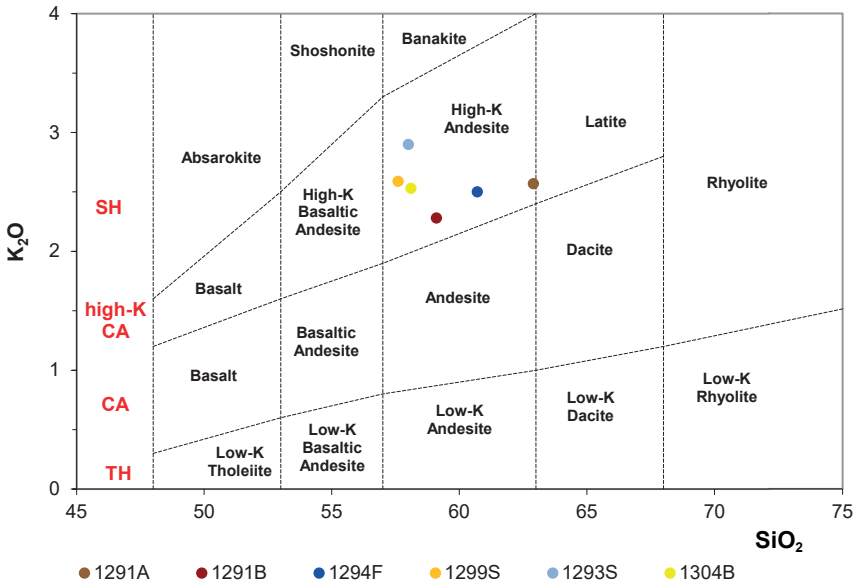

Fig. 6. Position of studied samples in classification diagram of SiO_2 vs. K_2O (sensu Pecerrillo & Taylor, 1976). Petrogenetic series: TH – tholeiitic, CA – calc-alkaline, high-K CA – high-potassium calc-alkaline, SH – shoshonitic.

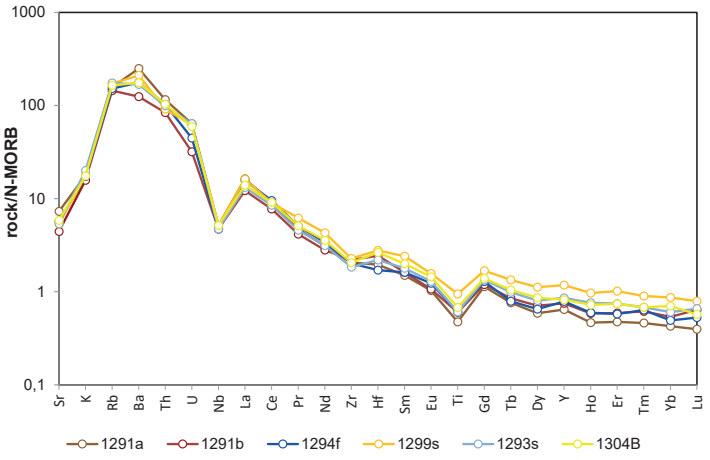

Fig. 7. Multi-element diagram (spiderogram; sensu Sun & McDonough, 1989). Contents of elements are normalized to N-MORB.

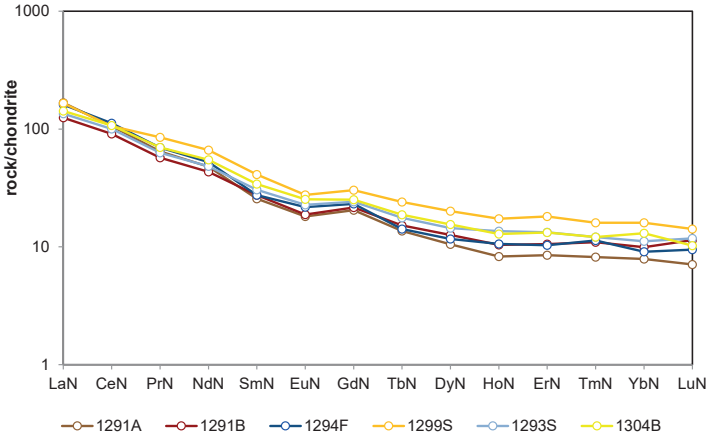

Fig. 8. Normalized REE patterns (normalization according to Evensen et al., 1978).

using multi-element diagrams (spiderograms, Fig. 7). On the diagram, we can see features typical for rocks of island arcs and active continental margins: the LILE enrichment (large-ion lithophile elements; K, Sr, Ba, Rb) and depletion in HFSE (high-field strength elements; Nb, Ti). The normalized REE patterns (REE = rare earth elements; Fig. 8) have a slight slope in the studied samples of andesites. The weak europium anomaly indicates that extensive fractionation of plagioclase did not take place in the genesis of andesite magmas.

Mineralogical and petrographic characteristics of volcanics of the Burda Formation

The studied samples are represented by fragments of andesites from volcanoclastic rocks, by andesites of intrusive bodies and by volcanoclastic rocks themselves. Andesites form two petrographic types: biotitic-amphibolic andesites with orthopyroxene and amphibolic andesites with biotite and pyroxene (Fig. 9).

Biotitic-amphibolic andesites with orthopyroxene have a porphyritic texture with a hyalopilitic (Fig. 9A, B) or microcrystalline (Fig. 9C, D, E) groundmass. There is one sample which can be identified as an andesite porphyry due to the more coarse-grained groundmass (sample 1310, Fig. 9F). The proportion of phenocrysts compared to the groundmass is 20–30 %. Plagioclase, amphibole and biotite are the main rock-forming minerals. This type of andesite occurs in the samples the most frequently.

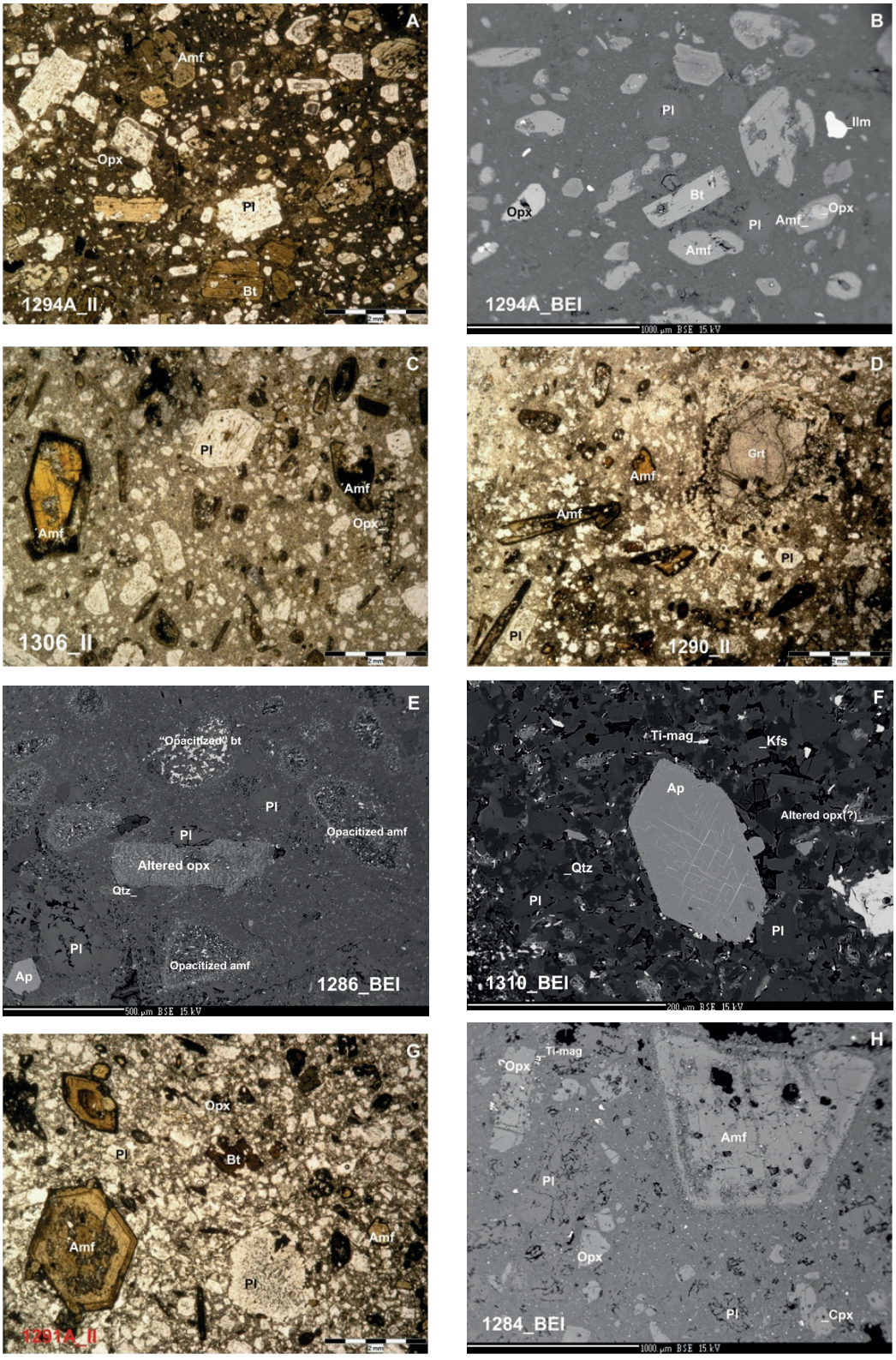

Fig. 9. A – photo of the sample 1294A, parallel polars, B – BEI of the same sample, C – photo of the sample 1306, parallel polars, D – photo of the sample 1290, parallel polars, E – BEI of sample 1286, F – BEI of the groundmass material, sample 1310, G – photo of the sample 1291A, parallel polars, H – BEI of the sample 1284.
Pl – plagioclase, Amf – amphibole, Bt – biotite, Opx – orthopyroxene, Cpx – clinopyroxene, Ilm – ilmenite, Ti-mag – Ti-magnetite, Kfs – potassium feldspar, Qtz – quartz, Ap – apatite, Grt – garnet, BEI –backscattered electron image.

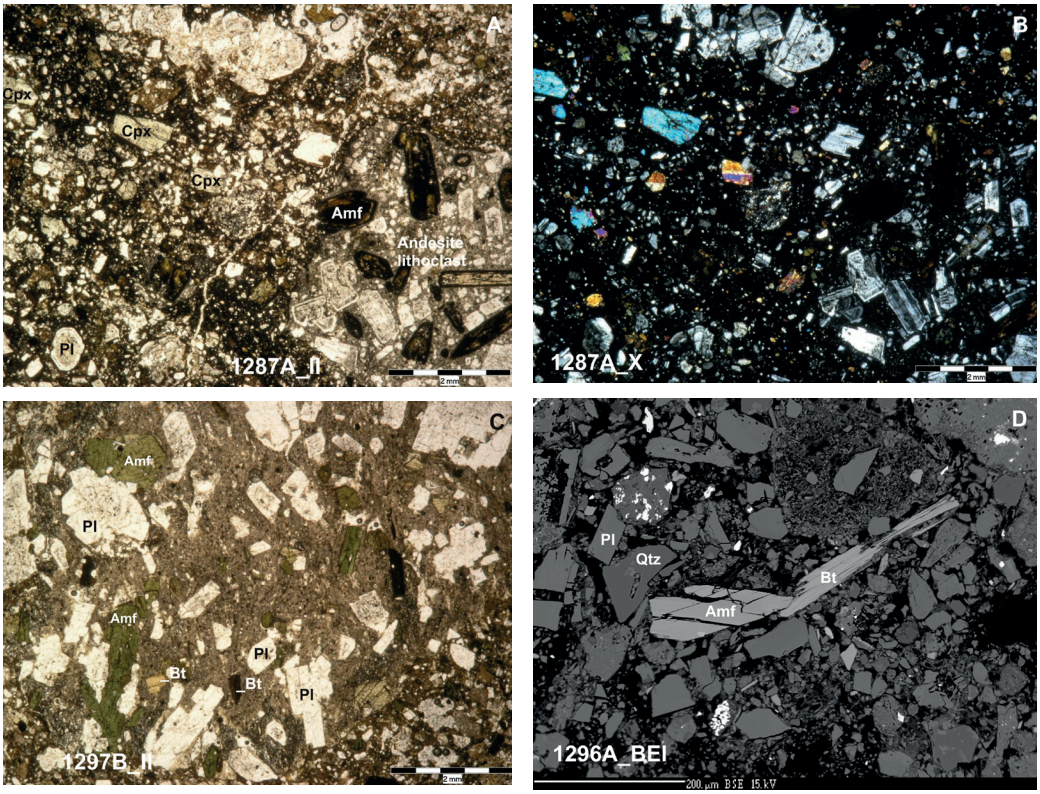

Fig. 10. Photo of the sample 1287A with parallel (A) and crossed (B) polars, C – lithoclast of biotitic-amphibolic andesite in the sample 1297B, parallel polars, D – crystalloclasts in the tuff sample 1296A, BEI. Pl – plagioclase, Amf – amphibole, Bt – biotite, Cpx – clinopyroxene, Qtz – quartz, BEI – backscattered electron image.

Amphibolic andesites with biotite and pyroxene (Fig. 9G, H) have a porphyritic texture with a microcrystalline groundmass. These rocks are characterized by a high proportion of phenocrysts compared to the groundmass (up to 50 %). Plagioclase and amphibole are the main rock-forming minerals. Sample 1297A has a special position in this group with plagioclase as the highly prevalent mineral, with mafic minerals rarer and smaller than in other samples and with the proportion of the phenocrysts compared to the groundmass about 30 %.

Plagioclase is the most abundant rock-forming mineral in both types of andesites. It forms phenocrysts and glomeroporphyric aggregates of tabular and lath shape and needles in the groundmass. Plagioclase is zoned and characteristically twinned. Amphibole forms idiomorphic to hypidiomorphic phenocrysts and aggregates which may enclose plagioclase. Preserved amphiboles are pleochroic, some of them are zoned. They are opacitized to the variable degree – from weakly opacitized crystal rims to complete opacitization. Biotite forms pleochroic tables and laths. It can enclose plagioclase. Biotites are preserved, or they show a phenomenon similar to the opacitization of amphibole: Fe-Ti oxides and potassium feldspar are formed at the expense of biotite (potassium feldspar instead of orthopyroxene in amphibole). Orthopyroxene forms idiomorphic to hypidiomorphic phenocrysts or is a part of glomeroporphyric aggregates. It also forms needles in the groundmass. It can be partially or completely altered. Very rare clinopyroxene is found in the sample 1284. Apatite is present as small phenocrysts or groundmass grains in some samples with crystallized groundmass. In three samples (1304B, 1290, 1310) there is garnet of almadine composition with a reaction rim. The crystallized groundmass consists of plagioclase, sanidine, quartz, orthopyroxene, Ti-magnetite, ilmenite, ± apatite.

Volcaniclastic material was studied in the samples 1287A and B, 1297B, and tuff in the samples 1296A and 1298.

The samples 1287A (Fig. 10A, B) and 1287B contain plagioclase, amphibole, orthopyroxene, and clinopyroxene crystalloclasts. There is no biotite in the samples. The presence of clinopyroxene may indicate their origin from pyroxenic andesites. Sample A contains orthopyroxene-amphibolic andesite lithoclast. Sample 1297B (Fig. 10C) contains rock lithoclasts and crystalloclasts of plagioclase, amphibole, and biotite. The lithoclasts are composed of biotitic-amphibolic andesite with plagioclase, green amphibole and hyalopilitic groundmass, of andesitic porphyry and of amphibolic(?)-pyroxenic andesite.

Sample 1296A (Fig. 10D) represents tuff. It contains amphibolic-pyroxenic andesite lithoclast (also with clinopyroxenes). Crystalloclasts are represented by plagioclase, amphibole, biotite, Fe-oxide, quartz and pyroxenes(?). In the tuff sample 1298, crystalloclasts are strongly predominant: plagioclase, green and brown amphiboles, biotite, clinopyroxene and orthopyroxene.

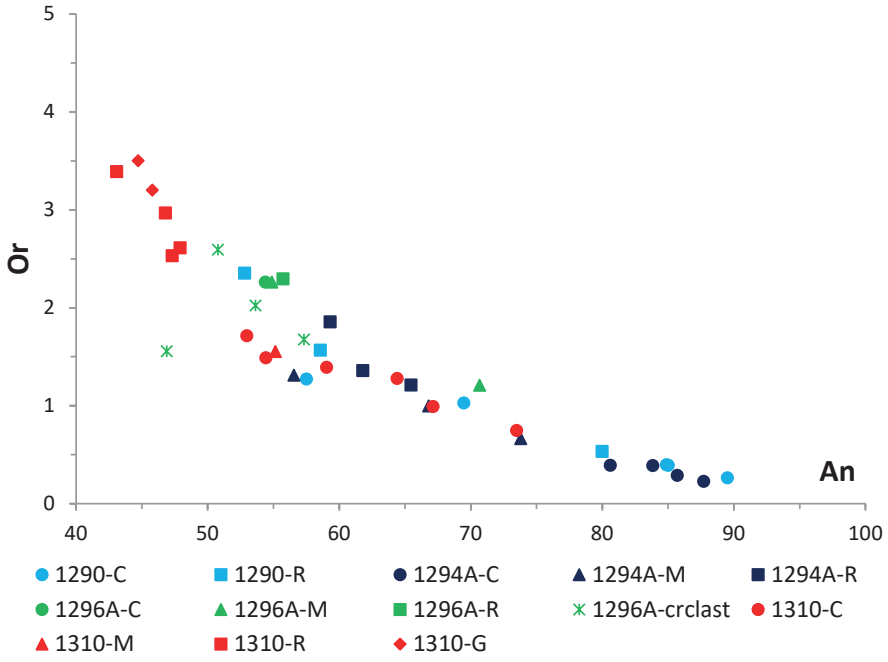

Fig. 11. Variability of plagioclase composition in the samples 1290, 1294A, 1296A and 1310. C – core, M – mantle, R – rim of plagioclase, G – groundmass plagioclase, crclast – plagioclase crystalloclast, An – anorthite, Or - orthoclase.

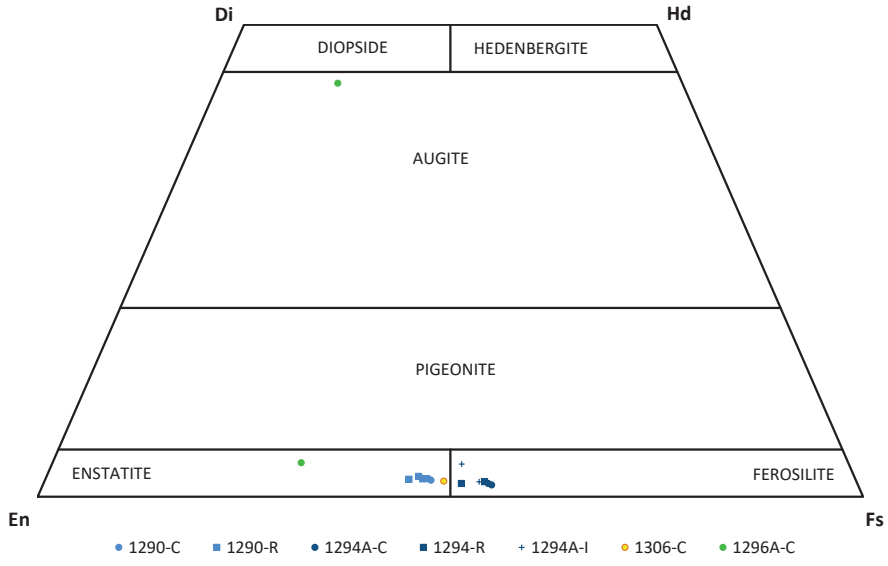

Fig. 12. Classification diagram for pyroxenes (Morimoto et al., 1988). C – core, M – mantle, R – rim of pyroxene, I – inclusion of orthopyroxene in another mineral, Di – diopside, Hd – hedenbergite, En – enstatite, Fs – ferosilite.

Characteristics of the chemical composition of andesite and tuff minerals

The analysed plagioclases in andesite samples 1290 and 1294A have the composition An52–An90. The composition trend of plagioclase in both samples is approximately the same. Diagram An vs. Or (Fig. 11) shows the normal plagioclase zonation: the cores are the most basic and the rims are the most acidic. Plagioclases of andesite porphyry sample 1310 are more acidic. Their composition varies from An43 to An74 and also indicates normal zonation. The composition of the groundmass plagioclase is similar to the composition of the plagioclase phenocryst rims. In addition, there is "gap" in the range of about 5 % of the An component between the composition of the inner part (core and mantle) of plagioclase (An53–74) and the plagioclase rims + groundmass plagioclase (An43–48). This gap may be caused by a change in chemical composition, or simply by an insufficient number of analyses. In the tuff sample 1296A, phenocrysts in the amphibolic-pyroxenic andesite clast and mineral crystalloclasts were analysed. The composition of the plagioclase phenocryst in the andesite clast is around An55, with a relatively significant zone with An70 in the phenocryst. The composition of plagioclase crystalloclast is variable, perhaps also related to which part of the crystal was analysed – whether it was the interior or the rim – it can be difficult to detect in crystalloclasts.

Only orthopyroxenes were analysed in the andesites of samples 1290, 1294A and 1306. There are no clinopyroxenes in these samples. The composition of analysed orthopyroxenes varies around the enstatite-ferrosilite boundary (Fig. 12), which reflects crystallization from a relatively differentiated magma. The analysed orthopyroxene in the amphibolic-pyroxenic andesite clast (tuff sample 1296A) has an ensta-

titic composition (Fig. 12), while En component is significantly higher than in other analysed orthopyroxenes. Clinopyroxene from the same andesite clast corresponds to augite and is found near the diopside field (Fig. 12). The composition of orthopyroxene and the presence of clinopyroxene indicates that they originated from a more basic magma than the other analysed orthopyroxenes.

Two classification diagrams (Hawthorne et al., 2012) were compiled for analysed amphiboles: diagram for amphiboles in andesites (Fig. 13A) and for amphiboles in volcaniclastics (Fig. 13B). Fe^{3+}min content (recalculated by Schumacher, in Hawthorne et al., 2012) was used for simplicity in both diagrams. According to the diagram on Fig. 13A, all amphiboles from andesites correspond to pargasite. Since there is no calcium in position A (y-axis), an increasing value on the y-axis indicates an increase in the alkali content of the amphibole. Amphibole from sample 1306 (analysed core, mantle and rim) has the highest alkali content. At the same time, this amphibole has the lowest Fe content of all analysed amphiboles. According to the diagram on Fig. 13B, all analysed amphiboles in the volcaniclastics also correspond to pargasite. The points on the diagram corresponding to the analysed phenocrysts in lithoclasts are less scattered than the points of the analysed crystalloclasts.

Paleogeography and paleovolcanic reconstruction of the Burda Mts

Paleogeography of the Burda Mts is demonstrated in Fig. 14 where the maximum range of Danube volcanics in the Da nube basin is indicated, while the

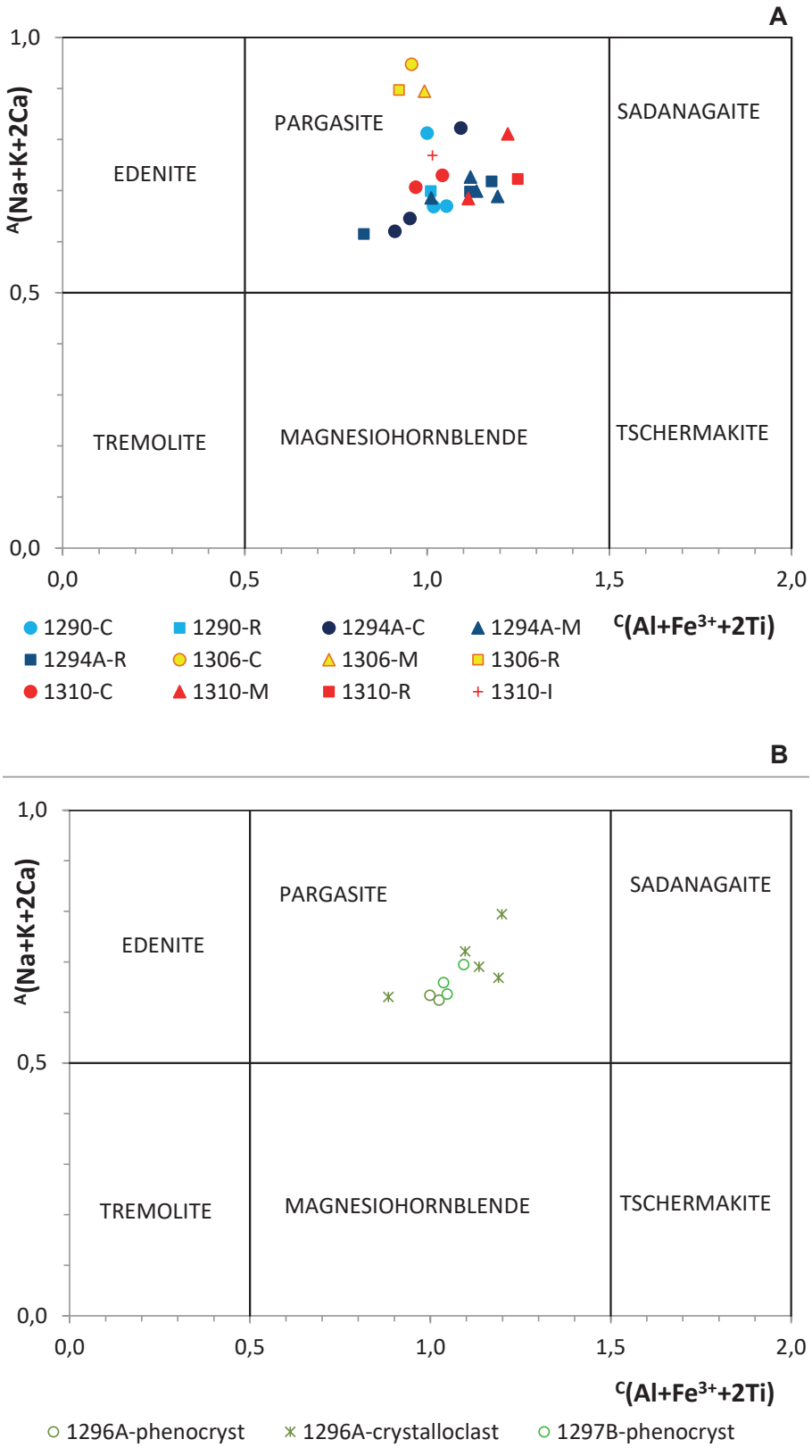

Fig. 13. Classification diagram for amphiboles (Hawthorne et al., 2012) for Fe^{3+}min. Diagram A is for amphiboles in andesites, diagram B for amphiboles in tuff. C – core, M – mantle, R – rim of pyroxene, I – inclusion of amphibole in another mineral.

designation of the volcanic centers of covered volcanics are numbers in the direction from west to east as follows: 1. Rusovce, 2. Gabčíkovo, 3. Tešedíkovo, 4. Palárikovo, 5. Kolárovo, 6. Šurany, 7. Bešeňov, 8. Dubník, 9. Bíňa and in the western part of the territory the volcanics of the Burda Mts near Štúrovo, the Börzsöny stratovolcano and the Visegrad volcanics are exposed (the central Slovakia volcanic field is located northeast of the territory; Šimon & Lacika, 2022). The volcanics of the Burda Mts nearby Štúrovo are included into the Burda Fm. At the base of the Burda Fm a succession of epiclastic volcanic rocks and pyroclastic rocks of amphibole-pyroxene andesites has developed. This horizon represents a succession of volcanoclastic rocks of volcanosedimentary origin with rare positions of autochthonous pyroclastic rocks. Their material has accumulated in the intervolcanic period, and partly also in the syneruptive period, when pyroclastic flows and pumice tuffs have formed. In the intervolcanic period, epiclastic material has formed, being represented by the positions of epiclastic volcanic breccias, conglomerates, sandstones formed at occasional flows, rapid flushes, lahars and mudflows, debris flows and debris avalanches. These epiclastic lithofacies occur in the transitional to marginal volcanic zone. From a petrographic point of view, the volcaniclastic material consists mainly of andesites, but we have rarely observed rocks of non-volcanic material and relics of a petrified wood from the original Badenian forest vegetation. Epiclastic volcanic sandstones of amphibole-pyroxene andesites are characterized by the presence of autochthonous light porous pumice fragments of angular to spherical shape. Epiclastic volcanic sandstones are predominantly coarse-grained, fairly well sorted, and occasionally show signs of stratification. There are also small or minor andesite sheets or lenticular positions of fine-grained epiclastic volcanic conglomerates with isolated blocks of andesites. In the beds, you can observe light porous pumice, which intergrows into individual beds. The material of epiclastic volcanic sandstones is represented by andesites of dark grey, grey and reddish brown colour. Porous pumice stone, predominantly light grey in colour, has an acidic dacite composition. Epiclastic volcanic sandstones with conglomerates of andesites crop out together with sandstones.

In the central part of the formation, volcanic products associated with the activity of submarine volcanism of the Badenian age developed. Submarine andesitic extrusive

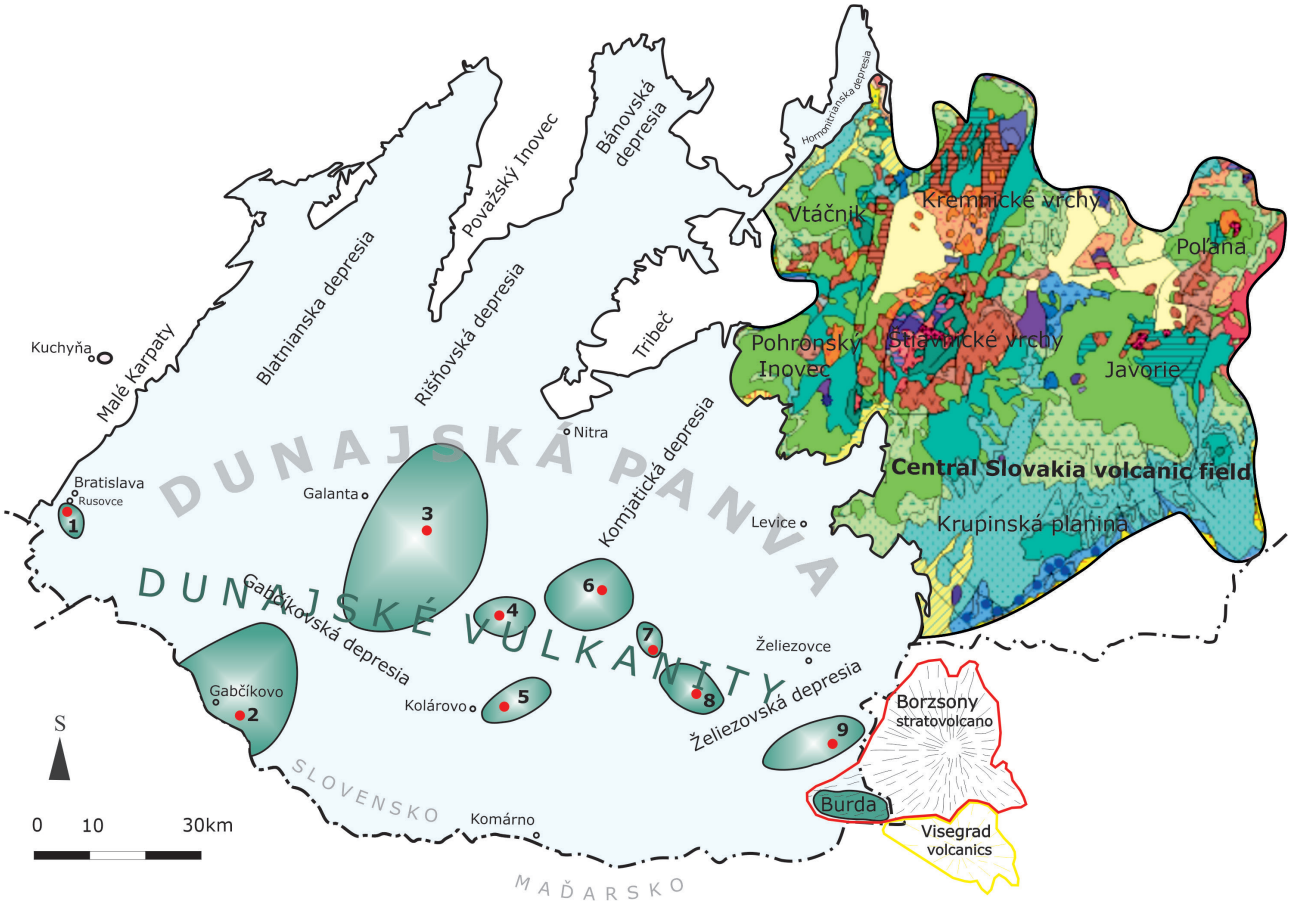

Fig. 14. Paleogeography of the Burda Mts near Štúrovo, the Börzsöny stratovolcano, the Visegrad volcanics and covered Danube volcanic centers: 1 – Rusovce, 2 – Gabčíkovo 3 – Tešedíkovo, 4 – Palárikovo, 5 – Kolárovo, 6 – Šurany, 7 – Bešeňov, 8 – Dubník, 9 – Bíňa.

volcanic domes of andesites are typical. They are formed of massive andesite with irregular blocky disintegration with a transition to brecciated andesite and up to breccia with a chaotic orientation of fragments. Extrusive domes of massive amphibole-pyroxene andesites have isometric shape, but occasionally also slightly elliptical bodies with dimensions of up to 200 m and vertical, blocky and roughly blocky disintegration. The indistinct fluid textures in the bodies were observed. The textures have a typical vertical to fan-like course. Zones of extrusive breccias developed at the edges of extrusive domes. The bodies are composed of light grey to greenish porphyritic andesite with phenocrysts of plagioclase, hypersthene, augite, amphibole and occasionally garnet in the ground mass, which is microlithic-grained in the middle part of the bodies and microlithic to microlithic-hyalopilitic at the edges of the bodies. As a result of the gradual destruction of these volcanic domes, debris-like material was formed and deposited even outside its volcanic center further into space applying the mass breccia flows, debris flows and deposits of coarse to blocky breccias. Intrusive-extrusive breccias of andesites represent marginal parts of intrusive-extrusive bodies. On the one hand, they are connected by a transition to their own body, on the other hand, they eventually pass into the breccias of subaqueous breccia flows. The brecciation zones are up to tens of meters thick. Extrusive breccias appear in facies with massive andesites of a light grey colour with solid texture and facies with angular fragments of grey non-porous andesite in a crushed lava matrix. Extrusive breccias are unsorted, chaotic, with a maximum fragment size of up to 100 cm. Fragments of andesites in extrusive breccias are present in amounts up to 80 %. Occasionally there was observed the presence of weakly oxidized red-brown andesite with a porous texture and spherical fragments of brown andesite with a porous texture. The matrix is formed by crushed andesites of light grey colour and porous texture. In the upper part of the Burda Formation, pyroclastic and epiclastic facies of pyroxene-amphibolic andesites were formed. Deposits of pyroclastic flows and redeposited pyroclastics are characterized with the presence of relics of petrified tree trunks, indicating transport from emergent forest-covered slopes in higher levels of the volcanic edifice of the Börzsöny Mts in present-day Hungary. This part of the Burda volcanics represents the transitional volcanic zone of the Börzsöny stratovolcano.

Acknowledgment

The geological mapping of the Burda volcanics and compilation of the geological map of the Burda mountain range were carried out as part of the project 02 17 *Geological map of the Danube Lowland region – south-east part at a scale of 1 : 50 000.* The research was financed by the Ministry of the Environment of the Slovak Republic and carried out by the State Geological Institute of Dionýz Štúr in Bratislava.

References

Bezák, V. (ed.), Biely, A., Broska, I., Bóna, J., Buček, S., Elečko, M., Filo, I., Fordinál, K., Gazdačko, Ľ., Grecula, P., Hraško, Ľ., Ivanička, J., Jacko st., S., Jacko ml., S., Janočko, J., Kaličiak, M., Kobulský, J., Kohút, M., Konečný, V., Kováčik, M. (Bratislava), Kováčik, M. (Košice), Lexa, J., Madarás, J., Maglay, J., Mello, J., Nagy, A., Németh, Z., Olšavský, M., Plašienka, D., Polák, M., Potfaj, M., Pristaš, J., Siman, P., Šimon, L., Teťák, F., Vozárová, A., Vozár, J. & Žec, B., 2009: Vysvetlivky k Prehľadnej geologickej mape Slovenskej republiky 1 : 200 000. *Bratislava, Št. Geol. Úst. D. Štúra, s. 53.* ISBN 978-80-89343-28-7.

Evensen, N. M., Hamilton, P. J. & O'Nions, R. K., 1978: Rare earth abundances in chondritic meteorites. *Geochim. cosmochim. Acta, 42, 1199–1212.*

Fordinál, K., Maglay, J., Moravcová, M., Vitovič, L., Nagy, A., Šimon, L. & Šefčík, P., 2022: Geologická mapa regiónu Podunajská nížina-juhovýchodná časť 1 : 50 000. *Bratislava, Št. Geol. Úst. D. Štúra.*

Fordinál, K. (ed.), Maglay, J., Moravcová, M., Vitovič, L., Nagy, A., Šimon, L., Šefčík, P., Benková, K., Dananaj, I., Demko, R., Dzurenda, Š., Fričovský, B., Gluch, A., Kollárová, V., Kováčiková, M., Kúšik, D., Laurinc, D., Marcin, D., Pelech, O., Šujan, M., Vlačiky, M., Zeman, I., Zlinská, A. & Žecová, K., 2023: Vysvetlivky ku geologickej mape Podunajskej nížiny-juhovýchodná časť 1 : 50 000. *Bratislava, Št. Geol. Úst. D. Štúra.*

Hawthorne, F. C., Oberti, R., Harlow, G. E., Maresch, W. V., Martin, R. F., Schumacher, J. C. & Welch, M. D., 2012: Nomenclature of the amphibole supergroup. *Amer. Mineralogist, 97, 2031–2048.*

Nagy, A., Halouzka, R., Konečný, V., Dublan, L., Lexa, J., Fordinál. K., Havrila, M., Vozár, J., Kubeš, P., Liščák, P., Stolár, M. & Dulovičová, K., 1998: Vysvetlivky ku geologickej mape Podunajskej nížiny-východná časť 1 : 50 000. *Bratislava, Št. Geol. Úst. D. Štúra, 1–187.*

Le Bas, M. J., Le Maitre, R. W., Streckeisen, A. & Zanettin, B., 1986: A chemical classification of volcanic rocks based on the total alkali – silica diagram. *J. Petrology, 27, 3, 745–750.*

Morimoto, N., Fabries, J., Ferguson, A. K., Ginzburg, I. V., Ross, M., Seifert, F. A., Zussman, J., Aoki, K. & Gottardi, G., 1988: Nomenclature of pyroxenes. *Amer. Mineralogist, 73, 1123–1133.*

Repčok, I., 1978: Vek niektorých stredoslovenských neovulkanitov zistených metódou stôp po delení uránu. *Geologické práce, Správy (Bratislava), 71.*

Pecerrillo, A. & Taylor, S. R., 1976: Geochemistry of Eocene calc-alkaline volcanic rocks from the Kastamonu area, Northern Turkey. *Contr. Mineral. Petrology, 58, 63–81.*

Šimon, L. & Lacika, J., 2022: Genesis and development of the volcanic landscape in the Slovenské stredohorie Mts., In: Lehotský, M. & Boltižiar, M. (eds.): Landscapes and landsforms of Slovakia, World Geomorphological Landscapes. *Springer Nature Switzeland AG 2022, 137–162.*

Sun, S. S. & McDonough, W. F., 1989: Chemical and isotopic systematics of oceanic basalts: implications for mantle composition and processes. In: Saunders, A. D. & Norry, M. J. (eds.): Magmatism in Ocean Basins. *Geol. Soc. Spec. Publ., London, 313–345.*

Vass, D., Konečný, V. & Šefara, J., 1979: Geologická stavba Ipeľskej kotliny a Krupinskej planiny. *Bratislava, Geol. Úst. D. Štúra, 1–277.*

Charakteristika neogénnych vulkanitov pohoria Burda pri Štúrove, Slovenská republika

Vulkanické pohorie Burda pri Štúrove je plošne najmenší geomorfologický celok na Slovensku. Nachádza sa na jz. Slovensku, na hraniciach s Maďarskom. Na západe hraničí s Podunajskou pahorkatinou. Južnú hranicu tvorí koryto Dunaja, ktorý sa prerezáva cez Vyšehradskú bránu a oddeľuje Burdu od maďarského pohoria Pilis. Východnú hranicu tvorí koryto rieky Ipeľ, ktorá oddeľuje Burdu od maďarského pohoria Börzsöny. Severozápadnú časť pohoria ohraničuje Bajtavská brána. Maximálna dĺžka pohoria je 7,5 km a maximálna šírka len 3,5 km. Najvyšším vrchom je Plešivec (395 m n. m.) v centrálnej časti pohoria. Vulkanity v pohorí Burda reprezentuje formácia Burda. Produkty formácie Burda vystupujú v rámci hrasťového bloku Burdy. Hrasťový blok je uklonený na SZ. Zlomovú zónu pri južnom okraji hrasti smeru V – Z sleduje tok Dunaja. Formácia Burda je bádenského veku. Horniny tejto formácie v smere na Z a SZ prechádzajú do bajtavského súvrstvia, ktoré vznikalo súčasne s formáciou. Súvrstvie obsahuje bohatú morskú faunu lagenidovej zóny a nanoplanktón spoločenstva zóny NN-5 zodpovedajúce spodnému bádenu. Na báze formácie sa vyvinula sukcesia epiklastík a pyroklastík amfibolicko-pyroxénických andezitov. V strednej časti formácie sa vyvinuli vulkanické produkty späté s aktivitou submarinného vulkanizmu bádenského veku. Typické sú podmorské andezitové extruzívne dómy amfibolicko-pyroxénických andezitov. Submarinné extruzívne dómy andezitov majú eliptický až izometrický prierez s dĺžkou do 220 m. Tvorí ich masívny andezit s nepravidelnou blokovitou odlučnosťou s prechodom do zbrekciovateného andezitu až do brekcie s chaotickou orientáciou úlomkov. Vplyvom postupnej deštrukcie týchto vulkanických dómov sa tvoril úlomkovitý materiál a ukladal sa aj mimo svojho vulkanického centra ďalej do priestoru prostredníctvom masových brekciovitých prúdov, úlomkových prúdov a uloženín hrubých až blokových brekcií. Vo vrchnej časti formácie Burda sa vytvorili fácie pyroklastík a epiklastík pyroxénicko-amfibolických andezitov. Uloženiny pyroklastických prúdov a laharov sú charakteristické prítomnosťou reliktov petrifikovaných kmeňov stromov. Formáciu Burda reprezentuje sukcesia fácií epiklastík, pyroklastík a produktov submarinných extruzívnych dómov. Je budovaná týmito fáciami: horizont epiklastík a pyroklastík, epiklastické vulkanické pieskovce s pemzami, epiklastické vulkanické pieskovce a konglomeráty, epiklastické vulkanické pieskovce, drobné epiklastické vulkanické konglomeráty, hrubé epiklastické vulkanické konglomeráty, epiklastické vulkanické brekcie a konglomeráty, epiklastické vulkanické brekcie, drobné redeponované pyroklastiká, hrubé redeponované pyroklastiká, blokovo-popolové pyroklastické prúdy, subakvatické brekciovité prúdy, chaotické brekcie redeponovaných pyroklastík, extruzívne brekcie dómov amfibolicko-pyroxénických andezitov a extruzívne dómy amfibolicko-pyroxénických andezitov.

Vzorky, z ktorých boli urobené celohorninové chemické analýzy, podľa klasifikačného TAS diagramu (obr. 5) zodpovedajú andezitu a vzorka 1291A dacitu. Pomerne blízke zloženie majú vzorky andezitu 1291B, 1293S, 1299S a 1304B. Vzorku 1294F možno považovať za acidný andezit. Podľa diagramu SiO_2 vs. K_2O (obr. 6) všetky vzorky zodpovedajú vysoko draselnému andezitu a patria do vysoko draselnej vápenato-alkalickej série. Obsah stopových prvkov v študovaných horninách možno znázorniť pomocou multiprvkových diagramov (tzv. spiderogramy, obr. 7). Na diagrame vidieť vlastnosti typické pre horniny ostrovných oblúkov a aktívnych okrajov kontinentov: obohatenie oproti N-MORB o tzv. LILE (K, Sr, Ba, Rb) a ochudobnenie o tzv. HFSE (Nb, Ti). Krivky normalizovaného obsahu vzácnych zemín (obr. 8) majú v prípade študovaných vzoriek andezitov mierny sklon. Nevýrazná európiová anomália poukazuje na to, že v genéze ich magiem neprebiehala rozsiahla frakcionácia plagioklasu. Študované vzorky predstavujú fragmenty andezitov z vulkanoklastík, andezity intruzívnych telies a samotné vulkanoklastiká. Andezity tvoria dva petrografické typy: biotiticko-amfibolické andezity s ortopyroxénom a amfibolické andezity s biotitom a pyroxénom (obr. 9). Biotiticko-amfibolické andezity s ortopyroxénom majú porfýrickú štruktúru so základnou hmotou hyalopilitickou (obr. 9A, B) alebo mikrokryštalickou (obr. 9C, D, E). V jednom prípade možno vzorku vďaka hrubšej zrnitosti základnej hmoty označiť ako andezitový porfýr

(vzorka 1310, obr. 1F). Podiel výrastlíc oproti základnej hmote je 20 – 30 %. Hlavné horninotvorné minerály sú plagioklas, amfibol a biotit. Tento typ andezitu sa vo vzorkách vyskytuje najčastejšie. Amfibolické andezity s biotitom a pyroxénom (obr. 9G, H) majú porfýrickú štruktúru s mikrokryštalickou základnou hmotou. Pre tieto horniny je charakteristický vysoký podiel výrastlíc oproti základnej hmote (až do 50 %). Hlavné horninotvorné minerály sú plagioklas a amfibol. Osobitné postavenie v skupine má vzorka 1297A, v ktorej je dominantným minerálom plagioklas, pričom mafické minerály sú zriedkavejšie a menšie ako v iných vzorkách. Podiel výrastlíc oproti základnej hmote je zhruba 30 %. Najpočetnejší horninotvorný minerál v oboch typoch andezitov je plagioklas, ktorý tvorí výrastlice a glomeroporfýrické agregáty tabuľkového a lištového tvaru a ihličky v základnej hmote. Plagioklasy sú zonálne a charakteristicky zdvojčatené. Variabilitu ich chemického zloženia znázorňuje diagram An vs. Or (obr. 11). Amfibol tvorí idiomorfné až hypidiomorfné výrastlice a agregáty. Môže uzatvárať plagioklas. Zachované amfiboly sú pleochroické, niektoré sú zonálne. Sú do rôzneho stupňa opacitizované – od nevýrazných opacitových lemov až po úplnú opacitizáciu. Analyzované amfiboly zodpovedajú pargasitu (obr. 13A). Biotit tvorí pleochroické tabuľky a lišty, môže uzatvárať plagioklas. Biotity sú zachované alebo sa pri nich prejavuje obdoba opacitizácie amfibolu. Na úkor biotitu vznikajú Fe-Ti oxidy a draselný živec (namiesto ortopyroxénu v amfibole). Ortopyroxén tvorí idiomorfné až hypidiomorfné výrastlice alebo je súčasťou glomeroporfýrických agregátov. Tvorí aj ihličky v základnej hmote. Môže byť čiastočne až úplne alterovaný. Zloženie analyzovaných ortopyroxénov je na rozhraní enstatit-ferosilit (obr. 12). Vo vzorke 1284 sa nachádza veľmi zriedkavý klinopyroxén. V niektorých vzorkách s vykryštalizovanou základnou hmotou je vo forme malých výrastlíc alebo v základnej hmote prítomný apatit. V troch vzorkách (1304B, 1290, 1310) sa nachádza granát s almadínovým zložením s reakčným lemom. Vykryštalizovanú základnú hmotu tvorí plagioklas, sanidín, kremeň, ortopyroxén, titanomagnetit, ilmenit ± apatit. Vulkanoklastický materiál bol študovaný vo vzorkách 1287A, B a 1297B a tuf vo vzorkách 1296A a 1298. Vzorky 1287A (obr. 10A, B) a 1287B obsahujú kryštaloklasty plagioklasu, amfibolu, ortopyroxénu a klinopyroxénu. Biotit vo vzorkách nie je. Prítomnosť klinopyroxénov môže poukazovať na ich pôvod z pyroxénických andezitov. Vzorka A obsahuje litoklast amfibolického andezitu s ortopyroxénom. Vzorka 1297B (obr. 10C) obsahuje litoklasty hornín a kryštaloklasty plagioklasu, amfibolu a biotitu. Litoklasty tvorí biotiticko-amfibolický andezit s čistými plagioklasmi, zelenými amfibolmi a hyalopilitickou základnou hmotou, andezitový porfýr a amfibolicko(?)-pyroxénický andezit. Vzorka 1296A (obr. 10D) je tuf. Obsahuje litoklast amfibolicko-pyroxénického andezitu (aj s klinopyroxénmi). Kryštaloklasty predstavuje plagioklas, amfibol, biotit, oxid Fe, kremeň a pyroxény(?). Vo vzorke tufu 1298 silne prevažujú kryštaloklasty: plagioklas, zelené a hnedé amfiboly, biotit, klinopyroxén a ortopyroxén. Variabilitu chemického zloženia minerálov vulkanoklastík odrážajú diagramy na obr. 11, 12 a 13B.

Paleogeografia pohoria Burda je znázornená na obr. 14, kde je vyznačený maximálny rozsah dunajských vulkanitov. Vulkanické centrá zakrytých vulkanitov sú označené číslami v smere zo západu na východ: 1 – Rusovce, 2 – Gabčíkovo, 3 – Tešedíkovo, 4 – Palárikovo, 5 – Kolárovo, 6 – Šurany, 7 – Bešeňov, 8 – Dubník, 9 – Bíňa. Na obrázku sú znázornené aj vulkanity pohoria Burda pri Štúrove, odkrytý stratovulkán Börzsöny a vyšehradské vulkanity (vulkanické pole stredného Slovenska sa nachádza na severovýchode územia; Šimon a Lacika, 2022). Na báze súvrstvia Burda sa vyvinula postupnosť epiklastických vulkanických hornín a pyroklastických hornín amfibolicko-pyroxénických andezitov. Horizont epiklastík a pyroklastík predstavuje postupnosť vulkanoklastických hornín vulkanosedimentárneho pôvodu so vzácnymi polohami autochtónnych pyroklastických hornín. Tento materiál sa nahromadil v medzivulkanickom období a čiastočne aj v období synerupcie, keď sa vytvárali pyroklastické prúdy a pemzové tufy. V medzivulkanickom období sa vytvoril epiklastický materiál, ktorý predstavuje polohy epiklastických vulkanických brekcií, zlepencov a pieskovcov vznikajúcich v občasných tokoch, rýchlych splachoch, laharoch a bahnotokoch, sutinových prúdoch a sutinových lavínach. Tieto epiklastické litofácie sa vyskytujú v prechodnej až okrajovej vulkanickej zóne. Z petrografického hľadiska vulkanoklastický materiál tvoria prevažne andezity. Ojedinele sme zaznamenali aj horniny nevulkanického materiálu a relikty skameneného dreva z pôvodnej vegetácie bádenského lesa. Epiklastické vulkanické pieskovce andezitov sú charakteristické prítomnosťou autochtónnej ľahkej poréznej pemzy hranatého až guľovitého tvaru. Sú prevažne hrubozrnné, pomerne dobre vytriedené a občas vykazujú známky stratifikácie. Vyskytujú sa tu aj malé andezitové pláty alebo šošovkovité polohy jemných epiklastických vulkanických konglomerátov s izolovanými blokmi andezitov. Vo vrstvách možno pozorovať svetlú pórovitú pemzu, ktorá sa prelína s jednotlivými vrstvami. Materiál epiklastických vulkanických pieskovcov predstavujú andezity tmavosivej, sivej a červenohnedej farby. Porézna pemza prevažne svetlosivej farby má kyslé dacitové zloženie. Spolu s pieskovcami vystupujú epiklastické vulkanické pieskovce so zlepencami andezitov.

Doručené / Received: 7. 12. 2023
Prijaté na publikovanie / Accepted: 21. 12. 2023

Mineralia Slovaca, Web ISSN 1338-3523, ISSN 0369-2086, https://doi.org/10.56623/ms.2023.55.2.3
55, 2 (2023), 133 – 142, © Authors 2023. CC BY 4.0

Geochemical characteristics and tectonic interpretation of garnet mica schists of Patharkhola area in Kumaun Lesser Himalaya, Uttarakhand Himalaya, India

[1]HARITABH RANA, [1]HAREL THOMAS and [1]RISHABH BATRI

[1]Department of Applied Geology, School of Engineering & Technology, Dr. Harisingh Gour Vishwavidyalaya, Sagar (A Central University) 470003 – INDIA
Corresponding Author: harelthomas@gmail.com; hthomas@dhsgsu.edu.in

Abstract: The Patharkhola area is exposed in the core of the southern limb of the Dudhatoli syncline in the Kumaun Lesser Himalaya. Garnet mica schists of the Patharkhola occur in the folded outcrop pattern being located in between the limbs. They are dominantly composed of garnet, biotite, muscovite, chlorite, plagioclase and a subordinate amount of quartz. Garnet, both xenoblastic as well as idioblastic, is wrapped round by phyllosilicates minerals. These investigated rocks exhibits slightly LREE depleted patterns ($La_N/Sm_N = 0.7$, $La_N/Yb_N = 0.64$) with flat HREE patterns ($Sm_N/Yb_N = 0.89$). Field evidence along with geochemical characteristics suggests that the Patharkhola schists are peraluminous in nature, showing sedimentary sources having silt to silty clay protolith. They were formed in active continental margins in arc-type setting where the sediments were received both from arc and continental crust.

Key words: Garnet, Schist, Geochemistry, Tectonic settings, Lesser Himalaya

Graphical abstract

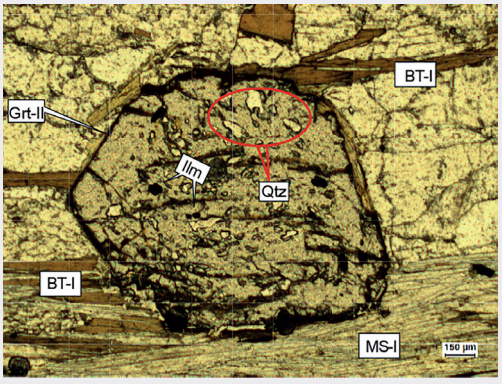

Highlights

- The garnet mica schists from Patharkhola, Kumaun Lesser Himalaya forms a part of Dudhatoli Almora group.
- The geochemical data clearly demonstrates that the Patharkhola schists are characterized by their high alkali content and silica-saturated nature exhibiting slightly LREE depleted patterns (LaN/SmN = 0.7, LaN/YbN = 0.64) with flat HREE patterns (SmN/YbN = 0.89).
- Shale dominated protolith representing nearby source sediments in arc type environment is inferred for the Patharkhola schists.

1 Introduction

The Himalaya, an arc-shaped mountain belt covering whole boundary of northern India is a type example of intercontinental collision between Indian and Asian plates around 55 Ma ago (Mukherjee, 2015; Yin, 2006). In the past, the structure, stratigraphy and tectonics of the Kumaun Lesser Himalaya have been described by Joshi & Tiwari (2009), Joshi et al. (2017) and Rana & Thomas (2018). In Kumaun region, the Lesser Himalayan sequence is delineated by Main Central Thrust (MCT) from the Higher Himalayan in the north and by Main Boundary Thrust (MBT) from the Siwaliks in south (Thakur et al., 2010). The rocks of the Dudhatoli group (Rana & Thomas, 2018) are exposed in the Patharkhola area. The "Inner Schistose Series" or the "Metamorphic and Crystalline Nappe' Tectonic Zone" of Lesser Himalaya forms a distinct structural unit which has witnessed multiple deformation and polyphase metamorphism. The Dudhatoli Crystallines extend from Garhwal in WNW to Kumaun in ESE. Kumar & Agarwal (1975) included Mandhali, Chandpur and Nagthat Formations and Dudhatoli-Almora Crystallines under a newly constituted group namely Dudhatoli group where the Dudhatoli-Almora Crystallines are the topmost horizon. Rocks of the Dudhatoli group have been considered to be of Precambrian age (Kumar & Agarwal, 1975). In Kumaun Himalaya, the Munsiari gneisses of Almora Group were dated as 1830 ± 200 Ma. old (Bhanot et al., 1977). Islam et al. (2005) proposed Proterozoic granitoids of Lesser Himalaya grouped into older clusters of 2200–1800 Ma and younger clusters of 1400–1200 Ma. Rana & Thomas (2023) studied the thermal and structural character of garnets from garnet mica schists of Patharkhola which is found to be of magnesian rich showing decomposition at higher temperatures. The metamorphic terrain exhibits multiple deformation patterns

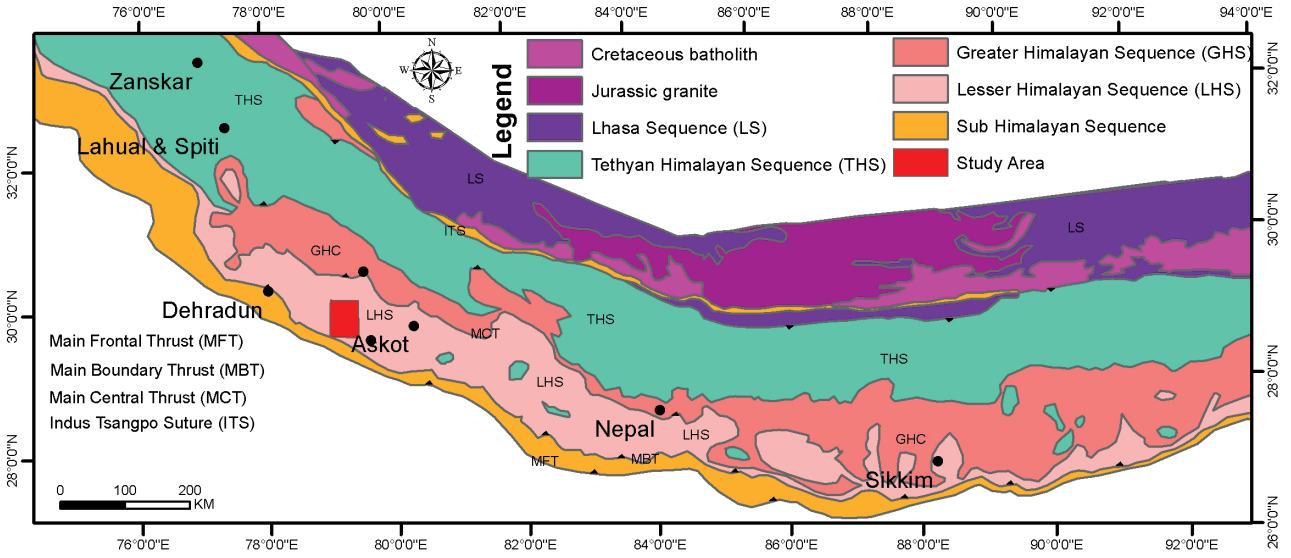

Fig. 1a. Generalized geological map of Himalaya, Modified after Yin (2006).

and polyphase metamorphism (Joshi & Tiwari, 2009) which is well exposed in the central part of Almora nappe.

In Lesser Kumaun Himalaya, extensive work has been carried out on the pelitic gneisses and granites, rather less on the low-grade metamorphic i.e. schists and phyllites (Phukon et al., 2018; Das et al., 2019). Rana et al. (2023) studied the phyllites of Patharkhola and opined that the phyllites have high alumina content with enrichment of trace elements formed in active continental margins. The area around Patharkhola, exposes rocks of Lesser Kumaun Himalaya, lies between longitude 79°09'E to 79°17'56"E and latitude 29°47'42"N to 29°56'69"N with an approximate area of around 120 square kilometres (Fig. 1a). The rock types exposed in the area are gneisses, schists and phyllites (Fig. 1b). The main aim of the present paper is to provide geochemical character and petrogenesis of schists.

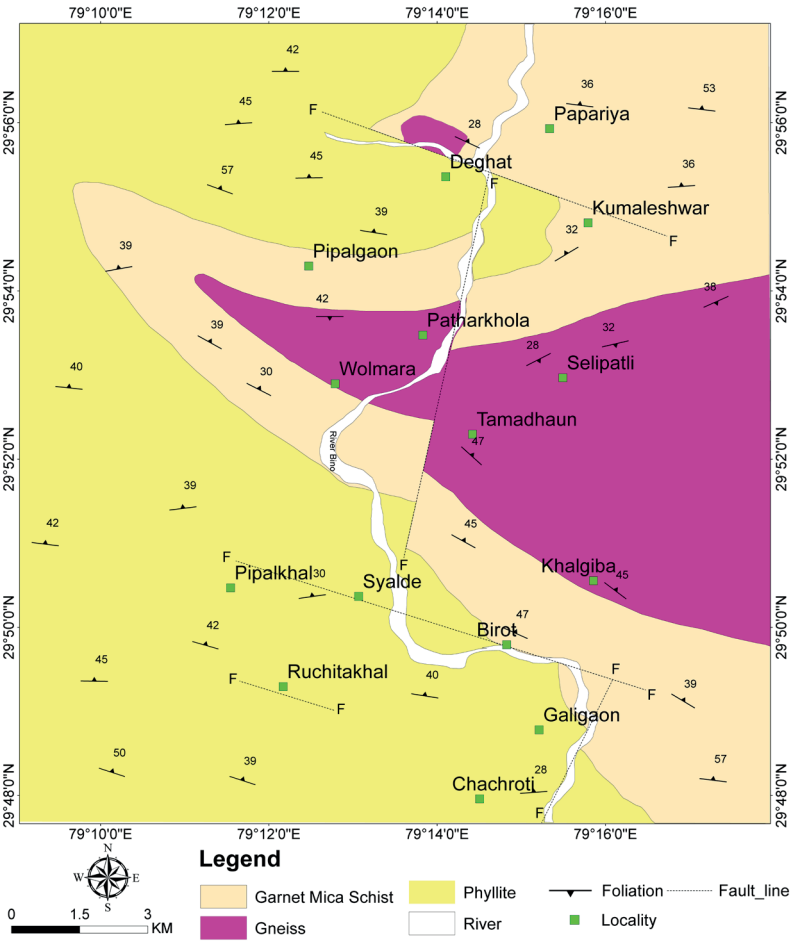

Fig. 1b. Geological map of the study area (Modified after Thomas & Thomas, 1992).

2 Macroscopic properties

In the area under investigation, schists are highly fragile and powdery in nature. Depending upon the biotite, muscovite and/or chlorite content, they exhibit a variation in colour from pinkish brown, dark brown, light grey to greenish green, (Fig. 2a, c). Increased percentage of quartz and feldspar imparts compaction. The schists of the area are characterized by the presence of garnet which ranges in size from 0.1 cm to 0.2 cm in hand

specimens (Fig. 2a). On weathering, pink garnet crystals impart a reddish brown tinge to the rock and when removed, leave behind small pits of reddish-brown colour. These are foliated medium to coarse-grained rocks where schistosity is defined by the parallel alignment of phyllosillicates showing folding and crenulations due to deformation.

3 Petrography

Rock samples have been collected from the entire area of the exposure of garnet mica schist terrain. Samples showing well-developed internal structures have been studied in detail and discussed here. Schists of the area is dominantly composed of garnet, biotite, muscovite, chlorite, plagioclase and subordinate amount of quartz. Two distinct varieties of garnet have been identified. Garnet-I occurs as pre-kinematic porphyroblasts, shattered and stretched parallel to the foliation, (Fig. 2c), containing ilmenite and quartz as inclusions and are highly fractured. Garnet has both xenoblastic as well as idioblastic textures suggesting the reaction:

Muscovite + Chlorite + Quartz = Garnet + Biotite + Water

Garnet-II occurs as rolled garnet wrapped round by flaky minerals and imparts a closed eye structure, (Fig. 2d). Two variants of Biotite recognised as Biotite-I, (Fig. 2b, d), as coarse lepidoblastic in intimate association with Muscovite-I defining the foliation while Biotite-II occurs as cross-cutting relationship with Biotite-I. Chlorite-I occurs as lepidoblasts, light greenish in colour showing pleochroism from light green to green in colour, defining the schistosity plane in close association with Biotite-I and Muscovite-I. Chlorite-II occurs as very similar to Chlorite-I, occurring as lepidoblasts cross cutting the schistosity plane varying from sub-parallel to low angles. Tiny shreds of plagioclase occur in the schists lying parallel to the schistosity plane in close association with quartz. At a few places, it is usually altered to sericite as a common alteration product. Apatite occurs as inclusion in feldspar and muscovite.

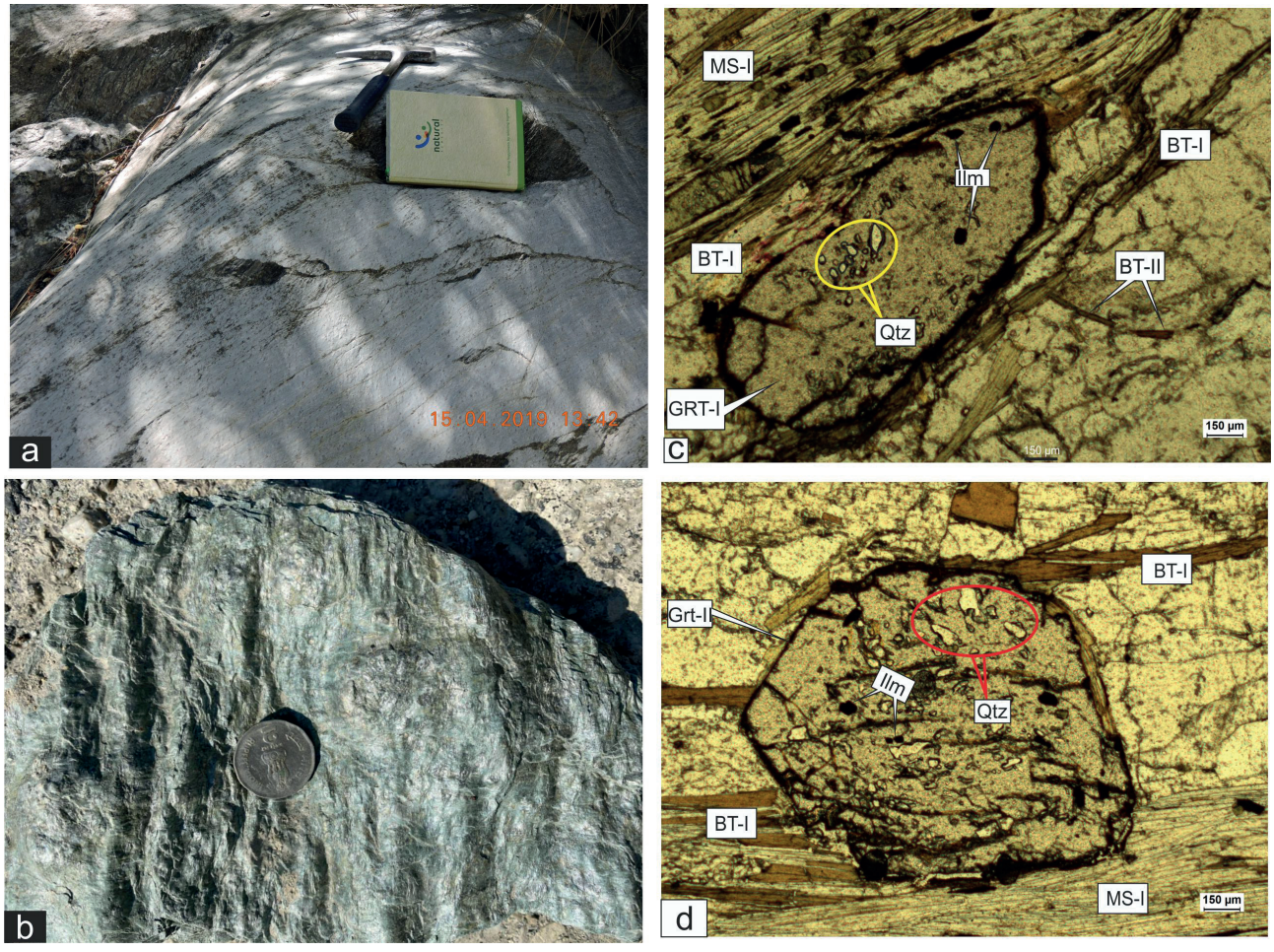

Fig. 2. (a, b) Field photograph showing pitted garnet; (c) Photomicrograph of stretched garnet parallel to foliation (d) Rolled garnet wrapped by flaky minerals (under plane polarised light).

4 Geochemistry and petrogenesis

The results of the major oxides, trace elements along with rare earth elements (REE) are tabulated below in Table 1. Rock samples were crushed, and then pulverized using an agate carbide ring grinder. Major oxides and selected trace element concentrations present in the rock were measured on powder pellets by X-ray Fluorescence Spectrometer (XRF; Siemens SRS-3000) in the Wadia Institute of Himalayan Geology (WIHG), Dehradun. The samples were analysed in the same institute for their REE and some trace elements by Inductively Couple Plasma-Mass Spectrometer (ICP-MS; PerkinElmer SCIEX ELAN DRC-e) using the open system rock digestion method. Rock powders were first thoroughly dissolved in HF and HNO_3 in Teflon crucibles and heated over a hot plate for three hours to prepare solutions from which trace elements and REE abundances were determined. Analytical precision for major elements is well within ± 2 – 3 % and ± 5 – 6 % for trace elements. Accuracy of rare earth elements ranges from 2 to 12 % and precision varies from 1 to 8 %.

The SiO_2 and Al_2O_3 content varies from 64.74 to 75.78 % and from 10.53 to 19.88 %, respectively. The average Na_2O and K_2O content in the schists is 2.59 % and 2.67 %, respectively. The average K_2O/Na_2O ratio of these rocks is 1.06; whereas TiO_2 content of the rocks varies from 0.61 to 0.8 %, as per Herron (1988), Fig. 3 (a) plot $\log(Fe_2O_3/K_2O)$ versus $\log(SiO_2/Al_2O_3)$ plot for classification of terrigenous sediments and shale, all studied samples of garnet mica schists fall within the shale to wacke-shale junction field specified for silty to silty clay protolith. This is due to the high Fe_2O_3/K_2O ratio with less SiO_2/Al_2O_3 ratio representing that the schists have been derived from shale-dominated environment.

The A/CNK values of schists ranging from 1.8 to 2.8 support its characterization as a strongly peraluminous, relatively potassic-rich source. The plot of K_2O/Al_2O_3 versus Na_2O/Al_2O_3, (Fig. 3b) has clearly differentiated the sedimentary from igneous rocks, Garrels and Mackenzie (1971). It is evident that all samples fall within the field specified for sedimentary rock. The plot between SiO_2 and other oxides, (Fig. 3c) shows good correlation, which indicates coherent behaviour of elements during different processes. SiO_2 versus Al_2O_3, CaO, K_2O, MnO and TiO_2 have shown positive regression while others have poor regression values. The representation of good regression values of alumina and potash with silica represents the dominance of peraluminous nature and is substantially supported by the good regression of silica with Rb, La, Y and Ce. The behaviour of trace elements in the schists has also been studied with the help of variation diagrams presented in (Fig. 3d). Trace elements show good correlation with respect to SiO_2.

During metamorphism, the REE are very little fractionated and also immobile during sedimentary processes. It is also considered that during metamorphism the REE remains unaffected up to the upper amphibolite facies regional metamorphism, (Taylor & McLennan, 1985). On the other hand,

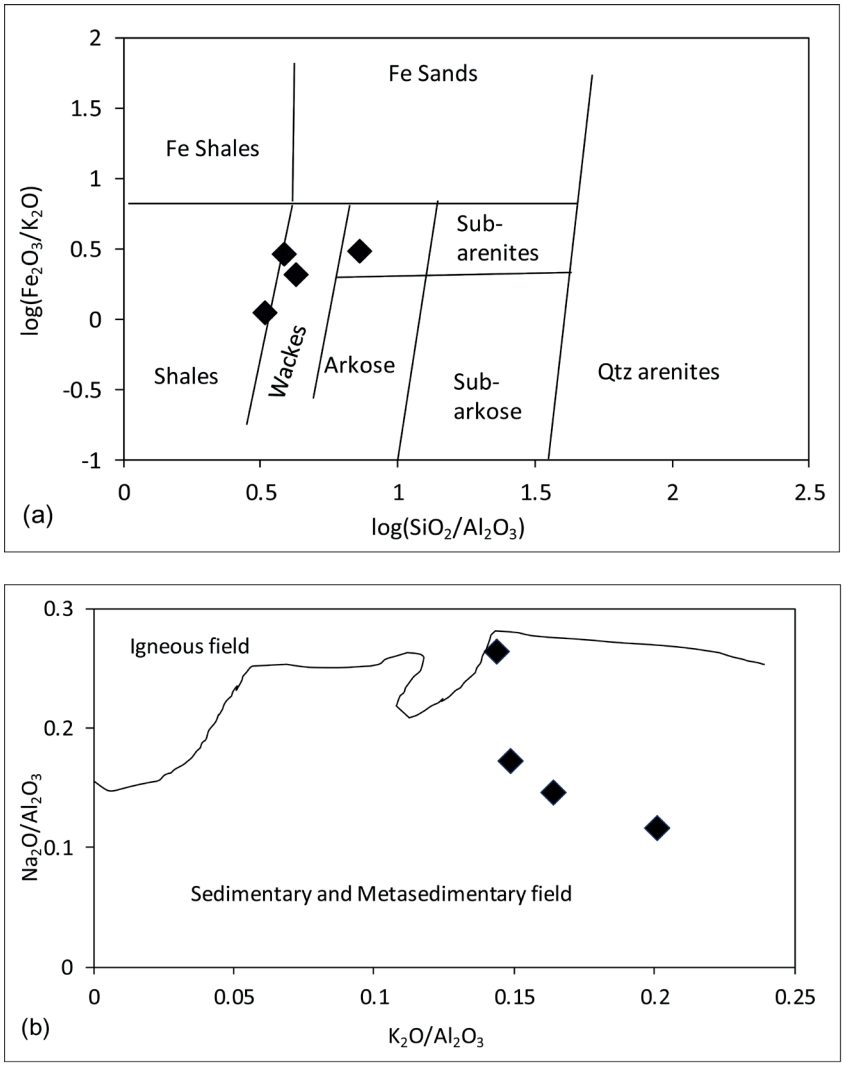

Fig. 3. (a) log (SiO_2/Al_2O_3) versus log (Fe_2O_3/K_2O) after Herron (1988) for classification of terrigenous sediments and shales; (b) K_2O/Al_2O_3 versus Na_2O/Al_2O_3 after Garrels & Mackenzie (1971).

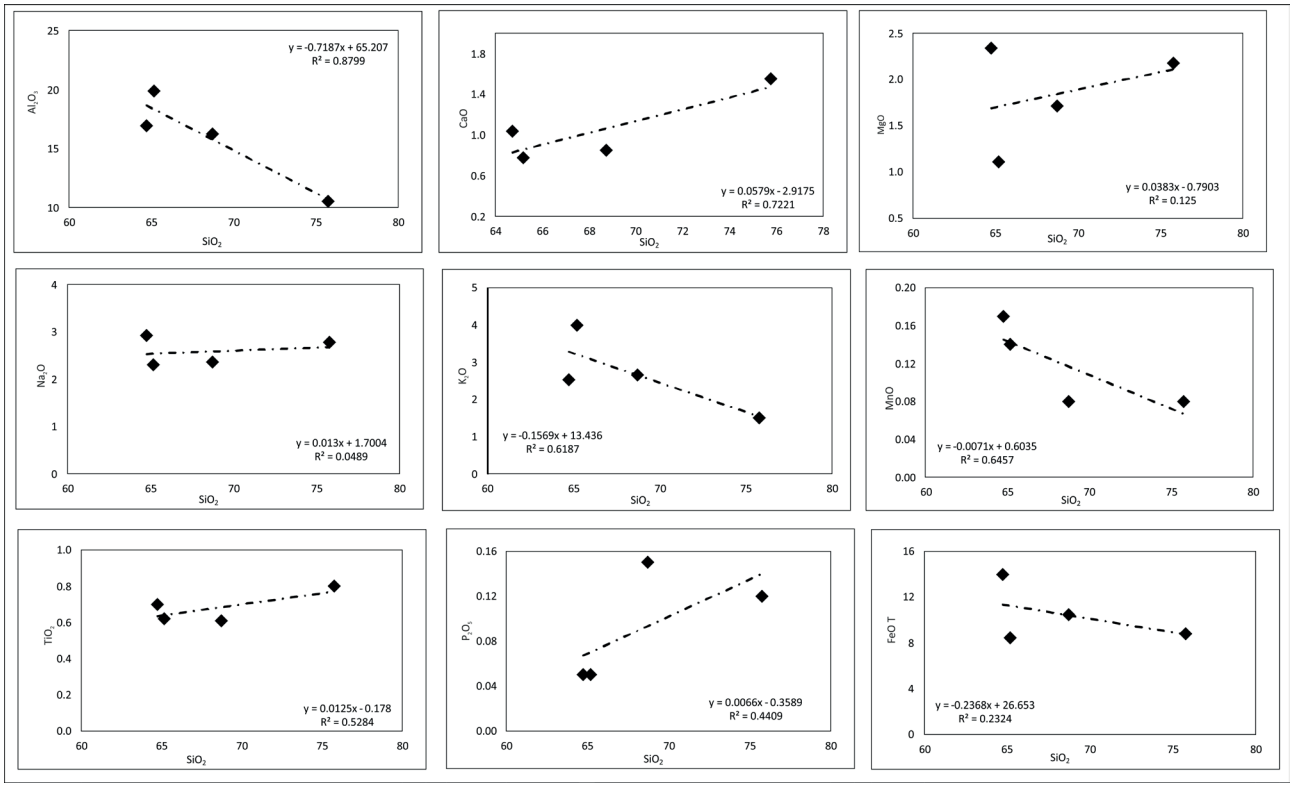

Fig. 3. (c) Silica versus major oxides for garnet mica schists.

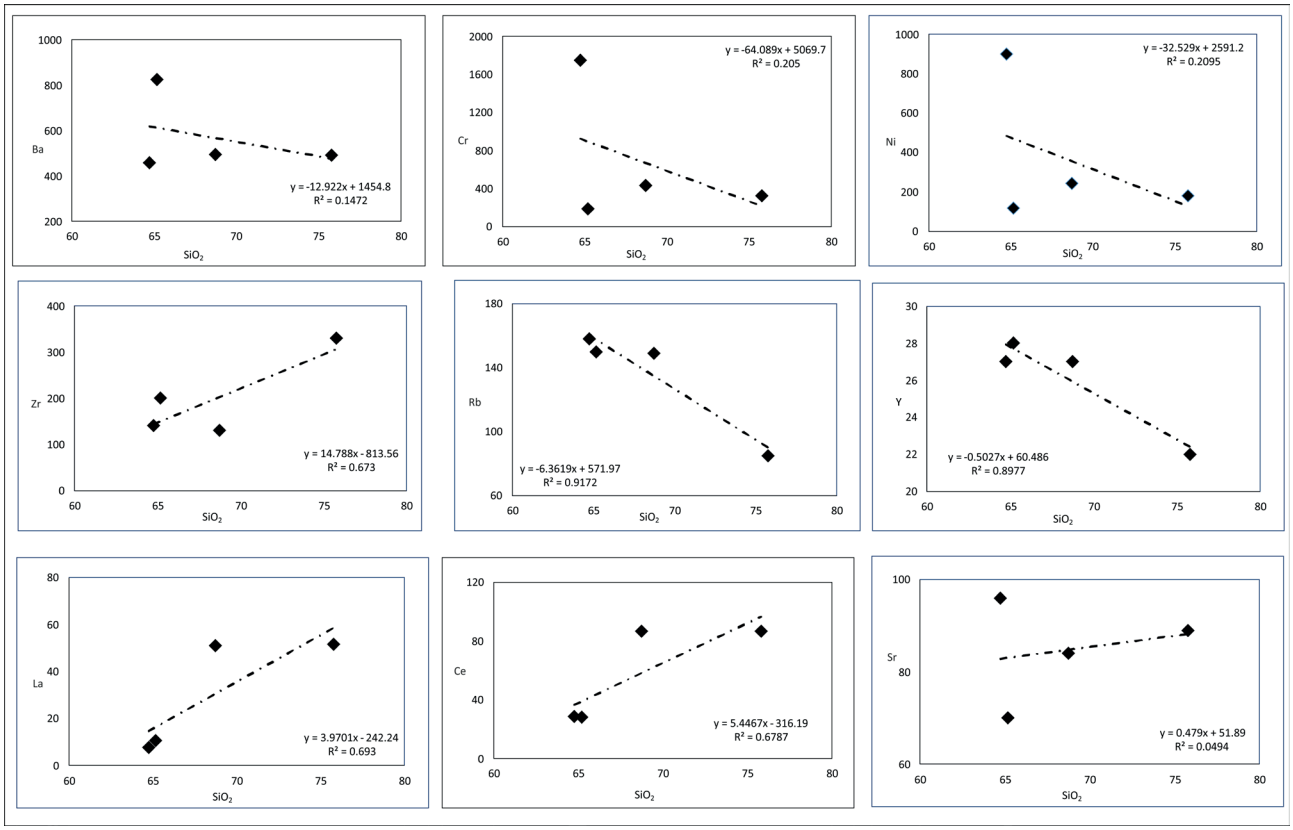

Fig. 3. (d) Silica versus trace elements.

REEs have been shown to be mobile to some extent during metamorphism (McLennan, 1982).

The REE content of a metamorphic rock directly mimics that of the protolith. This assumption has formed the basis for a great number of studies in which the evolution of the protolith was examined in detail without specifically testing for the immobility of the REEs (Grauch, 1989). In this context, the issue of REE migration during metamorphism has been long debated between proponents of isochemical metamorphism and those of metasomatism. The only certainty is that REEs are mobile in certain circumstances (Vocke et al., 1987) and immobile in others (Rolland et al., 2003). Despite some progress in this direction, the nature of these circumstances has rarely been determined. Further research on a typical lithologically and chemically distinct types of sample suites may help our understanding of REE contents in metamorphic rocks, because they may contain a record of REE mobility or immobility (Grauch, 1989).

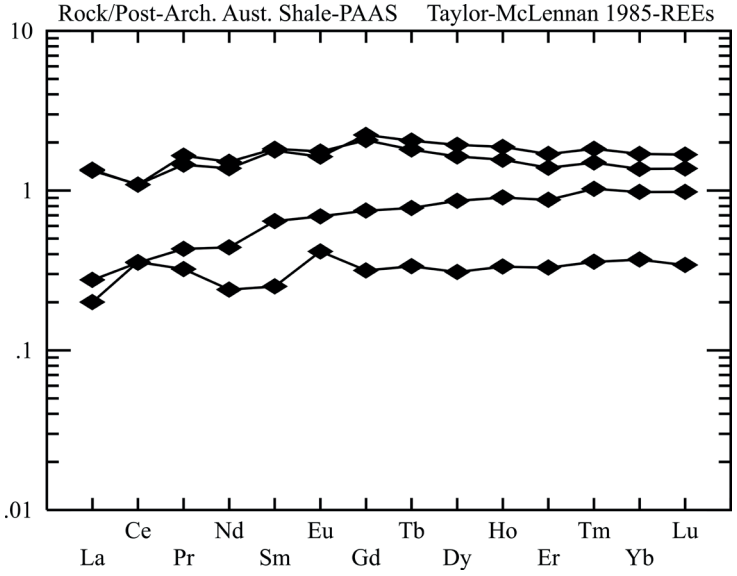

Fig. 3. (e) REE normalised plot (Taylor & Mclennan, 1985).

The analyzed REE data for the schists were normalized to Post Archean Australian Shales (PAAS), normalised values are from Taylor & Mclennan (1985).

They exhibits slightly LREE depleted patterns (LaN/SmN = 0.7, LaN/YbN = 0.64) with flat HREE patterns (SmN/YbN = 0.89). Concentration of lithophile elements (Rb, Cs, Ba and Sr) along with HFSE (Y, Nb and Zr) have shown values in close proximity to the PAAS. The higher LREE/HREE ratio indicates a high degree of fractionation during the metamorphic stage as no such chemical heterogeneity has been observed in the protolith. The steep LREE and gentle HREE with negative europium anomaly are depicted by the Patharkhola schists. The similarity in the values of schists with PAAS is interpreted to be steaming from the chemical homogeneity of the protolith which has changed a very little during the metamorphism (Likhanov, 2008). These aforementioned features are typical of post Archean clay shales which are caused by the occurrence of erosional products of upper continental crust material (an average of 23 Australian shales of Post Archean age), (Taylor & Mclennan, 1985) which imputes the presence of erosional products of sedimentary rocks in

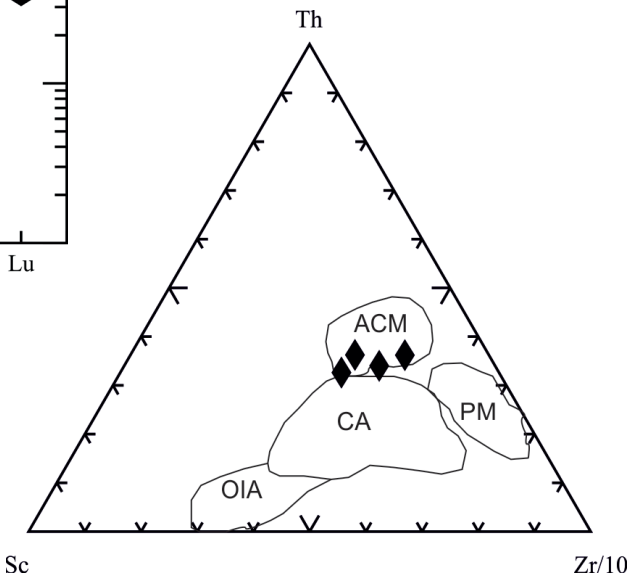

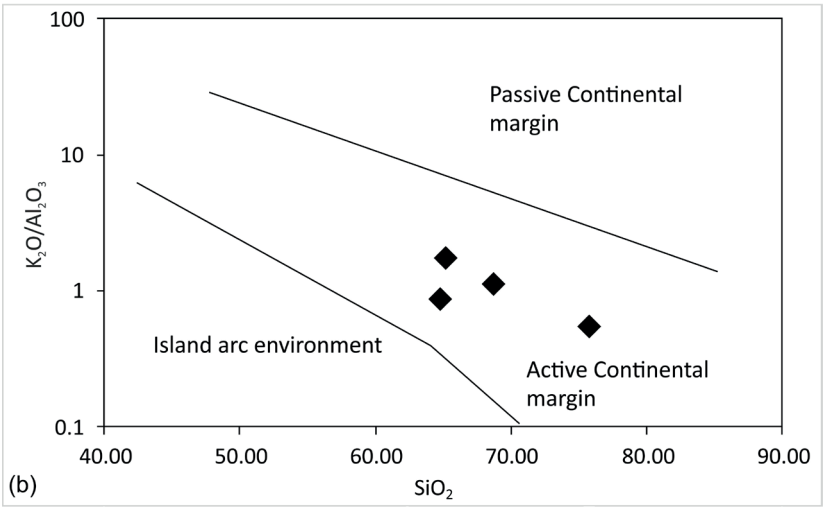

Fig. 4. (a) Th-Sc-Zr/10 triangular plot (Bhatia, 1983); (b) SiO_2 versus K_2O/Al_2O_3 (Bhatia, 1983).

the detritus accompanied by the decrease in the Eu content during the sedimentation process of residual plagioclase (Taylor & Mclennan, 1985).

5 Tectonic implications

Studies have traditionally shown that geochemistry plays a crucial role as sensitive indicator in determining the provenance of sedimentary and metasedimentary rocks and also to constrain the tectonic setting in which they were deposited (e.g., Bhatia, 1983; Bhatia & Crook, 1986; Roser & Korsch, 1986; Madukwe et al., 2015; Grizelj et al., 2017). Trace elements such as Co, Sc, Ni, Zr, Th, La and others are used for tectonic environment discrimination due to their fractionation and low mobility in sedimentary environments. Bhatia, (1983) proposed ternary plots of Sc-Th-Zr/10 and Sc-La-Th to ascertain the tectonic settings. The process of collisional tectonics and deformation is formed during the mechanism of orogeny or plate convergence leading to the formation of continental arc or active continental margin settings. These depositional environments forming in these regions are usually underlain by thick and elevated continental crust, (Bhatia & Crook, 1986). Geochemical composition of schists plotted in these ternary plots, falls in the active continental settings (Fig. 4a). Conversely, the plot of SiO_2 versus K_2O/Na_2O, shows that schists of Patharkhola have been formed in the active continental margin (Fig. 4b).

6 Conclusion

The garnet mica schists of the Patharkhola area forms a part of Dudhatoli Almora group in Kumaun Lesser Himalaya. Petrographically, the garnet mica schist is dominantly composed of garnet, biotite, muscovite, chlorite, plagioclase and a subordinate amount of quartz. It is observed that the prekinematic garnet wrapped round first generation biotite and muscovite. Second generation Biotite-II and Muscovite-II occur as cross-cutting relation with the Biotite-I and Muscovite-I.

The geochemical data reflects that Patharkhola schists are alkali rich with silica-saturated nature. These investigated schist exhibits slightly LREE depleted patterns (LaN/SmN = 0.7, LaN/YbN = 0.64) with flat HREE patterns (SmN/YbN = 0.89). The log(Fe_2O_3/K_2O) versus log(SiO_2/Al_2O_3) plot shows that the protolith of schists is mainly shale-dominated, representing nearby source sediments formed in arc-type environment. Their geochemical signature further suggests that the schists of Patharkhola have formed in active continental margins. Thus we considered that the Lesser Himalayan rocks have formed in arc-type active continental setting where the sediments where received from both from the arc and continental crust.

Acknowledgements

The authors thank the Head, Department of Applied Geology, Doctor Harisingh Gour Vishwavidyalaya, Sagar (M.P.) and the Department of Science and Technology, New Delhi, India, for providing facilities as including PURSE-Phase-II for conducting present research work. Thanks to Igor Petrík from Slovak Academy of Sciences and one anonymous reviewer for critical review for the improvement of manuscript.

References

Auden, J. B., 1937: Structure of the Himalaya in Garhwal. *Records Geol. Surv. of India, 71, 407–433.*

Bali, R. & Agarwal, K. K., 1999: Microstructures of mylonites in the Almora Crystalline Zone, Kumaun Lesser Himalaya. *Gondwana Res. Group Mem., 6, 111–116.*

Barker, F., 1979: Trondhjemite: definition, environment and hypotheses of origin. *In: Developments in petrology, Elsevier, 6, 1–12.*

Bhanot, V. B., Singh, V. P., Kansal, A. K. & Thakur, V. C., 1977: Early Proterozoic Rb-Sr whole-rock age for central crystalline gneiss of Higher Himalaya, Kumaun. *Geol. Soc. India, 18, 2, 90–91.*

Bhargava, O. N., Frank, W. & Bertle, R., 2011: Late Cambrian deformation in the Lesser Himalaya. *J. Asian Earth Sci., 40, 1, 201–212.*

Bhatia, M. R., 1983: Plate tectonics and geochemical composition of sandstones. *J. Geol., 91, 6, 611–627.*

Bhatia, M. R. & Crook, K. A., 1986: Trace element characteristics of graywackes and tectonic setting discrimination of sedimentary basins. *Contr. Mineral. Petrology, 92, 2, 181–193.*

Blevin, P., 2003: Metallogeny of granitic rocks. In The Ishihara Symposium. *Granites Assoc. Metallogen., 14, 5–8.*

Chappell, B. W., 1974: Two contrasting granite types. *Pacific Geol., 8, 173–174.*

Cullers, R. L., Chaudhuri, S., Arnold, B., Lee, M. & Wolf, W. J., 1975. REE distributions in clay minerals and in the clay-sized fraction of the lower Permian Havensville and Eskridge shales of Kansas and Oklahoma. *Geochim. cosmochim. Acta, 39, 1691–1703.*

De la Roche, H. D., Leterrier, J. T., Grandclaude, P. & Marchal, M., 1980: A classification of volcanic and plutonic rocks using R1R2-diagram and major-element analyses – its relationships with current nomenclature. *Chem. Geol., 29, 1–4, 183–210.*

Fleet, A. J., 1984: Aqueous and sedimentary geochemistry of the rare earth elements. *In: Developments in geochemistry, Elsevier, 2, 343–373.*

Frost, B. R., Barnes, C. G., Collins, W. J., Arculus, R. J., Ellis, D. J. & Frost, C. D., 2001: A geochemical classification for granitic rocks. *J. Petrology, 42, 11, 2033–2048.*

Gairola, V. K. & Joshi, M., 1978: Structure of a part of Dudatoli-Almora crystalline thrust sheet around Thalisain, district Pauri Garhwal – Structure d'une partie de la nappe charriée cristalline de Dudatoli-Almora dans la région de Thalisain, district de Pauri Garhwal Himal. *Geol., 8, 1, 379–398.*

Grizelj, A., Peh, Z., Tibljaš, D., Kovačić, M. & Kurečić, T., 2017: Mineralogical and geochemical characteristics of Miocene pelitic sedimentary rocks from the south-western part of the Pannonian Basin System (Croatia): Implications for provenance studies. *Geosci. Frontiers, 8, 1, 65–80.*

Humphris, S. E., 1984: The mobility of the rare earth elements in the crust. *In: Developments in Geochemistry, Elsevier, 2, 317–342.*

Irvine, T. N. & Baragar, W. R. A., 1971: A guide to the chemical classification of the common volcanic rocks. *Canad. J. Earth Sci., 8, 5, 523–548.*

Islam, R., Ahmad, T. & Khanna, P. P., 2005: An overview on the granitoids of the NW Himalaya. *Himalayan Geol., 26, 1, 49–60.*

Joshi, M. & Tiwari, A. N., 2007: Folded metamorphic reaction isograds in the Almora Nappe, Kumaun Lesser Himalaya: Field evidence and tectonic implications. *Neu. Jb. Geol. Paläont., Abh., 215–225.*

Joshi, M. & Tiwari, A. N., 2009: Structural events and metamorphic consequences in Almora Nappe, during Himalayan collision tectonics. *J. Asian Earth Sci., 34, 3, 326–335.*

Joshi, M. & Tiwari, A. N., 2004: Quartz C-axes and metastable phases in the metamorphic rocks of Almora Nappe: evidence of pre-Himalayan signatures. *Current Sci., 87, 995–998.*

Joshi, G., Agarwal, A., Agarwal, K. K., Srivastava, S. & Valdivia, L. A., 2017: Microstructures and strain variation: Evidence of multiple splays in the North Almora Thrust Zone, Kumaun Lesser Himalaya, Uttarakhand, India. *Tectonophysics, 694, 239–248.*

Joshi, M., Kumar, A., Ghosh, P., Das, B. P. & Devi, P. M., 2019: North Almora Fault: a crucial missing link in the strike slip tectonics of western Himalaya. *J. Asian Earth Sci., 172, 249–263.*

Karimpour, M. H., 1983: Application of trace elements and isotopes for discriminating between porphyry molybdenum, copper, and tin systems and the implications for predicting the grade. *Glob. Tecton. Metallog., 29–36.*

Mackenzie, F. T. & Garrels, R. M., 1971: Evolution of sedimentary rocks. *New York, Norton.*

Madukwe, H. Y., Obasi, R. A., Fakolade, O. R. & Bassey, C. E., 2015: Provenance, tectonic setting and source-area weathering of the coastal plain sediments, South West, Nigeria. *Sci. Res. J., 3, II, 20–31.*

McLennan, S. M., 1982: On the geochemical evolution of sedimentary rocks. *Chem. Geol., 37, 3–4, 35–350.*

Mehdi, S. H., Kumar, G. & Prakash, G., 1972: Tectonic evolution of eastern Kumaun Himalaya: a new approach. *Himalayan Geol., 2, 481–501.*

Molnar, P. & Tapponnier, P., 1975: Cenozoic Tectonics of Asia: Effects of a Continental Collision: Features of recent continental tectonics in Asia can be interpreted as results of the India-Eurasia collision. *Science, 189, 4201, 419–426.*

Muecke, G. K., Pride, C. & Sarkar, P., 1979: Rare-earth element geochemistry of regional metamorphic rocks. *Physics Chemistry Earth, 11, 449–464.*

Mukherjee, S., 2005: Channel flow, ductile extrusion and exhumation of lower-mid crust in continental collision zones. *Current Sci., 89, 3, 435–436.*

Mukherjee, S., 2007: Geodynamics, deformation and mathematical analysis of metamorphic belts of the NW Himalaya. Unpublished Ph. D. thesis. *Indian Institute of Technology Roorkee, 1–267.*

Mukherjee, S., 2013: Channel flow extrusion model to constrain dynamic viscosity and Prandtl number of the Higher Himalayan Shear Zone. *Int. J. Earth Sci., 102, 1811–1835.*

Mukherjee, S., Carosi, R., van der Beek, P., Mukherjee, B. K. & Robinson, D. M., 2015: Tectonics of the Himalaya: an introduction. *Spec. Publ., 412, 1, 1–3.*

Mukherjee, S., Punekar, J. N., Mahadani, T. & Mukherjee, R., 2015: Intrafolial folds: review and examples from the western Indian Higher Himalaya. Ductile shear zones: From micro-to macro-scales, *182–205.*

Nakata, T., 1989: Active faults of the Himalaya of India and Nepal. *Geol. Soc. Amer., Spec. Pap., 232, 1, 243–264.*

O'connor, J. T., 1965: A classification for quartz-rich igneous rocks based on feldspar ratios. *US Geol. Surv., Profess. Pap., 525B, B79–B84.*

Pearce, J. A., Harris, N. B. & Tindle, A. G., 1984: Trace element discrimination diagrams for the tectonic interpretation of granitic rocks. *J. Petrology, 25, 4, 956–983.*

Rana, H. & Thomas, H., 2018: Geology of the Patharkhola area, Almora District, Uttarakhand (India): with special reference to the lithology and field relation. *Bull. Depart. Geol., 1–6. DOI: https://doi.org/10.3126/bdg.v20i0.20716.*

Rana, H., Thomas, H., Soni, A. & Shukla, S., 2023: Petrochemistry of Phyllites from Patharkhola, Lesser Kumaun Himalaya with Reference to Tectonic Implications. *Earth Planet*, 2*, 2, 1–9. DOI: https://doi.org/10.36956/eps.v2i2.842.*

Rana, H. & Thomas, H., 2023: Structural, Micro-Structural and Thermal Characterizations of Natural Garnet of Regions of Patharkhola from the State of Uttarakhand of India. *Bull. Pure Appl. Sci., Geol., 1.*

Rao, Y. B., Chetty, T. R. K., Janardhan, A. S. & Gopalan, K., 1996: Sm-Nd and Rb-Sr ages and PT history of the Archean Sittampundi and Bhavani layered meta-anorthosite complexes in Cauvery shear zone, South India: evidence for Neoproterozoic reworking of Archean crust. *Contr. Mineral. Petrology., 125, 2–3, 237.*

Roser, B. P. & Korsch, R. J., 1986: Determination of tectonic setting of sandstone-mudstone suites using SiO_2 content and K_2O/Na_2O ratio. *J. Geol., 94, 5, 635–650.*

Rossi, J. N., Toselli, A. J., Basei, M. A., Sial, A. N. & Baez, M., 2011: Geochemical indicators of metalliferous fertility in the Carboniferous San Blas pluton, Sierra de Velasco, Argentina. *Geol. Soc. London, Spec. Publ., 350, 1, 175–186.*

Shand, S. J., 1943: Classic A/CNK vs A/NK Plot for Discriminating Metaluminous, Peraluminous and Peralkaline Compositions. *New York, Hafner Publishing*.

Thakur, V. C., 2004: Active tectonics of Himalayan frontal thrust and seismic hazard to Ganga Plain. *Current Sci., 1554–1560.*

Thakur, V. C., Jayangondaperumal, R. & Malik, M. A., 2010: Redefining Medlicott – Wadia's main boundary fault from Jhelum to Yamuna: An active fault strand of the main boundary thrust in northwest Himalaya. *Tectonophysics, 489, 1–4, 29–42.*

Thomas, T. & Thomas, H., 1992: Fold flattening and strain studies in a part of Almora Crystalline Zone, around Tamadhaun Kumaun Himalaya. *Indian Mining and Engineering Jour., 5–7.*

Taylor, S. R. & McLennan, S. M., The Continental Crust: its Composition and Evolution. *Oxford, Blackwell Scientific Publication, pp. 312.*

Valdiya, K. S., 1980: Stratigraphic scheme of the sedimentary units of the Kumaun Lesser Himalaya. In: Valdiya, K. S., Bhatia, S. B. (eds.): Stratigraphy and Correlation of the Lesser Himalayan Formation. *Delhi, Hindustan Pub. Corp., 7–48.*

Valdiya, K., 1980b: Geology of Kumaun lesser Himalaya. *W. I. H. G., 291–295.*

Valdiya, K. S., 1988: Tectonics and evolution of the central sector of the Himalaya. *Phil. Trans. Roy. Soc. London. Ser. A, Mathem. Phys. Sci., 326, 1589, 151–175.*

Webb, A. A. G., Yin, A., Harrison, T. M., Célérier, J., Gehrels, G. E., Manning, C. E. & Grove, M., 2011: Cenozoic tectonic history of the Himachal Himalaya (northwestern India) and its constraints on the formation mechanism of the Himalayan orogen. *Geosphere, 7, 4, 1013–1061.*

Webb, A. A. G., 2013: Preliminary balanced palinspastic reconstruction of Cenozoic deformation across the Himachal Himalaya (northwestern India). *Geosphere, 9, 3, 572–587.*

Yin, A., 2006: Cenozoic tectonic evolution of the Himalayan orogen as constrained by along-strike variation of structural geometry, exhumation history, and foreland sedimentation. *EarthSci. Rev., 76, 1–2, 1–131.*

Geochemické charakteristiky a tektonická interpretácia granatických svorov oblasti Patharkhola v Kumaunských Malých Himalájach, Uttarakhandské Himaláje, India

Pohorie Himaláje tvorí oblúkový horský pás pokrývajúci celú hraničnú zónu severnej Indie. Je typovým príkladom zrážky medzi indickou a ázijskou litosférickou platňou v období pred približne 55 miliónmi rokov (Mukherjee, 2015; Yin, 2006). Štruktúre, stratigrafii a tektonike územia Kumaun v Malých Himalájach sa venujú viaceré práce (Joshi a Tiwari, 2009; Joshi et al., 2017; Rana a Thomas, 2018). V oblasti Kumaun je sekvencia Malých Himalájí oddelená hlavnou centrálnou prešmykovou zónou (*Main Central Thrust;* MCT) od Vyšších Himalájí na severe. Hlavný hraničný prešmyk (*Main Bondary Thrust;* MBT) oddeľuje túto sekvenciu od oblasti Siwalikov na juhu (Thakur et al., 2010). Horninové súbory skupiny Dudhatoli (Rana a Thomas, 2018) vystupujú v oblasti Patharkhola.

Vnútorná bridličnatá séria, označovaná aj ako tektonická zóna príkrovu metamorfovaných a kryštalinických hornín, tvorí v Malých Himalájach výraznú štruktúrnu jednotku s polyfázovou deformáciou a metamorfózou. Kryštalinikum masívu Dudhatoli vystupuje od lokalít Garhwal na ZSZ po Kumaun na VSV. Kumar a Agarwal (1975) zahrnuli Mandhali a formácie Chandpur a Nagthat, rovnako ako kryštalinikum Dudhatoli-Almora, do novovytvorenej skupiny Dudhatoli, v ktorej kryštalinikum Dudhatoli-Almora reprezentuje najvyšší horizont. Horniny skupiny Dudhatoli sa považovali za prekambrické (Kumar a Agarwal, 1975). V Kumaunských Himalájach boli ruly jednotky Munsiari skupiny Almora datované na 1 830 ± 200 mil. r. (Bhanot et al., 1977). Islam et al. (2005) rozčlenili proterozoické veky granitoidov Malých Himalájí do dvoch skupín: 2 200 – 1 800 mil. r. a 1 400 – 1 200 mil. r. Rana a Thomas (2023) študovali termálny a štruktúrny charakter granátov z granatických svorov v bridliciach z lokality Patharkhola. Zistilo sa, že sú bohaté na Mg, čo dokladá ich vyššieteplotný rozklad.

Študovaný terén vykazuje polyfázovú deformáciu a metamorfózu (Joshi a Tiwari, 2009). Je to dobre pozorovateľné v centrálnej časti almorského príkrovu. V Kumaunských Malých Himalájach sa realizoval rozsiahly výskum pelitických rúl a granitov a v menšom rozsahu aj nízkostupňových bridlíc a fylitov (Phukon et al., 2018; Das et al., 2019). Rana et al. (2023) štúdiom patharkholských fylitov dospeli k záveru, že fylity s vysokým obsahom Al a obohatené stopovými prvkami vznikli na aktívnom kontinentálnom okraji.

Oblasť okolo lokality Patharkhola s vystupovaním hornín Malých Kumaunských Himalájí je ohraničená zemepisnou dĺžkou 79° 09' V až 79° 17' 56" V a zemepisnou šírkou 29° 47' 42" S až 29° 56' 69" S. Má rozlohu približne 120 km^2 (obr. 1a). Vystupujúcimi horninami sú ruly, bridlice a fylity (obr. 1b). Článok je zameraný na geochemický charakter a petrogenézu bridlíc.

Pri tektonickej interpretácii je dôležitý geochemický výskum sedimentárnych a metasedimentárnych hornín, ktorý dokáže citlivo preukázať ich pôvod a tektonické prostredie ich vzniku. Analyzované údaje o REE bridlíc boli normalizované podľa *Archean Australian Shales* (PAAS) s normalizovanými hodnotami podľa Taylora a Mclennana (1985).

Vykazujú mierne ochudobnené LREE (LaN/SmN = 0,7, LaN/YbN = 0,64) s plochým priebehom HREE (SmN/YbN = 0,89). Koncentrácia litofilných prvkov (Rb, Cs, Ba a Sr) spolu s HFSE (Y, Nb a Zr) má hodnoty v tesnej blízkosti PAAS. Vyšší pomer LREE/HREE označuje vysoký stupeň frakcionácie počas metamorfnej

fázy, keďže takáto chemická heterogenita sa nezistila v protolite. Patharkholské bridlice vykazujú strmé LREE a mierne HREE s negatívnou európskou anomáliou. Podobnosť hodnôt bridlíc s PAAS je interpretovaná ako kontaminácia z primárneho prostredia, pretože protolit sa málo zmenil počas metamorfózy (Likhanov, 2008). Uvedené znaky sú typické pre postarchaickú hlinu bridlíc s výskytom erozívnych produktov z vrchnej kontinentálnej kôry (priemer z 23 austrálskych bridlíc postarchaického veku). Prítomnosť erozívnych produktov sedimentárnych hornín v detrite je sprevádzaný poklesom obsahu Eu počas procesu sedimentácie zvyškov plagioklas (Taylor a Mclennan, 1985).

Štúdie mnohých autorov preukázali, že geochémia je citlivý indikátor určujúci provenienciu sedimentárnych a metasedimentárnych hornín a tektonické prostredie, v ktorom sa nachádzali (napr. Bhatia, 1983; Bhatia a Crook, 1986; Roser a Korsch, 1986; Madukwe et al., 2015; Grizelj et al., 2017). Na určenie tektonického prostredia sa využívajú predovšetkým stopové prvky ako Co, Sc, Ni, Zr, Th, La a ďalšie. Na určenie tektonického prostredia Bhatia (1983) navrhol ternárne diagramy Sc-Th-Zr/10 a Sc-La-Th. Prejavy kolíznej tektoniky a deformácie sú v rámci orogenézy produktom konvergencie litosférických platní vedúcej k vzniku kontinentálneho oblúka alebo prostredia aktívneho kontinentálneho okraja. Depozičné prostredia v takýchto regiónoch sú zvyčajne podostielané hrubou a vyklenutou kontinentálnou kôrou (Bhatia a Crook, 1986). Geochemické zloženie bridlíc zobrazených v ternárnych diagramoch spadá do prostredia kontinentálnej kolízie (obr. 4a). Naopak, diagram SiO_2 vs. K_2O/Na_2O indikuje, že bridlice z Patharkholy sa vytvorili na aktívnom kontinentálnom okraji (obr. 4b).

V záverečnom zhrnutí je možné konštatovať, že granatické svory v oblasti Patharkhola, ktoré sú súčasťou skupiny Dudhatoli-Almora v Kumaunských Malých Himalájach, petrograficky pozostávajú z granátu, biotitu, muskovitu, chloritu, plagioklasu a druhoradého množstva kremeňa. Zistilo sa, že predkinematický granát je obalený prvou generáciou biotitu a muskovitu. Druhá generácia biotitu-II a muskovitu-II sa vygenerovala priečne v mikrofraktúrach biotitu-I a muskovitu-I. Geochemické údaje dokladajú, že svory sú bohaté na alkálie a nasýtený SiO_2. Vykazujú mierne ochudobnené LREE (LaN/SmN = 0,7, LaN/YbN = 0,64) s plochým priebehom HREE (SmN/YbN = 0,89). Diagram $\log(Fe_2O_3/K_2O)$ vs. $\log(SiO_2/Al_2O_3)$ dokladá, že protolitom svorov bola predovšetkým bridlica reprezentujúca zdrojové sedimenty z aktívneho kontinentálneho okraja. To indikuje, že horniny z Malých Himalájí sa vytvorili v prostredí kontinentálneho oblúka, kde detrit sedimentov pochádzal z tohto oblúka, ako aj z kontinentálnej kôry.

Doručené / Received: 26. 9. 2023
Prijaté na publikovanie / Accepted: 21. 12. 2023

Mineralia Slovaca, Web ISSN 1338-3523, ISSN 0369-2086, https://doi.org/10.56623/ms.2023.55.2.4
55, 2 (2023), 143 – 156, © Authors 2023. CC BY 4.0

Characterization of ochre precipitate loaded with arsenic from mine water and study of its stability by using of leaching tests and sequential extraction analysis

ALEXANDRA BEKÉNYIOVÁ[1*], ZUZANA DANKOVÁ[1], KATARÍNA ČECHOVSKÁ[1], ERIKA FEDOROVÁ[1], JARMILA NOVÁKOVÁ[2], JAROSLAV BRIANČIN[3], LADISLAV VIZI[1] and DUŠAN KÚŠIK[4]

[1]State Geological Institute of Dionýz Štúr, Regional Centre Košice, Department of Applied Technology of Raw Materials, Slovak Republic; *alexandra.bekenyiova@geology.sk
[2]State Geological Institute of Dionýz Štúr, Regional Centre Spišská Nová Ves, Division of Geoanalytical Laboratories, Slovak Republic
[3]Slovak Academy of Sciences, Institute of Geotechnics, Košice, Slovak Republic
[4]State Geological Institute of Dionýz Štúr, Department of Raw Minerals and Geophysics, Bratislava, Slovak Republic

Abstract: This study is focused on the mobility of potential toxic elements release from the ochre precipitate sample after the leaching by using selected methods. The sequential extraction method was performed to characterize the stability of the sample after the leaching tests. The TCLP regulatory limit for arsenic of 5 mg/L in the ochre precipitate was not exceeded, thus meet the legislative regulations. The highest concentrations of As were achieved in the residual fraction (5) even after leaching tests. The lowest concentration values of As were found in the mobile fractions: water-soluble fraction (1) and ion-exchangeable and carbonate fraction (2). These results indicate the low mobility of arsenic and the tight bonding between As and Fe in formed ochre precipitates.

Key words: ochre precipitate, arsenic, leaching test, sequential extraction analysis

Graphical abstract

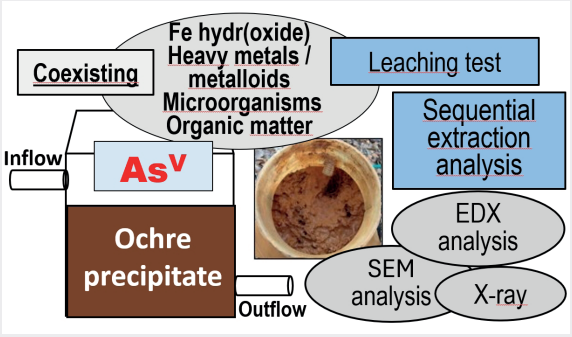

Highlights

- The regulatory TCLP limit (5 mg/L) for As in the leachate was not exceeded, which means that the waste (ochre precipitate) is stable under slightly acidic conditions.
- After TCLP and SPLP tests, the mobility of Fe and As was minimal, below 0.1 %. Mn was the most mobile element, with mobility value of 90 %, after the SBET and TCLP leaching tests.
- Arsenic is probably incorporated directly into the internal structure of the ochre precipitate (formed by hydrated iron oxides) and it binds in the form of internal complexes with iron.

1 Introduction

The Hauser adit is the deepest horizontal adit in the entire Zlatá Idka ore district. Mine water is characterised by a high arsenic content. This content significantly correlates with the content of divalent iron, which allows us to assume that this highly toxic micro-component of chemistry also originates from the primary environment of formation of the chemical composition of mine water – from the depth of the rock mass (the presence of arsenopyrite in the vein system of the locality Zlatá Idka), (Bačová, 2006). Outflows from the adit presented a permanent source of contamination (adit discharges, drainage water and mine heap leachate) and will recharge the surface waters of streams with elements of concern over the long term (Cicmanová & Baláž, 2007). Mine water discharge creates a pond – with no runoff – below the backfilled mouth of the adit. The mine water probably seeps into the Quaternary sediments of the Ida Valley.

The pH is a critical parameter for the mobility of metals, and thus their bioavailability. Dissolution of carbonates and silicates is an important type of reaction that shapes the pH of waters. In terms of the potency of arsenic present in waters, it has been found to be present only in the less toxic form of pentavalent ions. This points to a significant application of oxidizing conditions of the aquatic environment – probably in the final phase of mine water discharge (Cicmanová & Baláž, 2007). In an oxidizing environment, the arsenate species predominates,

and at a pH between 6 and 9, it exists as oxyanions of arsenic acid in the form of $H_2AsO_4^-$ and/or $HAsO_4^{2-}$ (average pH of mine water from the Hauser adit = 7.3).

The ochre phases are precipitated directly from mine waters (or tailings pond leakage). They are characteristic of mine sites, adit discharges and their surroundings due to oxidation of soluble Fe^{2+} to insoluble Fe^{3+} phases. HFO, also called hydrous iron oxides and iron (III) oxide-hydroxides, include several minerals, such as ferrihydrite, akaganeite, feroxyhyte, goethite, lepidocrocite and limonite. They are poorly crystalline, highly porous, have large surface areas and they are excellent sorbents of various potentially toxic elements. Hydrous ferric oxides (HFO) harbor a remarkable ability to sequester As and Sb from the environment by adsorbing arsenate [As(V)], arsenite [As(III)], antimonate [Sb(V)] and antimonite [Sb(III)] ions on its surface (in some cases even into the structure) under the neutral and low acidic conditions, which is the case of most groundwater and soil water conditions (Scheinost et al., 2006; Majzlan et al., 2007; Mitsunobu et al., 2006; Guo et al., 2014). Adsorption of As(V) species onto porous iron oxyhydroxides is known to take place via Coulombic and/or Lewis acid base interactions (ligand exchange reactions) and to form monodentate and bidentate inner sphere complexes (Zhang & Stanforth, 2005; Banerjee et al., 2008). Generally, it is believed that the porous nature of iron (oxy)hydroxides leads to As(V) adsorption at internal iron complexation sites (Sinha et al., 2002; Badruzzaman et al., 2004). Arsenic ions bound by the inner complexes are more strongly adsorbed than arsenic ions bound by the outer complexes (Stollenwerk, 2003).

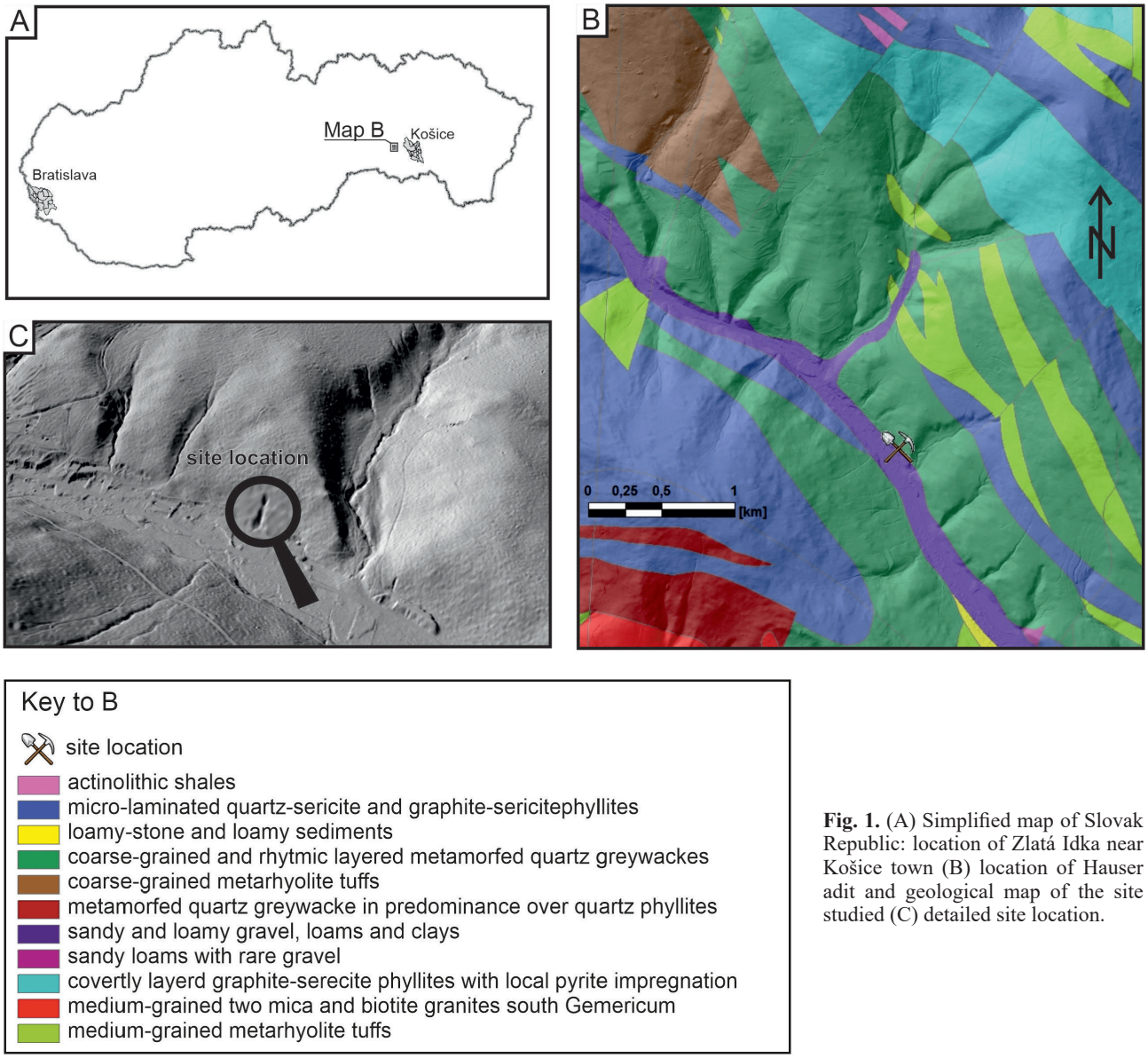

Fig. 1. (A) Simplified map of Slovak Republic: location of Zlatá Idka near Košice town (B) location of Hauser adit and geological map of the site studied (C) detailed site location.

A previous study focused on the elimination of As concentration from mine run-off water of

Hauser adit under flow conditions at the locality Zlatá Idka (Bekényiová et al., 2023), Fig. 1. The in situ field experiments consisted of designing a continuous mine water overflow system by placing two 50 L containers directly in the field, through which mine water flowed continuously by gravity flow. The mine water flowed through the two containers: a retention container and a filter container, in which different fractions of natural sorbents were deposited in layers. In the retention container, ochre precipitates naturally formed during the in situ experiment (4 months), binding a significant amount of arsenic.

The present study is focused on formed ochre precipitates and their characterization by X-ray diffraction, SEM and EDX analysis. The microbiology was discussed based on the results from the SEM analysis spectra, too. Furthermore, the main objective of the study was to determine the stability of the ochre precipitates. Leaching tests, namely SPLP, TCLP and SBET methods were used to assess the mobility of the investigated potentially toxic elements. Mobility and transport sequential extraction analysis (SEA) method was used to determine the content of potentially toxic elements in the bioavailable and unavailable fractions and to refine and understand the physicochemical processes of metal fixation.

2 Materials and Methods

2.1 Ochre precipitates

The ochre precipitates used in this study were obtained from previous in situ experiments, where they are naturally formed in 50 L container and binding a significant amount of arsenic (Bekényiová et al., 2023). Next they were used for the chemical and mineralogical analyses. Samples were collected using a field scoop into plastic bags. During collection, they were filtered through a 0.16 mm sieve to remove any residual organic matter (leaves, roots, etc.) and then washed with water. Then the precipitates were dried in a laboratory oven at a constant temperature of 60 °C to a stable mass during 3 days.

2.2 Ochre precipitate characterization

The powder X-ray diffraction (XRD) patterns of ochre precipitate sample was recorded using a diffractometer D2 Phaser (Bruker, Germany), equipped with a CuKα radiation source (30 kV, 10 mA) and Lynxeye detector. The data were qualitatively and quantitatively analysed using Software DIFFRAC.EVA with PDF-2 Database.

The ochre precipitates were studied by scanning electron microscopy FE MIRA 3 (Tescan, Czech Republic) equipped by energy-dispersive (EDX) analyser of chemical composition (Oxford Instruments).

2.3 Mobility of toxic elements and bioassessibility testing

Mobility of potential toxic elements present in the ochre sample was tested using Synthetic Precipitation Leaching Procedure (SPLP), US EPA Method 1312 based on the acid rain leaching; pH 4.2 (Fey et al., 2011). The ochre sample of 5 grams was extracted by solution of H_2SO_4 and HNO_3 (weight ratio 3 : 2). The ochre sample and extraction solution were placed into the extraction bottle and shaken for 18 hours on the laboratory shaker. Then the leachate was filtered and analysed.

Toxicity Characteristic Leaching Procedure (TCLP) was performed using the method (US EPA 1311) as follows: a 50 g sample was extracted with a 1 N solution of NaOH and acetic acid, pH 2.8, with stirring for 18 hours.

The bioassessibility of the toxic elements present in the ochre sample Fe-HB-Š was tested by Simply Bioavailability Extraction Test (SBET). The sediment sample of 5 grams was extracted by solution of 0.4 M glycine of pH 1.5 (adjusted by HCl) under the vigorous stirring for 1 hour at 37 °C (Report No.: 1542820-003-R-Rev0, 2016; Kim et al., 2009).

2.4 Sequential extraction analysis

The ochre sample was subjected to sequential extraction analysis with the aim to determine the content of toxic elements in biologically available and unavailable fractions. The sequential extraction analysis was provided according to the method described by Mackových et al. (2000). The extraction in each step was carried out in 3 measurements, the sample was shaken in suspension on a laboratory multirotator for 16 hours at laboratory temperature. After the extraction was completed, the solution was centrifuged at 3000 rpm for 20 minutes, the extraction leachate was filtered and fixed by the addition of HNO_3.

3 Results and discussion

3.1 Characteristics of the formed ochre precipitates

The resulting ochre precipitates (hydrated iron oxides, referred as HFO) contain high amount of arsenic, but under normal surface conditions are generally poorly soluble As compounds. They are commonly precipitated directly from mine waters as a result of the oxidation of soluble divalent iron to insoluble ferric iron phases and are characteristic of mine sites, adit outfalls and their surroundings. The water flows from the adit is neutral to slightly alkaline mine water with pH of 7.3 (an average) and with high arsenic content 360 µg/L (an average).

Sorptive properties of hydrous ferric oxides (HFO) depend on the pH of the surrounding water, the chemical composition of the water, and the ratio of the amount of dissolved trace metals to the amount of hydrous iron oxides

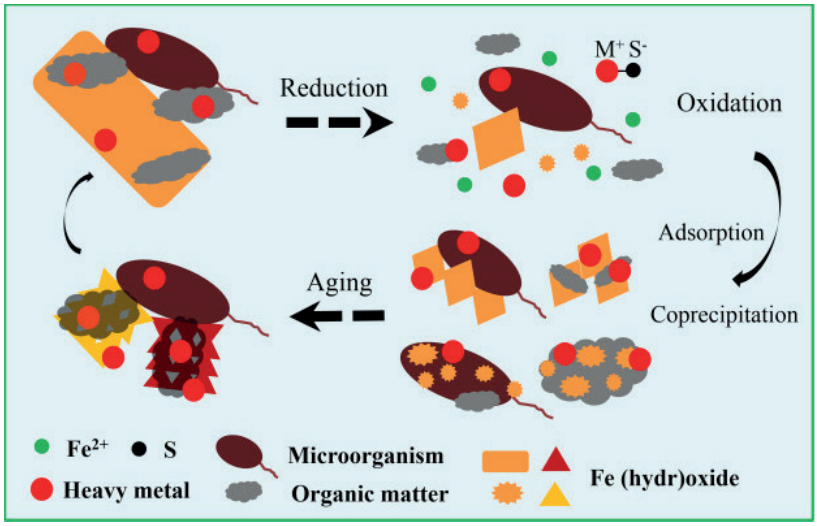

Fig. 2. Proposed scheme showing the influences of redox and aging on the behavior of heavy metals associated with Fe (hydr)oxides-organo complexes (Chenchen et al., 2019).

(Dzombak et al., 1987; Davis & Kent, 1990; Stumm, 1992). Behaviour of heavy metals in complex system of HFO is illustrated in Fig. 2.

After collection and processing ochre precipitates in the laboratory, they were further studied by using X-ray diffraction method, the morphology was studied by scanning electron microscopy with the EDX analysis.

The stability of Fe precipitates was studied by leaching tests (SBET, TCLP, SPLP). Sequential extraction (SEA) methodology was used to assess the mobility of potentially toxic elements bound in Fe precipitates before and after leaching tests, that would be released back into the water, and to refine and understand the physicochemical processes of metal fixation, mobility and transport.

The concentrations of Fe and As in the ochre precipitates formed in the container (after 4 months of filtration) are presented in Tab. 1. The data of As concentration were compared with the indication and intervention criteria of the *Directive of the Ministry of Environment of the Slovak Republic No. 1/2015-7 of 28 January 2015 for the preparation of risk analysis, listed in Annex 12a to the Directive (Indication and Intervention Criteria for the Rock Environment and Soil)*. The chemical analyses show that the concentrations for As expressively exceed the IT criteria for industry, Tab. 1.

The fine fibrous structure observed in some places may be related to the

Tab. 1

Concentration of selected elements in ochre precipitate and comparison of As concentration with the permissible and critical limits according to the guideline

Element	Permissible limit (ID)	Critical limit (IT)		Fe – HB – Š input
		Residential districts	Industrial districts	
	[mg.kg^{-1}]	[mg.kg^{-1}]	[mg.kg^{-1}]	[mg.kg^{-1}]
As	65	70	140	56 945
Fe	x	x	x	471 000

ID – Permissible limit of contaminant concentration in soils according to the Methodical Instruction of Ministry of Environment of the Slovak Republic, No. 1/2012-7

IT – Critical limit of contaminant concentration in soils according to the Methodical Instruction of Ministry of Environment of the Slovak Republic, No. 1/2012-7

Fig. 3. Formation of ochre precipitates in a 50 L sedimentation container, ochre sampling.

presence of Fe oxidizing bacteria, which may play an important role in the mobility of the elements. Formation of ochre precipitate during monitoring period and its sampling is illustrated in Fig. 3.

Processed Fe precipitate was subjected to X-ray analysis. The results showed a predominantly amorphous phase of ferric oxyhydroxides, consisted of weakly crystalline ferrihydrite, as can be seen in Fig. 4. Ferrihydrite is usually formed from mine drainage solutions that are rich in organic matter and/or have pH values greater than 5 (Bigham et al., 1992).

From X-ray and EDX analyses it can be assumed that the rusty red colour of the sediment as well as the surface coatings of the rocks around the lake is caused by amorphous phases of iron compounds (hydroxides, oxyhydroxides), binding a significant proportion of As from the outflowing mine water. The EDX analysis of rusty red precipitates from mine water collected on the filter confirmed the presence of both iron and arsenic in amount 52 wt. % and 13.2 wt. %, respectively (Fig. 5). Fig. 6 (A),

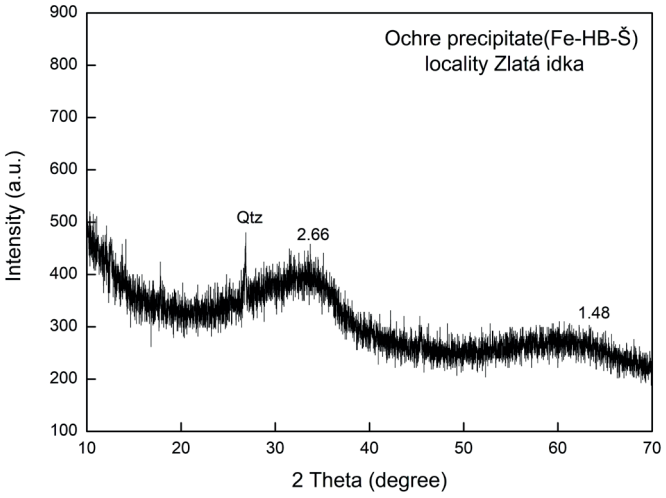

Fig. 4. X-ray diffraction of ochre precipitate.

shows Fe oxide aggregates (probably ferrihydrite) in the immediate neighbourhood of the two Fe-oxidizing bacterial species, *Gallionella ferruginea (G)* and *Lepthotrix ochracea (L)*, according to Cornell and Schwertmann

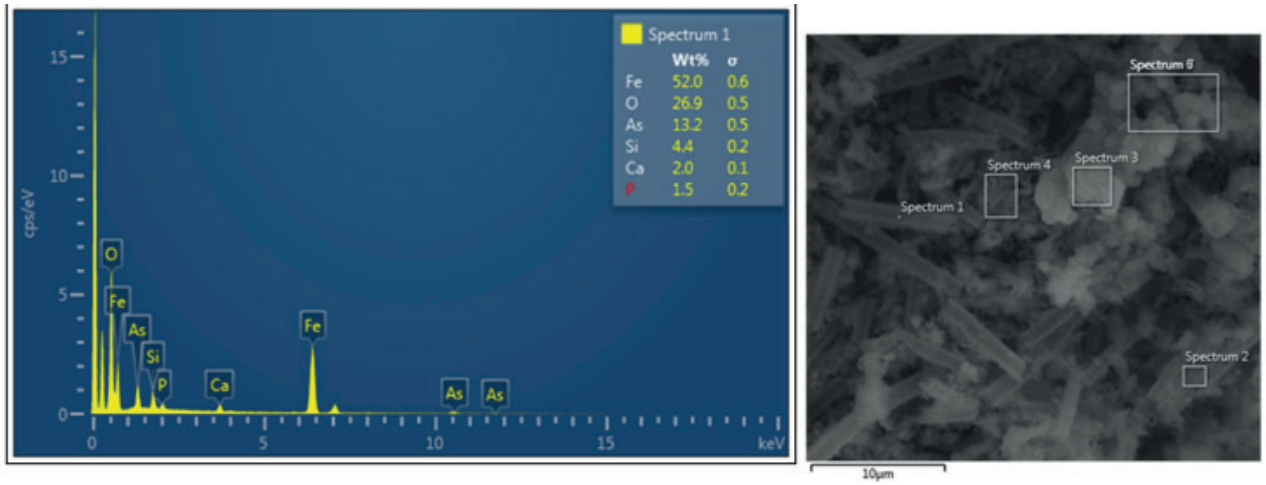

Fig. 5. EDX analysis of the ochre precipitate Fe-HB-Š.

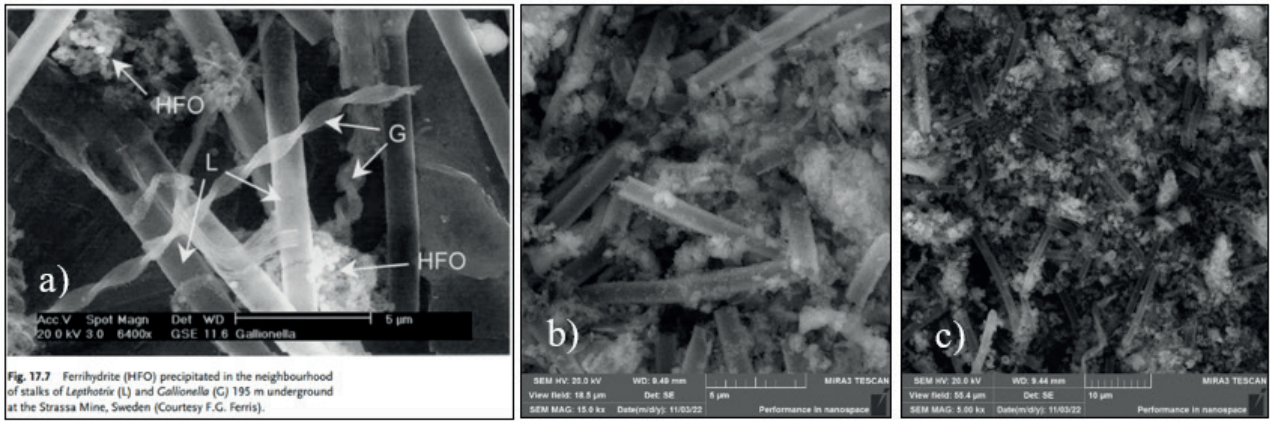

Fig. 6. Surface spectrum of HFO (Cornell & Schwertmann, 2003) (a), Fe-HB-Š sample – 15 000x magnification (b), Fe-HB-Š sample – 5 000x magnification (c).

(2003). From our observed scanning electron microscopy spectra at 15 000x and 5 000x magnification, hollow tubes are clearly visible, which probably correspond to bacterial species *Lepthotrix ochracea* (Fig. 6B, C). It is well known Fe-oxidizing bacteria that occurs in higher abundance in ochres, in addition to other facultatively aerobic or microaerophilic Fe-oxidizing bacteria (*Gallionella, Rhodobacter*, *Sphingopyxis*, *Dechloromonas*, *Azospira*, and others). These metal-oxidizing bacteria form robust populations, with significant effects on crystallization rate of hydrated iron oxides and adsorption of metal ions/metalloids (Volekova, 2022).

Fe oxidizing bacteria of the genus *Leptothrix* form iron-precipitating shells and oxidize divalent iron to trivalent iron hydroxide. These bacteria can either adaptively use metals (or other compounds) as electron acceptors (Roden, 2012; Bryce et al., 2018; Liu et al., 2019a). This allows them to live in changing conditions, e.g. the transition zone between aerobic and anaerobic environments, and adapt to changing oxygen availability.

To better understand the biochemical processes at the locality, the PCR analysis of the Fe-HB-Š sample to determine the specific bacterial species present in the precipitates is planned to be complemented.

3.2 Leaching tests

The leaching tests (SBET, TCLP, SPLP) were aimed to assess the mobility of the investigated potentially toxic elements (As, Sb, Fe and Mn) in the Fe precipitate sample. The bioavailability test by the SBET (Simply Bioavailability Extraction Test) method characterizes the proportion of toxic elements that are absorbed from the sample (soil, sediment) into the organism via the digestive tract. The method simulates an acidic gastric environment (pH = 1.5). These tests also indicate the possible effect of soil exposed to acid mine water to pH below 2.

The toxicity characteristic leaching procedure (TCLP) using US EPA Method 1311 assesses the mobility of hazardous substances from the solid phase into the aquatic environment. It simulates landfill leaching or simulated wetting (waste/solids exposed for 100 years in a landfill, pH = 2.8). It is a standardized method for determining whether a waste is hazardous or non-hazardous for disposal purposes. Concentration limits for individual elements according to the TCLP evaluation are given in Tab. 2.

Tab. 2

TCLP limits (US EPA 1311)

Element	Fe	As	Mn	Sb
TCLP limit [mg.L^{-1}]	–	5	–	–

The SPLP (Synthetic Precipitation Leaching Procedure) mobility test by US EPA Method 1312 simulates acid rain (waste exposed to 100 years of acid rain, pH = 4.2). The degree of waste/landfill stabilization is critical to the quality or composition of the leachate from the waste, which in turn affects the degree of groundwater contamination. The SPLP method is of limited use for the detection of metals that are present on the surface; therefore, it is considered to be not a fully suitable method for comprehensive toxicity testing. On the other hand, it simulates the effects of "normal" precipitation on waste.

When evaluating the results from the TCLP method, the total concentration is divided by 20 (the sample was diluted with extraction liquid weighing 20 times the sample weight) and compared to the TCLP regulatory limits. If the number is less than the TCLP limit, then the waste cannot leach enough of the chemical into the soil and groundwater to be considered a hazardous waste. If the initial concentrations of potentially toxic elements are not present or they are at such low levels that the TCLP limits cannot be exceeded – in this case a TCLP test may not be necessary.

The redox state of the metals found in the Fe complexes of the precipitates is important and the adsorption of As to the hydrated iron oxide (HFO) minerals may not be stable and may change continuously, either due to various geochemical interactions, or due to interactions with various living organisms, in particular bacteria, algae and fungi.

Iron oxidation by bacteria is a spatially and temporally tightly regulated process that ultimately leads to the formation of diverse biogenic Fe oxides, including HFOs, and thus form a perfect substrate for the adsorption of potentially toxic elements such as As(V) (Muehe et al., 2013; Xiu et al., 2019).

Ochre precipitates formed in a 50 L container

The longer time of water accumulation in the container and its slower outflow, led to the precipitation of Fe^{2+} into insoluble Fe^{3+} oxihydroxide phases, and the presence of potentially toxic elements bound in these Fe precipitates pose a risk of their release and mobilization. They can be highly toxic even at low concentrations and can have a negative impact on the environment.

The mobility of potentially toxic elements varied depending on the type of leaching method; the pH of buffering solution. While the bioavailability method simulates an acidic stomach environment with pH 1.5, the TCLP method leaches in a landfill with pH 2.8 and the SPLP method acidic precipitation with pH 4.2. Ochre precipitate (denoted as Fe-HB-Š) was subjected to leaching by all leaching methods. The results show that the mobility of both As and Fe were very low for both SPLP and TCLP

leaching methods. The mobility of As ranged from 0.01 % to 0.04 % for the SPLP and TCLP methods, respectively.

The highest mobility presented Mn above 90 % for the SBET and TCLP method and the least mobile was As. The concentration of As was under the limited values according to the regulatory TCLP limits in the leachate (5 mg/L).

The leachability of each element also depended on the input concentration of the selected element (Fig. 7 , Tab. 3). In the case of the SBET method used, although the mobility of arsenic was only 1.03 %, but due to the extremely high input concentration of As in the sample, the concentration in the leachate was relatively high for As (6.09 mg/L), Fig. 8. The Fe concentration in the leachate after the SBET method also presented a high value of concentration of 621 mg/L but the Fe mobility was minimal for the TCLP and SPLP methods.

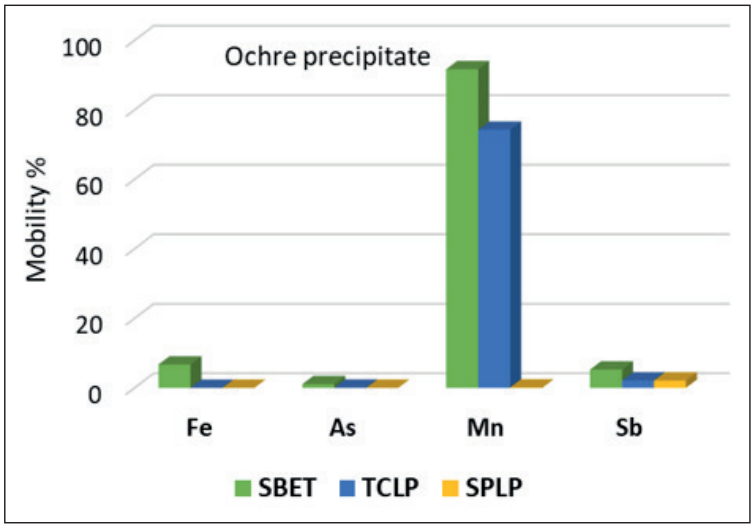

Fig. 7. Mobility of the potentially toxic elements after individual leaching tests in ochre precipitate Fe-HB-Š.

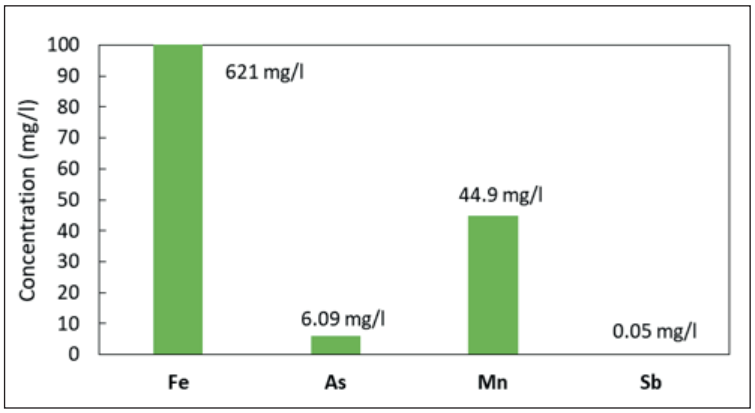

Fig. 8. Concentrations of potentially toxic elements in leachate after SBET bioavailability test in ochre precipitate Fe-HB-Š.

It can be concluded, that both As and Fe mobility were highest when the SBET method was used simulating acid aggressive environment at pH 1.5 and very low mobility was detected for the SPLP method using simulating acid precipitation at pH 4.2. Sb was the most mobile after the SBET method and the same 2 % mobility was shown after the TCLP and SPLP methods. The results indicate stable chemical bonds between Fe and As.

3.3 Sequential extraction analysis (SEA)

Chemical elements can be mobilized and retained in the rock environment by various processes, such as binding to primary and secondary minerals, formation of stable complexes with organic ligands, clays and metal oxyhydroxides (Bourg, 1995). Iron, manganese and aluminium oxyhydroxides are generally stable at neutral to alkaline environmental pH values, and their dissolution occurs under acidic or strongly alkaline conditions (Cheng & Yeh, 1998).

A sample of the resulting ochre precipitate (Fe-HB-Š) from a 50 L container was subjected to sequential extraction analysis to determine the content of potentially toxic elements in the bioavailable and non-available fractions. Each extraction step represents the leaching of a form of the element bound to a specific soil or sediment phase (Žemberyová et al., 2006). The fractions are indicated by the numbers 1–5, which according to the methodology (Mackových et al., 2000) means:

Tab. 3

Concentrations of potentially toxic elements in the ochre precipitate Fe-HB-Š before and after leaching tests

Sample	Element	Input [mg.kg^{-1}]	C_{SBET} [mg.kg^{-1}]	CV [mg.L^{-1}]	SBET [%]	C_{TCLP} [mg.kg^{-1}]	CV [mg.L^{-1}]	Mobility TCLP [%]	C_{SPLP} [mg.kg^{-1}]	CV [mg.L^{-1}]	Mobility SPLP [%]
Fe–HB–Š	Fe	462 190	31 050	621	6.72	9.10	0.46	0.00	6.79	0.34	0.00
	As	29 407	304	6.09	1.03	10.50	0.53	0.04	3.20	0.16	0.01
	Mn	2 449	2 245	44.9	91.7	1 818	90.9	74.2	2.56	0.13	0.10
	Sb	47.67	2.50	0.05	5.24	1.00	0.05	2.10	1.00	0.05	2.10

1. water-soluble fraction: characterizes the proportion of the element soluble in the aqueous phase in the form of inorganic salts;
2. ion-exchangeable and carbonate fraction: the fraction of the element adsorbed by inorganic salts and bound to carbonates, released into the environment when the pH changes from neutral to acidic;
3. reducible fraction; element bound to Fe and Mn oxides, from which it is released into the aquatic environment when Eh conditions change;
4. organic-sulphide fraction: element bound to organic matter and sulphides, released as a result of oxidation and subsequent degradation of organic matter and decomposition of sulphides under changing physicochemical conditions;
5. residual fraction called insoluble residue, encompasses the elements in form of no real risk for organisms present in given environment.

The most mobile fractions are fractions 1 and 2, i.e. the fractions present in the soil solution and in the soil sorption complex respectively.

3.3.1 Ochre precipitates formed in a 50 L container

To understand the physicochemical processes of metal fixation, mobility and transport the sequential extraction analysis of ochre sample was provided.

Based on the results of the sequential extraction analysis of the ochre sample (Fe-HB-Š), it can be concluded that both As and Sb are strongly bound and its amount in the mobile fractions (1) and (2) is almost zero. 98.82 % of arsenic is represented in the residual fraction (5), which means that they are bound to insoluble tertiary mineral phases. In fraction (4), As is present in the amount of 0.88 % where As is bound to organic matter and sulfides and 0.15 % of As is present in the reducible fraction (3). In the case of Fe, 81.98 % is also present in the residual fraction (5), 12.08 % in the reducible fraction (3) and 5.93 % in the organic-sulfide fraction (4). In the case of Mn, up to 52.26 % is bound to the mobile ion-exchangeable and carbonate fraction (2), the residue is represented most in the reducible (3), successively in the residual (5) and least in the organic-sulfidic fraction (4), Tab. 4, Fig. 9. This behaviour of elements correlate with the leaching test results, where the highest Mn mobility was observed after the TCLP test and SBET bioavailability test. The highest abundance in the ion-exchangeable and carbonate fractions (2), means that the element is readily released into the environment when the pH changes from neutral to acidic. These results from the sequential extraction analysis of ochre precipitate indicate, the tight binding of As to Fe oxyhydroxides, where it can bind to various complexes with Fe in $FeAsO^{4-}$, FeOHAs, etc. (Pitter, 1999).

The oxidation of primary minerals in mining areas often results in the formation of coatings or fringes on these minerals called tertiary minerals, which also affects the mobility of several elements. The resulting

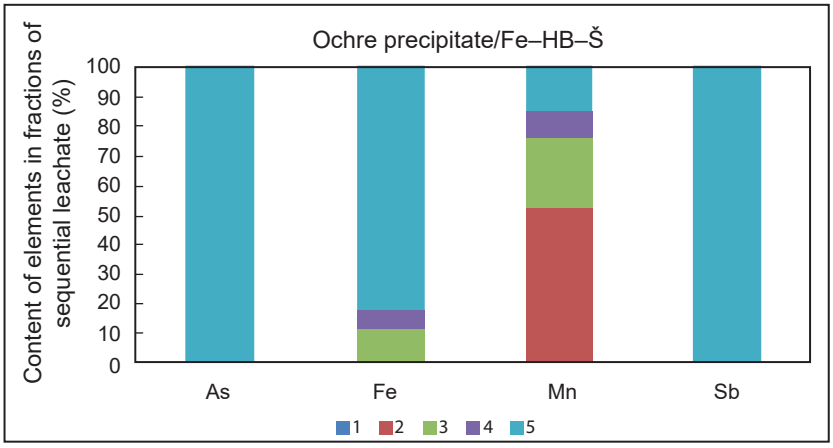

Fig. 9. Amount of extracted element in each extraction step in the ochre precipitate Fe-HB-Š.

Tab. 4

Results of sequential extraction analyses of elements in the ochre precipitate Fe-HB-Š and their amount in individual fractions (%)

Sample	Fraction	As_{TOT} [mg/kg]	As [mg/kg]	As %	Fe_{TOT} [mg/kg]	Fe [mg/kg]	Fe %	Mn_{TOT} [mg/kg]	Mn [mg/kg]	Mn %	Sb_{TOT} [mg/kg]	Sb [mg/kg]	Sb %
Fe–HB–Š	1	24 257	12.1	0.05	399.326	27.3	0.01	2 953	1.94	0.07	41	< 3	0.00
	2		23.2	0.10		16.40	0.00		1 543	52.3		< 3	0.00
	3		37.1	0.15		48 237	12.1		713	24.2		< 3	0.00
	4		214	0.88		23 679	5.93		271	9.18		< 3	0.00
	5		23.971	98.8		327 366	82.0		424	14.3		41	100

coatings may contain elevated concentrations of some elements, e.g. arsenic, iron or antimony. These elevated concentrations of elements in coatings may result from the incorporation of these elements originally present in solution into the coatings during their formation (Majzlan et al., 2011; Hiller et al., 2012). Tertiary precipitates also include gypsum coatings, or the most commonly occurring hydrated iron (or manganese, zinc, and aluminum) sulfates, which can also influence element mobility (Jambor, 1994). Grains of tertiary minerals can be formed by complete replacement of ore or by precipitation from solutions found in mine waste or tailings (Majzlan et al., 2011; Hiller et al., 2012).

3.3.2 Ochre precipitates subjected to leaching tests

The results of the sequential extraction analysis of the ochre precipitate performed after leaching tests is shown in Fig. 10. As was present in the residual insoluble fraction (5) with abundance above 99 % after all leaching tests. The amount of As in the organic-sulfide fraction (4) for each method were as follows: 0.28 % after SBET, 0.46 % after TCLP and 0.66 % after SPLP method. In the reducible fraction (3), 0.12 % As appear for all methods, where it is bound to Fe and Mn oxides, from which it can be released into the aquatic environment when Eh conditions change. A small concentration of As is also present in mobile fractions 1 and 2 (from 0.06–0.15 %), Tab. 5. Fe is also predominantly represented in the last insoluble fraction (5) above 80 % for all leaching methods, then in the reducible fraction (3) and the remainder in the organic-sulphidic fraction (4), Fig. 9. In the case of Mn, the highest proportion of the mobile form 44.01 % is found in the ion-exchangeable and carbonate fractions (2) after SPLP test. For the SBET and TCLP methods, Mn was found in the mobile phases in fraction (2) but also in the water-soluble fraction (1), and the proportion of Mn in the reducible fraction (3) decreased significantly and increased in the residual fraction (5), Fig. 10. The lowest Mn mobility was in the case of the SPLP test with simulated acid rain pH 4.2 , which corresponds with the leaching test results. Increasing the acidity of the

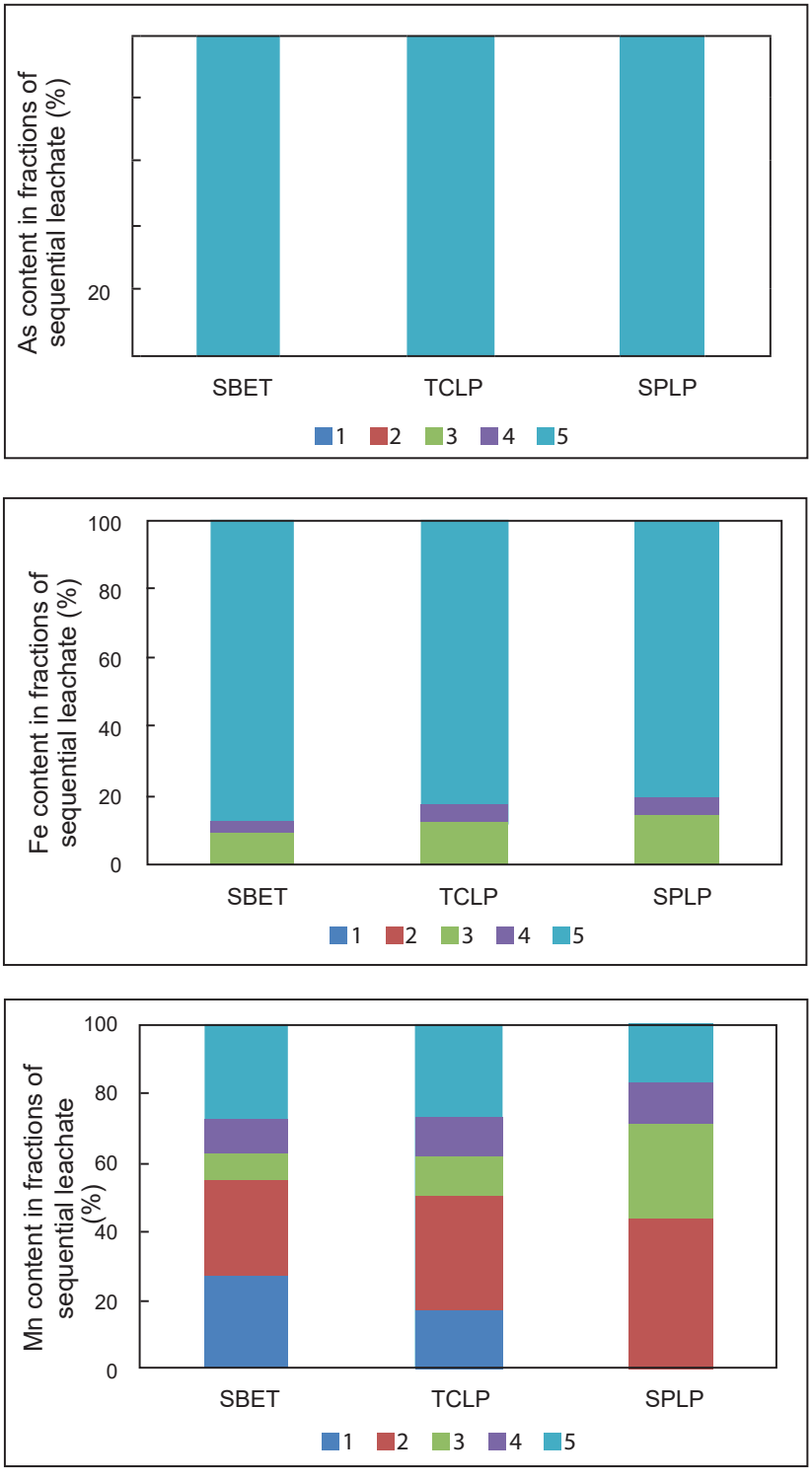

Fig. 10. Amount of extracted element in each exraction step in the ochre precipitate Fe-HB-Š after leaching tests.

Tab. 5

Results of sequential extraction analyses of elements in the ochre precipitate Fe-HB-Š using different leaching methods

Elements		As		Fe		Mn		Sb	
Fe–HB–Š	Fraction	[mg/kg]	%	[mg/kg]	%	[mg/kg]	%	[mg/kg]	%
Ci		**36 693**		**530 948**		**1 314**			
SBET	1	55.0	0.15	1 252	0.24	355	27.0	< 3	0.00
	2	43.0	0.12	1 539	0.29	369	28.1	< 3	0.00
	3	45.0	0.12	46 115	8.69	91.64	6.97	< 3	0.00
	4	102	0.28	20 623	3.88	128	9.72	< 3	0.00
	5	36.448	99.3	461 420	86.9	370	28.2	46.0	100
Ci		**26 111**		**430 725**		**1 589**		**55**	
TCLP	1	16.0	0.06	68.0	0.02	264	16.6	< 3	0.00
	2	19.0	0.07	477	0.11	527	33.2	< 3	0.00
	3	36.0	0.14	53 190	12.35	184	11.6	< 3	0.00
	4	119	0.46	20 736	4.81	185	11.6	< 3	0.00
	5	25 921	99.3	356 254	82.7	429	27.0	55.0	100
Ci		**25 418**		**424 896**		**3 081**		**42**	
SPLP	1	16.0	0.06	55.5	0.01	1.74	0.06	< 3	0.00
	2	21.0	0.08	75.4	0.02	1 356	44.0	< 3	0.00
	3	31.0	0.12	57 680.8	13.6	831	27.0	< 3	0.00
	4	167	0.66	24 803	5.84	361	11.7	< 3	0.00
	5	25 183	99.08	342 281	80.56	531	17.2	42.0	100

Explanatory notes:
Ci – input concentrations of elements in the sample mg/kg
% – percentage of elements in each fraction

leaching solution increased the amount of Mn in the mobile fraction, which seems to be related to the binding of Mn in the form of oxides, from which it is readily released into the aqueous environment when the pH and Eh conditions are changed. Mn becomes soluble at low pH and probably binds to tertiary mineral phases in the residual fraction (5). The elemental amounts and concentration (%) in each fraction are given in Tab. 5.

4 Conclusion

The aim of this study was to study the mobility of potentially toxic elements (As, Sb, Fe and Mn) and to determine their content in the bioavailable and unavailable fractions in the resulting ochre precipitates (Fe precipitates from a 50 L container from previous in situ field experiments) using leaching tests (SBET, TCLP, SPLP) and sequential extraction analysis. The bioavailability of iron was relatively high, 621 mg/L in the leachate, but this represents a mobility of 6.72 % from the input Fe concentration (input 471 000 mg/kg Fe). For As, the mobility was 1.03 % (input 56 945 mg/kg). After TCLP tests (pH = 2.8) simulating conditions of 100 years of leaching in a landfill and SPLP test (pH = 4.2) simulating conditions of waste exposed to 100 years of acid rain, the mobility of Fe and As was minimal, below 0.1 %. Mn was the most mobile element with removed amount above 90 % after the bioavailability and TCLP tests.

The regulatory TCLP limit (5 mg/L) for As in the leachate was not exceeded, indicating that the waste is unable to leach sufficient amounts of the contaminant. Arsenic is probably incorporated directly into the internal structure of the Fe precipitate (formed by hydrated iron oxides) and is bounded to it in internal complexes. It is generally assumed that the porous nature of iron (oxy) hydroxides leads to adsorption of As(V) on internal iron complexation sites.

Even after leaching tests, a sample of ochre precipitate was subjected to a five-step sequential extraction analysis to determine the content of potentially toxic elements in the bioavailable and unavailable fractions. The results from the SEA for Mn correlated with the results from the leaching tests, where the highest Mn mobility was observed after SBET and TCLP tests. Mn was the most mobile element represented predominantly in the (2) ion-exchangeable and carbonate fractions, progressively less in the (5) residual, (3) reducible, and (4) organic-sulfide fractions. In the case of Fe, As and Sb, they were predominantly represented in the residual fraction – non biologically available (5) after all leaching tests. In summary, except of Mn, As and Sb are bounded to tertiary insoluble minerals.

Acknowledgements

The information used in this paper was obtained within the framework of the Operational Programme Quality Environment Programme *Ensuring the monitoring of environmental burdens in Slovakia – Part 2*, which is co-financed by the European Union / Cohesion Fund (application code: NFP310010AXF2). This material is a contribution to the EuroGeoSurveys HORIZON-CSA Geological Service for Europe project. Authors are grateful to reviewers of primary manuscript.

References

Bačová, N., 2006: Niektoré poznatky o banských vodách priestoru Medzev – Zlatá Idka. *Podzemná voda, XII, 1, 39–49.*

Badruzzaman, M., Westerhoff, P. & Knappe, D. R. U., 2004: Intraparticle diffusion and adsorption of arsenate onto granular ferric hydroxide (GFH). *Water Res. 38, 18, 4002–4012, https://doi.org/10.1016/j.watres.2004.07.007.*

Banerjee, K., Aamy, G. L., Prevost, M., Nour, S., Jekel, M., Gallagher, P. M. & Blumenschein, C. D., 2008: Kinetic and thermodynamic aspects of adsorption of arsenic onto granular ferric hydroxide (GFH). *Water Res., 42, 13, 3371–3378, https://doi.org/10.1016/j.watres. 2008.04.019.*

Bekényiová, A., Danková, Z. & Kúšik, D., 2023: Eliminácia arzénu z podzemnej banskej vody – lokalita Zlatá Idka. *e-zborník, Odpadové fórum 2023, Hustopeče, ISBN: 978-80-85990-41-6.*

Bigham, J. M., Schwertmann, U. & Carlson, L., 1992: Mineralogy of precipitates formed by the biogeochemical oxidation of Fe (II) in mine drainage. In: Skinner, H. C. W., Fitzpatrick, R. W. (eds.): Biomineralization Processes of Iron and Manganese: Modern and Ancient Environments. *Catena Suppl., 21, 219–232.*

Bourg, A. C. M., 1995: Speciation of heavy metals in soils and groundwater and implications for their natural and provoked mobility. In: Salomons, W., Förstner, U. & Mader, P. (eds.): Heavy Metals Problems and Solutions. *Springer, 19–31.*

Bryce, C., Blackwell, N., Schmidt, C., Otte, J., Huang, Y., Kleindienst, S., Tomaszewski, E., Schad, M., Warter, V., Peng, C., Byrne & J. M., Kappler, A., 2018: Microbial anaerobic Fe (II) oxidation – ecology, mechanisms and environmental implications. *Environ. Microbiol., 20, 10, 3462–3483, https://doi.org/10.1111/1462-2920.14328.*

Cicmanová, S. & Baláž, P., 2007: Historická ťažba rúd a kvalita prírodného prostredia v okolí obce Zlatá Idka. *Podzemná voda, XIII, 1, 89–99.*

Cornell, R. M. & Schwertmann, U., 2003: The Iron Oxides: Structure, Properties, reactions, Occurences and uses. *Weinheim Publ., ISBN 3-527-30274-3.*

Davis, J. A. & Kent, D. B., 1990: Chapter 5. Surface complexation modeling in aqueous geochemistry. In: Hochella, M. F., White, A. F. (eds.): Mineral-Water Interface Geochemistry. *Rev. Miner., 23, 1, 177–260, https://doi.org/10.1515/9781501509131-009.*

Dzombak, D. A., Asce, A. M. & Morel, F. M. M., 1987: Adsorption of inorganic pollutants in aquatic systems. *Hydraul. Eng., 113, 4, 430–475, https://doi.org/10.1061/(ASCE)0733-9429(1987)113:4(430).*

Fey, D. L., Church, S., Driscoll, R. & Adams, M. G., 2011: Multiple applications of the U.S. EPA 1312 leach procedure. *Geochem.: Explor., Environ., Anal., 11, 163–178.*

Ferris, F. G., Konhauser, K. O., Lyvén, B & Pedersen, K., 1999: Accumulation of metals by bacteriogenic iron oxides in a subterranean environment. *Geomicrobiol. J., 16., 181–192.*

Guo, X., Wu, Z., He, M., Meng, X., Jin, X., Qiu, N. & Zhang, J., 2014: Adsorption of antimony onto iron oxyhydroxides: adsorption behavior and surface structure. *J. Hazard. Mater., 276, 339–345, https://doi.org/10.1016/j.jhazmat.2014.05.025.*

Hiller, E., Petrák, M., Tóth, R., Lalinská-Voleková, B., Jurkovič, Ľ., Kučerová, G., Radková, A., Šottník, P. & Vozár, J., 2013: Geochemical and mineralogical characterization of a neutral, low-sulfide/high-carbonate tailings impoundment, Markušovce, eastern Slovakia. *Environ. Sci. Pollut. Res., 20, 7627–7642, https://doi.org/10.1007/s11356-013-1581-5.*

Chenchen, Q., Wenli, CH., Xiping, H., Peng, C., Chengrong, CH., Xiao-Ying, Y. & Qiaoyun, H., 2019: Review article: Heavy metal behaviour at mineral-organo interfaces: Mechanisms, modelling and influence factors. *Environ. Intern., 131, 104995, https://doi.org/10.1016/j.envint.2019.104995.*

Cheng, H. & Yeh, G., 1998: Development of a three-dimensional model of subsurface flow, heat transfer, and reactive chemical transport: 3dhydrogeochem. *J. Contamin. Hydrol., 34, 1–2, 47–83.*

Jambor, J., Blowes, D. & Ptacek, C., 1994: Mineralogy of mine wastes and strategies for remediation. In: Vaughan, D. & Wogelius, R. (eds.): Environmental mineralogy. *Budapest, Eötvös Univ. press, Eur. Miner. Union Notes miner.*

Kim, K. R., Owens, G. & Naidu, R., 2009: Heavy metal distribution, bioaccessibility and phytoavailability in longterm contaminated soils from Lake Macquarie, Australia. *Aust. J. Soil Res., 47, 166–176.*

Lalinská-Voleková, B., Majerová, H., Kautmanová, I., Brachtýr, O., Szabóová, D., Arendt, D., Brčeková, J. & Šottník, P., 2022: Hydrous ferric oxides (HFO's) precipitated from contaminated waters at several abandoned Sb deposits – Interdisciplinary assessment. *Sci. Total Environ., 821, 153 248, 2–19.*

Liu, T., Chen, D., Li, X. & Li, F., 2019: Microbially mediated coupling of nitrate reduction and Fe (II) oxidation under anoxic conditions. *FEMS Microbiol. Ecol., 95, 4, fiz030, https://doi.org/10.1093/femsec/fiz030.*

Mackových, D., Nováková, N., Šoltýsová, H. & Lučivjanský, P., 2000: Determination of some toxic elements specific forms in soils and sediments after sequential extraction. *4th European Furnace Symposium and 15th Slovak Spectroscopic Conference, Podbanské, 125.*

Majzlan, J., Lalinská, B., Chovan, M., Jurkovič, Ľ., Milovská, S. & Göttlicher, J., 2007: The formation, structure, and ageing of As-rich hydrous ferric oxide at the abandoned Sb deposit Pezinok (Slovakia). *Geochim. Cosmochim. Acta, 71, 17, 4206–4220, https://doi.org/10. 1016/j.gca.2007.06.053.*

Majzlan, J., Lalinská, B., Chovan, M., Bläss, U., Brecht, B., Göttlicher, J., Steininger, R., Hug, K., Ziegler, S. & Gescher, J., 2011: A mineralogical, geochemical, and microbiological assessment of the antimony – and arsenic-rich neutral mine drainage tailings near Pezinok, Slovakia. *Amer. Mineralogist, 96, 1, 1–13, https://doi.org/10.2138/am.2011.3556.*

Mitsunobu, S., Harada, T. & Takahashi, Y., 2006: Comparison of antimony behavior with that of arsenic under various soil redox conditions. *Environ. Sci. Technol., 40, 23, 7270–7276, https://doi.org/10.1021/es060694x.*

Muehe, E. M., Scheer, L., Daus, B. & Kappler, A., 2013: Fate of arsenic during microbial reduction of biogenic versus abiogenic As-Fe(III)-mineral coprecipitates. *Environ. Sci. Technol., 47, 15, 8297–8307, https://doi.org/10.1021/es400801z.*

Pitter, P., 1999: Hydrochemie. 3. vyd. *Praha, VŠCHT.*

Roden, E. E., 2012: Microbial iron-redox cycling in subsurface environments. *Biochem. Soc. Trans., 40, 6, 1249–1256, https://doi.org/10.1042/bst20120202.*

Scheinost, A. C., Rossberg, A., Vantelon, D., Xifra, I. O., Kretzschmar, R., Leuz, A. K., Funke, H. & Johnson, A., 2006: Quantitative antimony speciation in shooting-range soils by EXAFS spectroscopy. *Geochim. Cosmochim. Acta, 70, 13, 3299–3312, https://doi.org/10. 1016/j.gca.2006.03.020.*

Sinha, S., Lee, N. & Amy, G., 2002: Innovative technologies for arsenic removal. *Water Quality and Treatment Conference Seattle, WA.*

Stollenwerk, K., 2003: Geochemical Processes Controlling Transport of Arsenic in Groundwater: *Rev. Adsorpt., Springer, 67–100.*

Stumm, W., 1992: Chemistry of the Solid-Water Interface. *New York, John Wiley, 448 p., ISBN 978-0-471-57672-3.*

Zhang, J. & Stanforth, R., 2005: Slow adsorption reaction between arsenic species and goethite (α-FeOOH). Diffusion or heterogeneous surface reaction control. *Langmuir, 21, 7, 2895–2901, https://doi.org/10.1021/la047636e.*

Žemberyová, M., Barteková, J. & Hagarová, I., 2006: The utilization of modified BCR three-step sequential extraction procedure for the fractionation of Cd, Cr, Cu, Ni, Pb and Zn in soil reference materials of different origins. *Talanta, 70, 973–978.*

Xiu, W., Yu, X., Guo, H., Yuan, W., Ke, T., Liu, G., Tao, J., Hou, W. & Dong, H., 2019: Facilitated arsenic immobilization by biogenic ferrihydrite-goethite biphasic Fe(III) minerals (Fh-Gt Bio-bi-minerals). *Chemosphere, 255, 755–764, https://doi.org/10.1016/j.chemosphere. 2019.02.098.*

Legislative standards

Directive of the Ministry of the Environment of the Slovak Republic of 28 January 2015 No. 1/2015-7 Coll. for the preparation of risk analysis.

US EPA 1311: Hazardous Waste Test Methods / SW-846. https://www.epa.gov/hw-sw846/sw-846-compendium

US EPA 1312: Hazardous Waste Test Methods / SW-846. https://www.epa.gov/hw-sw846/sw-846-compendium

Charakteristika okrových precipitátov obsahujúcich arzén z banskej vody a štúdium ich stability pomocou lúhovacích testov a sekvenčnej extrakčnej analýzy

Štôlňa Hauser je najhlbšie položené horizontálne úvodné banské dielo v celej rudnej oblasti Zlatej Idky. Zo štôlne vyteká neutrálna až slabo alkalická banská voda s priemerným pH 7,3 a vysokým obsahom arzénu (360 µg/l). Vysoký obsah arzénu významne koreluje s obsahom dvojmocného železa. To nám umožňuje predpokladať, že táto vysoko toxická mikrozložka chemického zloženia pochádza z primárneho prostredia formovania chemického zloženia banskej vody – z hĺbky horninového masívu (prítomnosť arzenopyritu v zlatoidčianskom žilnom systéme) (Bačová, 2006). Ide o zdroj kontaminácie, ktorý je permanentný (výtoky zo štôlní, drenážne vody a výluhy banských háld) a bude dlhodobo dotovať povrchovú vodu potokov rizikovými prvkami (Cicmanová a Baláž, 2007). Výtok banskej vody vytvára pod zavaleným ústím štôlne jazierko bez odtoku. Banská voda pravdepodobne vsakuje do sedimentov kvartéru v údolí Idy.

Kritickým parametrom mobility kovov, a teda aj ich biopríustupnosti, je pH. Rozpúšťanie karbonátov a silikátov je dôležitým typom reakcií, ktoré formujú pH vôd. Z hľadiska mocenstva arzénu prítomného vo vodách sa zistilo, že vystupuje len v menej toxickej forme päťmocných iónov. Poukazuje to na výrazné uplatnenie oxidačných podmienok vodného prostredia – pravdepodobne v záverečnej fáze výstupu banskej vody (Cicmanová a Baláž, 2007).

Okrové fázy sa vyzrážajú priamo z banskej vody (alebo úniku z odkaliska). Sú charakteristické pre banské lokality, výtoky zo štôlní a ich okolie v dôsledku oxidácie rozpustného Fe^{2+} na nerozpustné fázy Fe^{3+}. Ide o hydratované oxidy železa (HFO), ktoré môžu zahŕňať niekoľko minerálov, ako napríklad ferihydrit, akaganéit, feroxyhyt, goethit, lepidokrokit a limonit. Sú slabo kryštalické, veľmi pórovité, majú veľký povrch a vďaka tomu sú vynikajúcimi sorbentmi rôznych potenciálne toxických prvkov. Sorpčné vlastnosti hydroxidov železa (HFO) závisia od pH okolitej vody, chemického zloženia vody a pomeru rozpustených stopových kovov k množstvu hydratovaných oxidov železa (Dzombak et al., 1987; Davis a Kent, 1990; Stumm, 1992).

Predchádzajúca štúdia bola zameraná na zníženie koncentrácie As z vytekajúcej banskej vody v dynamických/prietočných podmienkach (Bekényiová et al., 2023). Terénne pokusy in situ pozostávali z navrhnutého systému kontinuálneho pretekania banskej vody tak, že priamo v teréne sa osadili dve 50 l nádoby, cez ktoré nepretržite samospádom pretekala banská voda. Vytekajúca banská voda pretekala cez obe nádoby: odkaľovaciu (osadená vyššie) a filtračnú (osadená nižšie), v ktorej boli do vrstiev uložené rôzne frakcie prírodných sorbentov. V odkaľovacej nádobe sa počas celého trvania experimentu in situ (4 mesiace) prirodzene tvorili okrové zrazeniny viažuce významnú časť arzénu. V priebehu experimentu sme v 50 l odkaľovacej nádobe postupne pozorovali tvorbu a vznik veľkého množstva prirodzene sa vytvárajúcich Fe zrazenín. Pozorovaná jemná vláknitá štruktúra na niektorých miestach súvisí s prítomnosťou železitých baktérií, ktoré zohrávajú významnú rolu v mobilite prvkov. Na základe výsledkov rtg. analýzy možno uvažovať o prevažne amorfnej fáze železitých oxyhydroxidov s malým podielom kryštalického ferihydritu. EDX analýza hrdzavočervených precipitátov z banskej vody zachytených na filtri potvrdila prítomnosť železa v množstve 52 hmot. % aj arzénu 13,2 hmot. % . Z pozorovaného spektra skenovacej elektrónovej mikroskopie boli zreteľne viditeľné duté rúrky, ktoré vzhľadom pravdepodobne zodpovedajú Fe oxidujúcej baktérii *Lepthotrix ochracea*. Ide o známu baktériu, ktorá sa v okroch vyskytuje vo vyššom počte, s pravdepodobným významným vplyvom na rýchlosť kryštalizácie hydratovaných oxidov železa a adsorpciu iónov kovov/metaloidov. Železité baktérie rodu *Leptothrix* tvoria schránky s vyzrážaným železom a oxidujú dvojmocné železo na trojmocný hydroxid železa. To, že môžu adaptívne využívať kovy (alebo iné zlúčeniny) ako akceptory elektrónov, im umožňuje žiť v meniacich sa podmienkach, napr. v prechodnej zóne medzi aeróbnym a anaeróbnym prostredím, a prispôsobiť sa meniacej sa dostupnosti kyslíka.

Cieľom tejto štúdie bolo aj posúdiť mobilitu potenciálne toxických prvkov a stanoviť obsah potenciálne toxických prvkov v biologicky dostupných a nedostupných frakciách vo vzniknutých okrových zrazeninách (Fe precipitáty z 50 l nádoby z predchádzajúcich terénnych experimentov in situ) pomocou lúhovacích testov (SBET, TCLP, SPLP) a sekvenčnej extrakčnej analýzy. Zistená biopríustupnosť železa pomocou metódy SBET bola relatívne vysoká, vo výluhu 621 mg/l, čo ale pri vstupnej hodnote koncentrácie Fe (vstup 471 000 mg/kg Fe) predstavuje mobilitu 6,72 %. V prípade As bola mobilita 1,03 % (vstup 56 945 mg/kg). Po teste TCLP (pH = 2,8), ktorý simuluje podmienky 100-ročného lúhovania odpadu na skládke, a teste SPLP (pH = 4,2) simulujúcom podmienky odpadu vystaveného 100 rokov kyslým dažďom bola mobilita Fe a As minimálna, nižšia ako 0,1 %. Najmobilnejším prvkom bol jednoznačne Mn so zastúpením vo výluhu vyše 90 % po použitej metóde biopríustupnosti SBET a teste TCLP.

Aj napriek pravidelnej závlahe plodín kontaminovanou banskou vodou v susediacej záhrade boli hraničné hodnoty arzénu stanovené len vo vzorke zemiakov. Tento fakt svedčí o nízkej mobilite arzénu.

Regulačný limit TCLP (5 mg/l) As vo výluhu nebol prekročený. To značí, že odpad nedokáže vylúhovať dostatočné množstvo kontaminujúcej látky. Arzén je pravdepodobne zabudovaný priamo do vnútornej štruktúry Fe precipitátu (tvoreného hydratovanými oxidmi železa) a je s ním viazaný do vnútorných komplexov. Vo všeobecnosti sa predpokladá, že porézna povaha (oxy)-hydroxidov železa vedie k adsorpcii As(V) na vnútorných miestach komplexácie železa. Vzorka vzniknutého Fe precipitátu aj po lúhovacích testoch bola podrobená päťstupňovej sekvenčnej extrakčnej analýze s cieľom stanoviť obsah potenciálne toxických prvkov v biologicky dostupných a nedostupných frakciách. Výsledky zo SEA v prípade **Mn** korelujú s výsledkami lúhovacích testov, kde sa najvyššia mobilita Mn prejavila po metóde SBET a TCLP. Mn bol najviac mobilným prvkom zastúpeným prevažne vo (1) vodorozpustnej a (2) v ionovymeniteľnej a karbonátovej frakcii, postupne menej v reziduálnej (5), redukovateľnej (3) a najmenej v organicko-sulfidickej frakcii (4) po týchto testoch. Po lúhovaní metódou SPLP s pH 4,2 došlo k prestúpeniu Mn v prospech (2) ionovymeniteľnej a karbonátovej frakcie, úbytku v (5) reziduálnej frakcii a navýšeniu v (3) redukovateľnej frakcii. **Fe, As** a **Sb** boli vo všetkých vzorkách po všetkých lúhovacích testoch zastúpené prevažne v (5) reziduálnej, teda nemobilnej frakcii. Súhrnne možno konštatovať, že tieto prvky, okrem mangánu, sú viazané na terciárne, ťažko rozpustné minerály.

Tam, kde v okolí výtokov banskej vody dochádza k intenzívnej sedimentácii okra, je potrebné posúdiť, či nie je vhodné tento sediment preventívne odstraňovať a ukladať ho na miesto, kde nespôsobí kontamináciu pôdy a vodných tokov.

Doručené / Received: 21. 11. 2023
Prijaté na publikovanie / Accepted: 21. 12. 2023

Mineralia Slovaca, Web ISSN 1338-3523, ISSN 0369-2086, https://doi.org/10.56623/ms.2023.55.2.5
55, 2 (2023), 157 – 166, © Authors 2023. CC BY 4.0

The impact of increased calcium and magnesium content in drinking water on arterial stiffness and the cardiovascular system in humans: A case study in Kokava nad Rimavicou, Slovak Republic

PATRIK ČERMÁK[1], VERONIKA CVEČKOVÁ[2], IGOR HAJDUK[3], ĽUBOMÍR JURKOVIČ[1] and STANISLAV RAPANT[1]

[1]Faculty of Natural Sciences, Comenius University, Ilkovičova 6, Bratislava, Slovak Republic; cermak25@uniba.sk; lubomir.jurkovic@uniba.sk
[2]State Geological Institute of Dionýz Štúr, Mlynská dolina 1, Bratislava, Slovak Republic
[3]Institute for Occupational Rehabilitation of Citizens with Disabilities, Mokrohájska 1, Bratislava, Slovak Republic

Abstract: In the village of Kokava nad Rimavicou, we enriched the drinking water with Ca and Mg using a recarbonatization reactor (RR). In the RR, carbonate rock is dissolved using CO_2. In the RR, we produce a concentrate with a Ca and Mg content of approximately 100 mg.l^{-1}, which is then added directly to the water reservoir at a ratio of approximately 1 : 10. On average, the Ca and Mg content in the drinking water increased by 10–15 mg.l^{-1}. Subsequently, we monitored the positive effect of the increased Ca and Mg content in the drinking water by measuring the arterial stiffness of the residents, which characterizes the state of the cardiovascular system (CVS) of people. We measured the arterial stiffness four times in six-month intervals. The first time was before the start of the enrichment of the drinking water with Ca and Mg, and subsequently three times after the enrichment. The increased content of Ca and Mg in the drinking water resulted in a significant improvement in the arterial stiffness. The arterial age of the people improved by approximately ten years, and the speed of the pulse wave velocity decreased by 0.9 m.s^{-1}.

Key words: Arterial stiffness, Ca, Mg, cardiovascular system, drinking water, recarbonatization

Graphical abstract

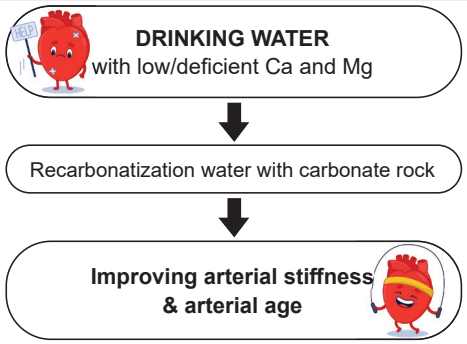

Highlights

- **Cardiovascular Impact:** Increased Ca and Mg content improves arterial stiffness, demonstrating potential health benefits and offering a practical intervention for mineral deficiencies.
- **Innovative Solution:** The study introduces a recarbonatization reactor to address calcium and magnesium deficiency in drinking water.

Introduction

The impact of deficient levels of Ca and Mg in drinking water on the cardiovascular system of humans has been known for over 70 years (Kobayashi, 1957). Since then, this influence has been confirmed by thousands of studies conducted in various countries around the world, including several meta-analyses (e.g., Catling et al., 2008). The deficient levels of Ca and Mg in drinking water have also been associated with increased incidence/mortality of oncological diseases and diabetes mellitus over the past 20–30 years (e.g., Yang et al., 1998; Naumann et al., 2017). Furthermore, it has been confirmed that individuals supplied with "soft" drinking water have a shorter lifespan by 4–5 years compared to those supplied with "hard" drinking water (Rapant et al., 2021). A very illustrative example of the impact of deficient levels of Ca and Mg in drinking water is observed in countries where drinking water produced from seawater using reverse osmosis has been used for drinking purposes. This water is characterized by an extremely low content of Ca and Mg, resulting in increased incidence/mortality of cardiovascular and oncological diseases in these countries (e.g., WHO, 2011; Lesimple et al., 2020).

In this study, we address the issue of deficient levels of Ca (< 30 mg.l^{-1}) and Mg (< 10 mg.l^{-1}) in drinking water by enriching (recarbonating) drinking water using RR. We increase the content of Ca and Mg by approximately

10–15 mg.l^{-1}. Subsequently, we observe how this increased content of Ca and Mg in drinking water affects arterial stiffness. The main objective of this study is to determine whether there is an improvement in the cardiovascular system of individuals (which is monitored by measuring arterial stiffness) originally supplied with "soft" drinking water after enriching this water with Ca and Mg.

Area description

The village of Kokava nad Rimavicou (KnR) has a population of approximately 3,000 inhabitants and is located in the southern part of the Slovak Republic (SR) (Fig. 1). It is supplied with potable water from the Klenovec reservoir. After treatment and disinfection, the potable water is led by pipeline to the local water reservoir in the village Kokava nad Rimavicou. The rock environment around the Klenovec reservoir is mainly composed of granitoid and metamorphic rocks, resulting in water with very low mineralization and very low levels of Ca and Mg (Tab. 1). The reservoir in the village Kokava nad Rimavicou is supplied by water quantity according to the current consumption, which averages at approximately 100,000 m^3 per year. In the summer months, consumption is approximately 20–30 % higher than in the winter months, with an average consumption of approximately 3.0 l.s^{-1}.

The Slovak drinking water standard only provides recommended values for Ca and Mg contents and water hardness (measured as Ca + Mg in mmol.l^{-1}). As shown in Tab. 1, the values for these parameters are at the lower end of the recommended range. The health status of the inhabitants of the village of KnR is significantly worse compared to the average of the Slovak Republic, especially regarding cardiovascular diseases (CVD). The relative mortality rate from CVD in the KnR village is 882.4 (period 1995–2006), almost 65 % higher compared to the SR average of 531.2 (Rapant et al., 2019; Cvečková & Rapant, 2022). The aforementioned increased mortality from CVD is mainly associated with low content of Ca (19 mg.l^{-1}) and Mg (3.5 mg.l^{-1}) in drinking water. Based on the risk analysis, an increased health risk from Ca and Mg deficiency and low hardness of water for the local population has been confirmed (Rapant et al., 2020; Cvečková & Rapant, 2022). The mean hazard quotient level for deficient elements (HQ_d) was found to be 1.59 for Ca, 1.59 for Mg, and 1.56 for hardness water, which is a medium level of health risk. The hazard index for deficient elements (HI_d) for these three parameters was 4.7, which is at a high risk level of developing chronic diseases. To reduce the level of health risk to a low risk level, it is necessary to increase the content of Ca and Mg in drinking water in the KnR village by approximately 10 mg.l^{-1}.

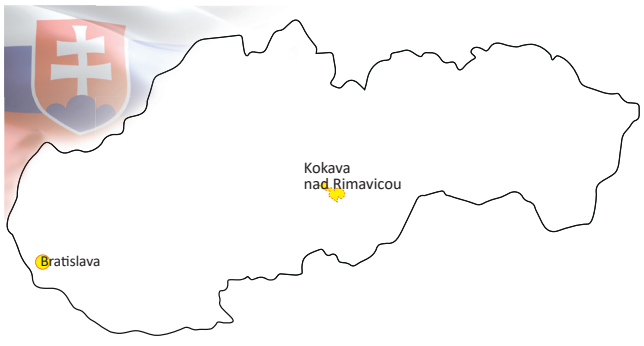

Fig. 1. Position of studied locality Kokava nad Rimavicou in Slovakia.

Ta b. 1

Ca, Mg and water hardness contents of drinking water in Kokava nad Rimavicou compared to the standard values of the Slovak drinking water standard and proposed concentrations of Ca, Mg and water hardness after recarbonatization (RC)

	Ca	Mg	Water hardness
	[mg.l^{-1}]		[mmol.l^{-1}]
Kokava nad Rimavicou	19.1	3.52	0.62
Slovak drinking water standard*	> 30	10–30	1.1–5.0
Proposed values after RC**	25–30	8–12	1.1–1.3

* Decree of the Ministry of Health No. 247/2017 Coll.
**The proposed values are based on a risk analysis.

Materials and Methods

Carbonate Rock Leaching

To increase the mineral content of drinking water, Half-burnt dolomite (HBD) is utilized as a rock material due to its high solubility of carbonatic rocks (Tuček et al., 2017). HBD is produced by annealing dolomite [$CaMg(CO_3)_2$] at a temperature range of 600–800 °C, which results in the conversion of magnesium carbonate to magnesium oxide. When HBD is dissolved in the liquid phase, magnesium ions are preferentially released due to the higher solubility of magnesium oxide compared to magnesium carbonate. Magno-Dol, a type of HBD with a size fraction of 2.0–4.5 mm and approved for drinking water treatment in the European Union (EU), contains approximately 98.2 % Ca and Mg oxides and carbonates, 0.9 % Si, Al, and Fe oxides, 0.8 % water, and less than 0.1 % of other elements. Only trace amounts of toxic heavy metals are present. For dissolving HBD, food CO_2 from Messer Tatragas, which is approved for food purposes by the EU and contains over 99 % CO_2 is used.

Design of a Fluidized Bed Recarbonatization Reactor

The process of recarbonatization is used to increase the content of Ca and Mg in drinking water. Various processes and carbonate rocks are used for RC, typically under CO_2 saturation. Flow-through systems are often used, where carbonate rock is added to a device through which the treated water flows (e.g., Al-Rqobah & Al-Munayyis, 1989; Withers, 2005; Luptáková & Derco, 2015). To enrich the drinking water in the village of KnR with Ca and Mg, a prototype of a fluidized bed recarbonatization reactor (RRF) was developed (Fig. 2, 3). The RRF contains a layer of solid particles of half-burnt dolomite, which is kept in motion by the bottom-up flow of water to intensify the dissolution process of the carbonate rock. The recarbonatization reactor was placed directly into the water reservoir without any technical interventions. The device consists of two main parts, the reactor and a circulation tank. The reactor is approximately 3.5 meters tall, cylindrical with a diameter of 40 centimeters, and has a dosing tank on top for adding HBD. The volume of the reactor is approximately 2 m^3, and it is connected to the circulation tank with a volume of approximately 10 m^3. The system is powered by two pumps: one serves as a circulation pump to circulate water between the reactor and the circulation tank, while the other pumps the produced concentrate into the water reservoir. Carbon dioxide is supplied from pressurized bottles with serial concentration. Three circulation pumps with a capacity of 6.8 $m^3.sec^{-1}$ were used. The dosing pump has a capacity of up to 2 $m^3.h^{-1}$, while the output of the circulation pump is approximately 10 times higher.

This allows for multiple rinsing of the carbonate rock, which results in the formation of a concentrate with a Ca and Mg content ranging from 500 to 1,000

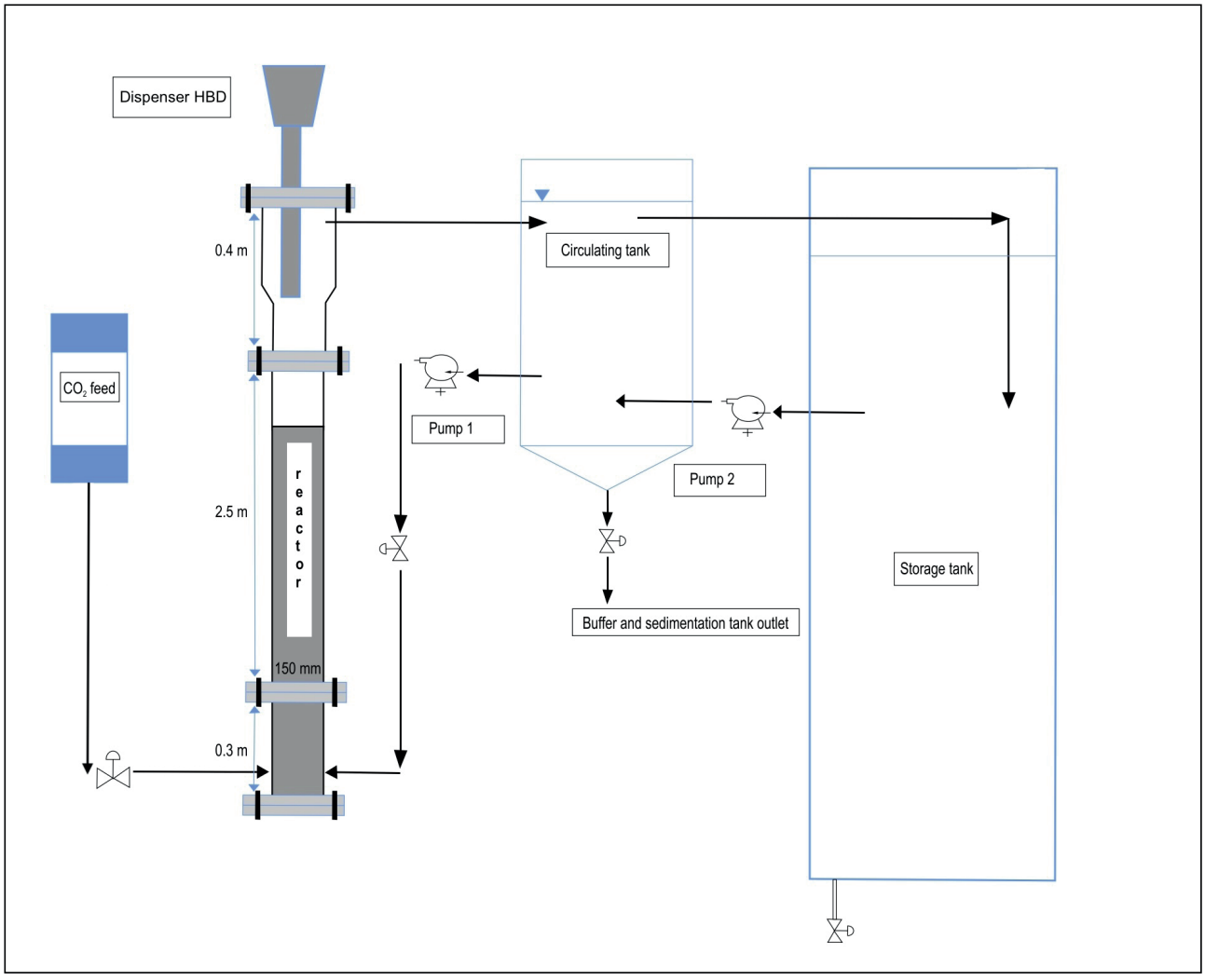

Fig. 2. Schematic diagram of the drinking water recarbonatization plant at the water source in the village of Kokava nad Rimavicou.

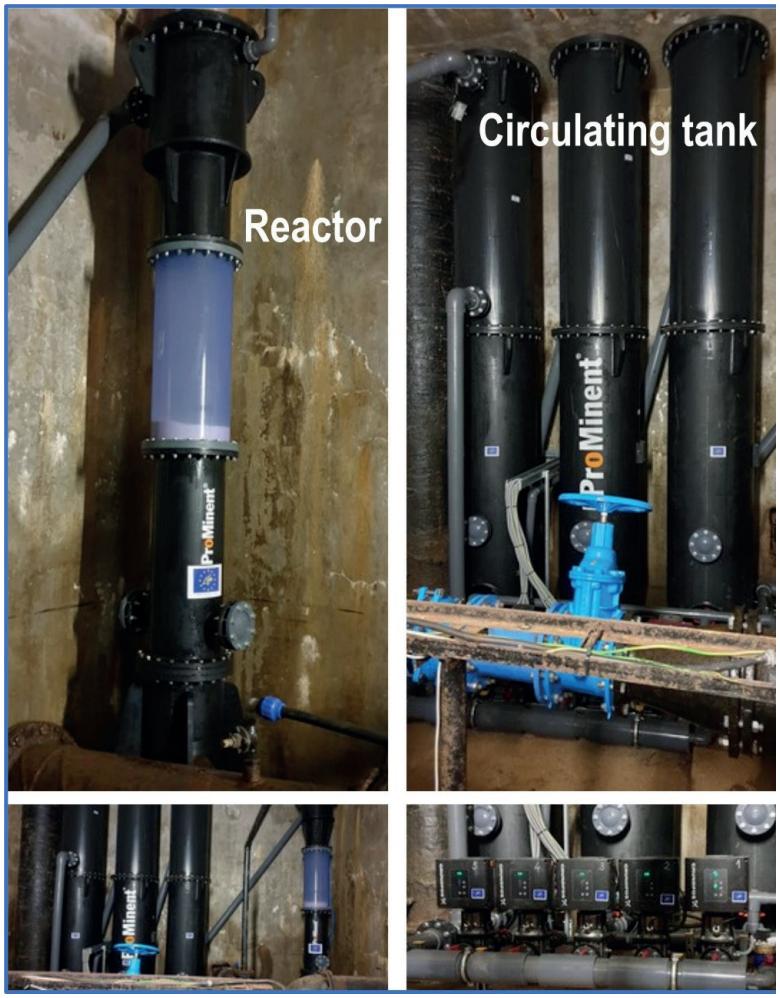

Fig. 3. Recarbonatization reactor at the Kokava nad Rimavicou water source.

milligrams per liter. The concentrate is added directly to the water reservoir in a ratio of approximately 1 : 10 to the water consumption. The circulation and dosing pumps are equipped with frequency converters, which can be easily adjusted as needed. A photovoltaic system was built to provide electricity for powering the pumps. Detailed technical documentation of the recarbonatization reactor is available on the website https://fns.uniba.sk/lifewaterhealth/or Cvečková & Rapant (2022). The production of RR in KnR drew upon the expertise gained from manufacturing a comparable RR in the village of Devičie (Rapant et al., 2022).

Measurement of arterial stiffness

The concept of "arterial stiffness" has only entered our awareness in the last 20–30 years. This phrase is a general term that refers to the loss of arterial compliance or changes in vessel wall properties, or both (Shirwany et al., 2010). The measurement of arterial stiffness is a simple technique that has become a useful non-invasive approach to health prevention in the past 20 to 25 years (DeLoach et al., 2008). Markers of arterial stiffness, such as increased aortic pulse wave velocity and increased central aortic pressure, are independent predictors of cardiovascular risk (Illyes, 2005). These markers represent tissue biomarkers of the arteries and have been shown to be better prognosticators than traditional blood pressure measurements, as well as biomarkers in the bloodstream. Furthermore, their significant predictive value specifies the risk assessment provided by traditional risk factors. The measurement of arterial stiffness provides insights into the actual pathological processes through the evaluation of the loss of elasticity of the aorta. Over time, endothelial damage progresses and causes damage to the arterial elasticity, resulting in the loss of elasticity of the vessel wall. In this study, measurements were performed with an arteriograph (Fig. 4) developed in Hungary and patented in over 30 countries (Arteriograph, TensioMed Ltd., Budapest, Hungary). The arteriograph can easily measure, without any health risk, physiological parameters characterizing the state of arteries that are independent of other known risk factors (age, sex, blood pressure, cholesterol, smoking) and can reliably assess the state of the car-

Fig. 4. Arterial stiffness measurement with arteriograph.

diovascular system and predict the risk of complications in asymptomatic, apparently "healthy" patients. These parameters are also confirmed by international guidelines for the diagnosis of target organ damage (Williams et al., 2018). The influence of Ca and Mg content in drinking water on the improvement of arterial stiffness has been demonstrated in the work of Rapant et al. (2019). The Ca and Mg content in drinking water had a greater impact on arterial elasticity than other factors such as obesity, BMI index, smoking, and so on.

We measured arterial stiffness on approximately 60 volunteers in the village of KnR. The basic condition was that the volunteers had a permanent residence in the village for at least five years. People who had been treated for cardiovascular diseases and other diagnoses (especially diabetes mellitus and kidney diseases) were excluded from the measurements. All participants in the measurement gave written consent for the study, and before the measurement, they completed a short questionnaire about their health status, age, height, weight (BMI index), smoking, and alcohol consumption. For the purpose of the study, an ethical commission was established at the Regional Public Health Office based in Zvolen (minutes 1/2021 dated 05. 09. 2021). The basic characteristics of the volunteers from the KnR village are presented in the Tab. 2.

Tab. 2

Basic characteristics of volunteers from the KnR village

Age	BMI	Gender	Smoking habbits	Alcohol consumption
53*	28.5*	Male 15	Yes 14	Regularly 0
56**	27.45**	Female 41	No 41	Occasionally 31
16–69***	19.5–53***			Abstinent 25

* average ** median *** dispersion

Selected volunteers underwent four measurements of arterial stiffness. The first measurement was conducted before the enrichment of drinking water with Ca and Mg, and the following three measurements were conducted approximately every six months after the enrichment of drinking water with Ca and Mg. The results of arterial stiffness measurement are expressed using pulse wave velocity PWVao ($m.s^{-1}$) and arterial age. The lower the pulse wave velocity, the better the condition of the arteries. Similarly, the lower the arterial age (age of the arteries), the better the condition. In a normal case, arterial age corresponds to the actual age. If the condition of the arteries is unfavorable, the arterial age is higher than the actual age and vice versa. Therefore, the results of arterial age are expressed as the difference between arterial age and actual age. The lower this difference, the more favorable the condition of the arteries. In the best case, this difference takes negative values, which means that the age of the arteries is lower than the actual age. Further details on the methodology of arterial stiffness measurement depending on the content of Ca and Mg in drinking water are available in the work of Rapant et al. (2019) and directly in KnR in the work of Cvečková and Rapant (2022).

Results

Recarbonatization of drinking water

The recarbonatization reactor in the KnR village was put into operation on July 12, 2021.

The basic conditions for recarbonatization were as follows:

- Average daily water consumption in KnR: 275–300 m^3.
- Average daily dose of produced and added concentrate: 25–30 $m^3.day^{-1}$.
- Mixing ratio of concentrate and water from the reservoir: 1 : 9 (1 : 10).
- Performance of the circulation pump: approximately 10 $m^3.h^{-1}$.
- Average dose of added HBD: 50 kg per week.
- Average amount of added CO_2: 230–240 kg per week.
- Total volume of the reservoir: 1,300 m^3.
- Target values for recarbonatization: Ca 25–30 $mg.l^{-1}$, Mg 8–12 $mg.l^{-1}$, (Ca + Mg) 1.1–1.3 $mmol.l^{-1}$.

After the RR was put into operation, a malfunction occurred in the reactor hydraulics. The reactor operated at only about 20 % capacity. Due to the COVID-19 pandemic, it took approximately 90 days to resolve the issue and ensure the reactor was operating at full capacity. After that, the RR worked reliably until the end of the LIFE-WATER and HEALTH project (December 31, 2022). The results of the recarbonatization of drinking water in KnR for the years 2021–2022 are shown in Tab. 3.

The Tab. 3 shows values of Ca, Mg, water hardness, and conductivity at the output in the village (in the branch of the local waterworks center), approximately 2 km from the water source. From April 2022, the local water company began to enrich drinking water with Ca using calcium hydroxide [$(Ca(OH)_2$]. This was reflected by an increase in the content of Ca in drinking water in KnR.

Tab. 3

Results of drinking water recarbonatization in KnR for the years 2021–2022

Month	Ca	Mg	Water hardness	Conductivity
	[mg.l^{-1}]		[mmol.l^{-1}]	[µS.cm^{-1}]
2021				
Original state	19.1	3.5	0.62	110
August	19.9	4.1	0.66	116
September	25.6	4.9	0.83	145
October	30.7	6.9	1.04	165
November	30	8.8	1.11	202
December	32.5	9.2	1.18	222
2022				
January	32.9	14.0	1.39	202
February	33.2	13.2	1.33	210
March	35.6	12.8	1.41	225
April	46.4	12.6	1.68	259
May	31.3	9.9	1.19	205
June	42.7	12.5	1.58	235
July	44.8	13.2	1.64	242
August	38.6	11.7	1.44	250
September	42.4	12.8	1.58	239
October	39.6	11.1	1.44	225
November	44.8	15.2	1.74	261
December	40.2	12.8	1.53	229

Measurement of arterial stiffness

The first initial measurement of arterial stiffness was carried out in the village of KnR in May 2021. Sixty-four volunteers participated in the measurements. Due to their advanced age (over 67 years), four volunteers were excluded from the sample. This stage took place during a period when the residents were supplied with "soft" drinking water (Ca 19 mg.l^{-1}, Mg 3.5 mg.l^{-1}). The next three stages of arterial elasticity measurements were carried out at approximately six-month intervals after enriching drinking water with Ca and Mg (Ca 45 mg.l^{-1}, Mg 10–15 mg.l^{-1}). Due to the COVID-19 pandemic, we could not follow the planned six-month interval for the measurements. Measurements were conducted at 5–7 month intervals due to quarantine. Additionally, not all respondents who participated in the first arterial stiffness measurement were able to participate in the measurements of the II.–IV. stages due to COVID-19. Therefore, we also used a smaller sample of substitute volunteers. For this reason, we present the results first without substitute volunteers, and also with substitute volunteers. The results of the arterial stiffness measurement of the inhabitants of the KnR village are shown in tables 4 and 5, and the entire arterial stiffness measurement database is available on the project website (http://fns.uniba.sk/lifewaterhealth/).

Tab. 4

Results of the arterial stiffness measurement of respondents in the village of Kokava nad Rimavicou, all respondents

	Measurement date	Number of respondents	PWVao	Actual age	Arterial age	Difference Arterial age – actual age
			[m.s^{-1}]	[years]		
I.	May 2021	60	**9.7**	54.11	64.18	**10.07**
II.	December 2021	53	**9.54**	53.69	62.77	**9.08**
III.	June 2022	56	**9.37**	52.3	61.35	**9.5**
IV.	December 2022	73	**8.91**	54.43	55.58	**1.15**

Tab. 5

Results of the arterial stiffness measurement of respondents in the village of Kokava nad Rimavicou, excluding substitute respondents

Measurement stage	Measurement date	Number of espondents	PWVao	Actual age	Arterial age	Difference Arterial age – actual age
			[m.s^{-1}]	[years]		
I.	May 2021	60	**9.7**	54.11	64.18	**10.07**
II.	December 2021	46	**9.42**	53.74	61.24	**7.5**
III.	June 2022	49	**9.25**	53.4	59.76	**6.36**
IV.	December 2022	52	**8.83**	54.53	54.67	**0.14**

Discussion

Calcium and magnesium are very important essential elements. For healthy human development, their content in drinking water should be at least at the level of Mg 10–20 mg.l^{-1} and Ca 30–50 mg.l^{-1} (e.g., Rosborg & Kožíšek, 2020). As can be seen from Tab. 3, after the initial technical problems (first 90 days of operation), the reservoir operated reliably. We increased the Ca and Mg content in the drinking water in KnR to the desired level without any problems, by approximately 10–20 mg.l^{-1}. We then tested the reactor, varying the performance of the circulation pumps, the amount of concentrate discharged, the amount of HBD added, and also the amount of CO_2. The process of dissolving HBD is mainly influenced by the performance of the circulation pump and the amount of added rock. The amount of added CO_2 needs to be limited to such an extent that the residual free CO_2 does not exceed the level of 60–80 mg.l^{-1}. A relatively large amount of rock micro-particles is released during the fluidization process. The produced concentrate is turbid. However, these micro-particles dissolve in the reservoir water due to the residual free CO_2, thereby increasing the Ca and Mg content in the drinking water by 10–15 %. Therefore, there is no risk of acidification. The resulting pH of the water in the village increased only slightly, from about 7.2 to 7.3 and the free CO_2 content from about 4 mg.l^{-1} to 8 mg.l^{-1}. The optimal reactor setting, at which we can ensure an increase in the Ca and Mg content in drinking water by 10–15 mg.l^{-1} at the lowest possible operating costs, was a circulation pump performance in the range of 7–9 m^3. h^{-1}, the amount of added HBD of 7–8 kg.day^{-1}, and the amount of CO_2 of 15–17 kg.day^{-1}. It is clear from the above that the reactor operated at only about half power, and at maximum reactor output, we can increase the Ca and Mg content by up to for Ca 50 mg.l^{-1} and for Mg 25 mg.l^{-1}. An advantage of the RRF prototype we developed is the relatively low operating costs, which are approximately €0.1 per m^3 of drinking water. More detailed results of recarbonatization under different conditions are available on the website http://fns.uniba.sk/lifewaterhealth/ and in the work of Cvečková and Rapant (2022). From the results of the measurements of arterial stiffness (Tab. 4, 5), it is evident that there was a significant improvement in the condition of the arteries of the residents of the KnR village after enriching the drinking water with Ca and Mg. This was reflected in the decrease in the pulse wave velocity and the reduction in the arterial age of the people. The pulse wave velocity decreased in all volunteers (9.7 to 8.91) and also in the case of volunteers without replacements (9.7 to 8.83). Similarly, the arterial age of the people, expressed as the difference between the arterial age and the actual age, was significantly reduced. In the case of all volunteers, it decreased from 10.07 to 1.15 years and in the case of volunteers without replacements, it decreased from 10.07 to 0.14 years. The values of PWVao and arterial age of the KnR residents have already approached the level of the Central European average (Rapant et al., 2019). Improvement in arterial age and PWVao is truly significant. It can be explained only by the fact that we increased the content of Ca and Mg in drinking water, up to 2–3 times compared to their original levels. These results can hardly be confronted with other works because, to our best knowledge, there is no literature documenting the relationship between arterial stiffness and water hardness, with the exception of older publications by the authors (Rapant et al., 2019). However, it should be noted that medical studies clearly show the protective role of Mg and Ca for arteries (Hruby et al., 2014; Uemura et al., 2014). Magnesium deficiency has been shown to have a detrimental effect on arterial elasticity (Joris et al., 2016; Kostov & Halacheva, 2018), and it is well known that the state of arteries has a direct relationship to the development of cardio-vascular diseases (Shirwany et al., 2010).

Other risk factors for the development of cardiovascular diseases, such as stress, genetic predisposition, BMI, excessive alcohol consumption, and smoking, also influence the cardiovascular system and consequently the arterial stiffness, in addition to the content of calcium and magnesium in drinking water. However, statistical testing has shown that the content of Ca and Mg in drinking water has a much greater impact on arterial stiffness than, for example, BMI and smoking (Rapant et al., 2019).

Conclusion

The results presented in the article clearly confirmed the improvement of arterial stiffness, thus the cardiovascular system of KnR residents, after consuming drinking water enriched with Ca and Mg. This improvement was reflected in a significant reduction in pulse wave velocity and arterial age of people. The findings unambiguously substantiate that, beyond the conventional risk factors associated with the onset of CVD, such as stress, obesity, genetic predisposition, smoking, and excessive alcohol consumption, the content of Ca and Mg in drinking water constitutes an equally significant contributing factor to the emergence of CVD. The deficient content of Ca and Mg in drinking water not only worsens the condition of the human cardiovascular system but also increases the mortality rate from other diseases, especially cancer and diabetes mellitus. It also results in a shorter lifespan by up to five years compared to people who are supplied with "hard" drinking water. Therefore, we believe that, based on many studies published in the world literature, Ca and Mg should be included among the regulated parameters of drinking water. We also believe that the content of Ca and Mg in bottled drinking water should be regulated, especially in cases where bottled drinking water is produced by desalination of seawater.

Acknowledgments

This research was funded by the project *Improvement of health status of population of the Slovak Republic through drinking water recarbonization LIFE – Water and Health LIFE17 ENV/SK/000036*.

References

Al-Rqobah, H. E. & Al-Munayyis, A. H., 1989: A recarbonation process for treatment of distilled water produced by MSF plants in Kuwait. *Desalination, 73, 2595–2312.* https://doi.org/10.1016/0011-9164(89)87020-1.

Catling, L. A., Abubakar, I., Lake, I. R., Swift, L. & Hunter, P. R., 2008: A systematic review of analytical observational studies investigating the association between cardiovascular disease and drinking water hardness. *J. Water Health, 6, 4, 433–442.* https://doi.org/10.2166/wh.2008.054.

Cvečková, V. & Rapant, S., 2022: Improvement of health status of population of the Slovak Republic through drinking water re-carbonization. *Bratislava, Comenius University, Faculty of Natural Sciences*, https://fns.uniba.sk/lifewaterhealth/. Accessed 2 May 2023. ISBN 978-80-223-5488-2. – ISBN 978-80-223-5489-9. In Slovak.

DeLoach, S. S. & Townsend, R. R., 2008: Vascular stiffness: Its measurements and significance for epidemiologic and outcome studies. *Clin. J. Am. Soc. Nephrol., 3, 184–192*. https://doi.org/10.2215/cjn.03340807.

Hruby, A., O'Donnell, C. J., Jacques, P. F., Meigs, J. B., Hoffmann, U. & McKeown, N. M., 2014: Magnesium intake is inversely associated with coronary artery calcification. The Framingham Heart Study. *Jacc Cardiovasc. Imaging, 7, 59–69*. doi:10.1016/j.jcmg.2013.10.006.

Illyes, M., 2005: A new and fast screening method for measuring complex hemodynamical parameters and arterial stiffness non-invasively with a simple arm cuff. *American Journal of Hypertension, 18, S4, 15A.* https://doi.org/10.1016/j.amjhyper.2005.03.035.

Joris, P. J., Plat, J., Bakker, S. J. L. & Mensink, R. P., 2016: Long-term magnesium supplementation improves arterial stiffness in overweight and obese adults: Results of a randomized, double-blind, placebo-controlled intervention trial. *Am. J. Clin. Nutr. 2016, 103, 1260–1266*, doi:10.3945/ajcn.116.131466.

Kobayashi, J., 1957: Studies on the drinking water of Japanese. Archives of *Environmental Health*: *An International Journal, 14, 3, 305–317*.

Kostov, K. & Halacheva, L., 2018: Role of magnesium deficiency in promoting atherosclerosis, endothelial dysfunction, and arterial stiffening as risk factors for hypertension. *Int. J. Mol. Sci. 2018, 19, 1724*. doi:10.3390/ijms19061724.

Lesimple, A., Ahmed, F. E. & Hilal, N., 2020: Remineralization of desalinated water: Methods and environmental impact. *Desalination, 496, 15*, *114692*. https://doi.org/10.1016/j.desal.2020.114692.

Luptáková, A. & Derco, J., 2015: Improving Drinking Water Quality by Remineralisation. *Acta Chim Slov., 62, 4, 859–866.* https://doi.org/10.17344/acsi.2015.1590. PMID: 26680713.

Naumann, J., Biehler, D., Lüty, T. & Sadaghiani, C., 2017: Prevention and Therapy of Type 2 Diabetes-What Is the Potential of Daily Water Intake and Its Mineral Nutrients? *Nutrients*. *Aug 22, 9, 8, 914.* https://doi.org/10.3390/nu9080914. PMID: 28829398; PMCID: PMC5579707.

Rapant, S., Cvečková, V. & Čermák, P., 2022: Enrichment of drinking water with Ca and Mg by a fluidized bed recarbonization reactor: a case study of Devičie, Slovak Republic. *Journal of Water and Health, 20, 4, 630.* doi: 10.2166/wh.2022.252.

Rapant, S., Cvečková, V., Fajčíková, K., Hajdúk, I., Hiller, E. & Stehlíková, B., 2019: Hard Water, More Elastic Arteries: A Case Study from Krupina District, Slovakia. *Int. J. Environ. Res. Public Health, 16, 1521.* https://doi.org/10.3390/ijerph16091521.

Rapant, S., Cvečková, V., Hiller, E., Jurkovičová, D., Kožíšek, F. & Stehlíková, B., 2020: Proposal of New Health Risk Assessment Method for Deficient Essential Elements in Drinking Water-Case Study of the Slovak Republic. *Int. J. Environ. Res. Public Health*. *Aug. 14, 17, 16, 5915.* https://doi.org/10.3390%2Fijerph17165915. PMID: 32824039; PMCID: PMC7459771.

Rapant, S., Letkovičová, A., Jurkovičová, D., Kosmovský, V., Kožíšek, F. & Jurkovič, Ľ., 2020: Differences in health status of Slovak municipalities supplied with drinking water of different hardness values. *Environ. Geochem. Health, 2021 Jul, 43, 7, 2665–2677.* https://doi.org/10.1007/s10653-020-00664-6. Epub Jul 22. PMID: 32700094.

Rosborg, I. & Kožíšek, F. (ed.), 2020: Drinking water minerals and mineral balance. Importance, health significance, safety precautions. 2nd ed. *Springer International Publishing Switzerland, Springer Verlag,* ISBN 978-3-03018033-1 (Print), 978-3-030-18034-8 (eBook).

Shirwany, N. & Zou, M. H., 2010: AMPK in cardiovascular health and disease. *Acta Pharmacol., 31, 1075–1084.* https://doi.org/10.1038/aps.2010.139.

Tuček, Ľ., Rapant, S., Čechovská, K. & Németh, Z., 2017: Increasing of drinking water quality by adding carbonate rocks to low mineralized groundwater: Case study from the Krupina district, Slovakia. *Mineralia Slovaca*, *49, 95–112.*

Uemura, H., Katsuura-Kamano, S., Yamaguchi, M. & Nakamoto, M., 2014: Association between dietary calcium intake and arterial stiffness according to dietary vitamin D intake in men. *Br. J. Nutr., 2014, 112, 1333–1340*. doi:10.1017/S0007114514002153.

WHO, 2011: Safe Drinking-water from Desalination. https://apps.who.int/iris/bitstream/handle/10665/70621/WHO_HSE_WSH_11.03_eng.pdf?sequence=1

Williams, B., Mancia, G., Spiering, W., Agabiti, Rosei E., Azizi, M., Burnier, M., Clement, D. L., Coca, A., de Simone, G., Dominiczak, A., Kahan, T., Mahfoud, F., Redon, J., Ruilope, L., Zanchetti, A., Kerins, M., Kjeldsen, S. E., Kreutz, R., Laurent, S., Lip, G. Y. H., McManus, R., Narkiewicz, K., Ruschitzka, F., Schmieder, R. E., Shlyakhto, E., Tsioufis, C., Aboyans, V. & Desormais, I., 2018: Authors/Task Force Members: 2018 ESC/ESH Guidelines for the management of arterial hypertension: The Task Force for the management of arterial hypertension of the European Society of Cardiology and the

European Society of Hypertension: The Task Force for the management of arterial hypertension of the European Society of Cardiology and the European Society of Hypertension. *J. Hypertens. Oct., 36, 10, 1953–2041.* https://doi.org/10.1097/hjh.0000000000001940. Erratum in: *J. Hypertens., Jan.* 2019, 37, 1, 226. PMID: 30234752.

Withers, A., 2005: Options for recarbonation, remineralisation and disinfection for desalination plants. *Desalination, 179, 1–3, 11–24.* ISSN 0011-9164. https://doi.org/10.1016/j.desal.2004.11.051.

Yang, C. Y., Cheng, M. F., Tsai, S. S. & Hsieh, Y. L., 1998: Calcium, magnesium, and nitrate in drinking water and gastric cancer mortality. *Jpn. J. Cancer Res. Feb., 89, 2, 124–130.* https://doi.org/10.1111/j.1349-7006.1998.tb00539.x PMID: 9548438; PMCID: PMC5921760.

Vplyv zvýšeného obsahu vápnika a horčíka v pitnej vode na arteriálnu tuhosť a kardiovaskulárny systém u ľudí: prípadová štúdia v Kokave nad Rimavicou, Slovenská republika

Negatívny vplyv deficitného obsahu Ca (približne 30 mg . l^{-1} a menej) a Mg (približne 10 mg . l^{-1} a menej) v podobe zvýšenej incidencie kardiovaskulárnych ochorení (KVO) a zvýšenej mortality na tieto ochorenia je známy už takmer 70 rokov (Kobayashi, 1957). Tento vplyv bol potvrdený približne v 50 krajinách sveta vrátane Slovenskej republiky. Potvrdil sa aj viacerými metaanalýzami (napr. Catling et al., 2008). Hlavným cieľom príspevku je zistiť, či sa kardiovaskulárny systém (KVS) u ľudí, ktorí pôvodne konzumovali mäkkú pitnú vodu, zlepší, keď začnú konzumovať pitnú vodu so zvýšeným obsahom Ca a Mg. Obohacovanie pitnej vody o Ca a Mg sme realizovali na vodárenskom zdroji v obci Kokava nad Rimavicou (KnR) v rámci riešenia projektu *LIFE – WATER and HEALTH*. Pitná voda na vodárenskom zdroji KnR sa vyznačuje veľmi nízkym obsahom Ca (18 – 20 mg . l^{-1}) a Mg (3 – 4 mg . l^{-1}), ktorý je výrazne nižší ako odporúčané hodnoty slovenskej vyhlášky pre pitnú vodu (tab. 1). Relatívna úmrtnosť na KVO u obyvateľov v KnR je 882,4, čo je takmer o 65 % vyššia hodnota ako priemer Slovenskej republiky (531,2). Kardiovaskulárny systém obyvateľov KnR sme sledovali pomocou merania pružnosti ciev (MPC). Meranie pružnosti ciev sa realizovalo pomocou arteriografu (obr. 4), ktorý bol vyvinutý v Maďarsku a patentovaný vo viac než 30 krajinách sveta. Veľkou výhodou MPC je, že sa ním dajú odhaliť riziká a náchylnosť na KVO ešte pred klinickými príznakmi (Illes, 2005). Pri MPC sa meria rýchlosť pulznej vlny aorty a hlavných tepien (PWVao). Čím je rýchlosť PWVao nižšia, tým je stav tepien lepší a sú priechodnejšie. Z hodnôt PWVao sa následne pri zohľadnení priemerných hodnôt pre stredoeurópsku populáciu vypočíta arteriálny vek (AV) ľudí. Následne sa stanovuje rozdiel medzi arteriálnym vekom a skutočným vekom. V prípade priaznivého stavu KVS ľudí je tento rozdiel záporný a naopak. Obohacovanie pitnej vody na vodárenskom zdroji v obci KnR sme realizovali pomocou rekarbonatizačného reaktora (RR), v ktorom sa rozpúšťa karbonatická hornina – polovypálený dolomit za pôsobenia CO_2 (obr. 2, 3). V RR sme vyrábali koncentrát približne so 100 mg . l^{-1} horčíka, ktorý sa pridával priamo do vodárenského zdroja v pomere približne 1 : 10. Takto sme zvyšovali obsah Ca a Mg v pitnej vode vo vodárenskom zdroji v obci KnR približne o 10 – 15 mg . l^{-1}. Tým sme zvýšili pôvodný obsah dva- až štyrikrát (tab. 4). Vplyv zvýšeného obsahu Ca a Mg na KVS ľudí bol sledovaný pomocou MPC. Meranie sme realizovali približne na 60 vybraných respondentoch z obce KnR. Vybraní občania museli mať najmenej päť rokov trvalý pobyt v obci a nesmeli byť liečení na KVO a ďalšie závažné diagnózy, najmä na diabetes mellitus a ochorenie obličiek. Merania sme realizovali štyrikrát v šesťmesačných intervaloch – prvýkrát pred obohacovaním pitnej vody o Ca a Mg a trikrát po obohacovaní pitnej vody o Ca a Mg. Druhá až štvrtá fáza merania pružnosti ciev bola negatívne ovplyvnená pandemickou situáciou spojenou s ochorením COVID-19. Nie všetci respondenti, ktorí sa zúčastnili na prvej fáze merania, sa mohli pre karanténu zúčastniť na ďalších fázach merania. Aby sme splnili technické zadanie projektu *LIFE – WATER and HEALTH* (60 respondentov), museli sme pružnosť ciev zmerať aj náhradným respondentom z obce KnR. Určite to mohlo čiastočne negatívne ovplyvniť dosiahnuté výsledky. Preto výsledky MPC podávame dvakrát – najprv len

z merania respondentov, ktorí sa zúčastnili na prvej fáze merania (tab. 5), a potom výsledky všetkých meraných respondentov aj s náhradnými (tab. 4). V obidvoch prípadoch je však zrejmý pokles PWVao, pokles arteriálneho veku a pokles rozdielu medzi arteriálnym vekom a skutočným vekom. Dosiahnuté výsledky presvedčivo potvrdili výrazné zlepšenie KVS ľudí. Došlo k výraznému poklesu PWVao, a to z 9,7 na 8,8 m . s^{-1}, a veľmi výraznému zníženiu hodnôt rozdielu medzi arteriálnym vekom a skutočným vekom, a to z 10,07 na 0,14. Tento rozdiel (0,14), zistený po 18-mesačnej konzumácii pitnej vody obohatenej o Ca a Mg, je už na úrovni stredoeurópskeho priemeru. Zlepšenie hodnôt PWVao a AV po 18-mesačnej konzumácii pitnej vody obohatenej o Ca a Mg je naozaj signifikantný. Preto je možné plne ho spájať so zvýšenou dennou dávkou Ca a Mg z pitnej vody. Výsledky jednoznačne potvrdzujú, že okrem tradičných rizikových faktorov vzniku KVO (stres, obezita, genetické faktory, fajčenie a nadmerná konzumácia alkoholu) je obsah Ca a Mg v pitnej vode rovnako významným faktorom rizika vzniku KVO.

Doručené / Received: 23. 10. 2023
Prijaté na publikovanie / Accepted: 21. 12. 2023

Inštrukcie autorom

Etika publikovania, záväzná pri publikovaní v časopise Mineralia Slovaca: *www.geology.sk/mineralia položka* ***Publikačná etika***

1. Geovedný časopis Mineralia Slovaca publikuje scientometricky hodnotné recenzované pôvodné vedecké články s vysokým citačným potenciálom. V úvode príspevku musí autor jasne deklarovať, čím konkrétnym je jeho príspevok prínosný pre rozvoj geovied. Rešeršné štúdie sa publikujú len ojedinele.

2. Články na publikovanie (manuskripty) sa do redakcie zasielajú poštou (dva vytlačené exempláre a CD so všetkými súbormi v editovateľnej podobe) alebo e-mailom (editovateľné súbory a kompletná verzia vo formáte PDF).

3. Súčasne s článkom je potrebné redakcii poslať autorské vyhlásenie o originalite textu a obrázkov. Kópie obrázkov z iných publikácií musia byť legalizované získaním práva na publikovanie. Vyhlásenie musí obsahovať meno autora (autorov), akademický titul a trvalé bydlisko.

4. Rozsah manuskriptu na publikovanie je najviac 25 rukopisných strán (MS Word, Times New Roman, veľkosť písmen 12 bodov, riadkovanie 1,5) vrátane literatúry, obrázkov a vysvetliviek. V prípade veľkého odborného prínosu sú v ojedinelých prípadoch povolené aj dlhšie články.

5. Články sú publikované v angličtine so slovenským resumé v závere článku (za zoznamom citovanej literatúry).

Text

1. Abstrakt stručne sumarizuje článok. Môže mať najviac 200 slov a nemá obsahovať citácie. Počet kľúčových slov je maximálne 6. Text má mať úvod, charakteristiku (stav) skúmaného problému, použitú metodiku, nové zistenia, ich interpretáciu, diskusiu, záver a zoznam literatúry. Východiskové údaje musia byť zreteľne odlíšené od interpretácií. V texte musia byť odvolávky na všetky použité obrázky a tabuľky.

2. Hierarchiu nadpisov v texte je potrebné vyznačiť ceruzkou na ľavom okraji strany manuskriptu: 1 – najvyššia, 2 – nižšia, 3 – najnižšia.

3. V texte sa uprednostňuje citácia v zátvorke, napr. (Dubčák, 1987; Hrubý et al., 1988), pred formou ... podľa Dubčáka (1987).

4. Pozícia obrázkov a tabuliek v texte sa označí. Nie je vhodné, aby text v editore MS Word obsahoval vložené obrázky, ale náhľadová verzia v pdf ich má obsahovať.

5. Grécke písmená treba identifikovať na ľavom okraji slovom (napr. sigma). Potrebné je odlišovať pomlčku od spojovníka. Symboly, matematické značky, názvy skamenelín a pod., ktoré sa majú vysádzať kurzívou, autor v rukopise podčiarkne vlnovkou.

Obrázky a tabuľky

1. Ilustrácie a tabuľky vysokej kvality bývajú publikované buď **na šírku stĺpca (81 mm), alebo strany (170 mm).** Optimálna veľkosť písma a čísiel v publikovaných obrázkoch je 2 mm. Všetky texty v obrázkoch a tabuľkách, rovnako ako popisy k nim musia byť v angličtine. **Maximálny rozmer ilustrácie a tabuľky vytlačený v časopise je 170 x 230 mm.** Väčšie (skladané) ilustrácie sú publikované len v ojedinelých prípadoch.

2. Pri počítačovej tvorbe obrázkov odporúčame používať programy s vektorovým zobrazením (Corel Draw, Adobe Illustrator a pod.). Čiary tzv. vlasovej hrúbky, softvérová alebo rastrová výplň plôch (napr. v Corel Draw) nie sú prípustné. Výplne v obrázkoch musia pozostávať zo samostatne vysádzaných objektov.

3. Ilustrácie vrátane fotografií musia obsahovať **grafickú mierku** v centimetrovej či metrovej škále, prípadne sa rozmer zobrazených objektov vyjadrí v popise obrázka. Mapy a profily musia mať aj **azimutálnu orientáciu** a jednotné vysvetlivky, ktoré sa uvedú pri prvom obrázku. Zoskupené obrázky, napr. fotografie a diagramy, sa uvádzajú ako jeden obrázok s jednotlivými časťami označenými písmenami (a, b, c atď.).

4. Pri zasielaní fotografií vo forme počítačových súborov (formáty JPG alebo TIF) sa požaduje rozlíšenie minimálne 600 DPI. Publikovanie farebných ilustrácií môže byť spoplatnené.

Literatúra

1. Minimálne 50 % citácií musí reprezentovať publikácie od roku 2000. V zozname literatúry sa v abecednom poradí uvádza len literatúra citovaná v danom článku.

2. Spôsob uvádzania literatúry v zozname literatúry

Knižná publikácia: Gazda, L. & Čech, M., 1988: Paleozoikum medzevského príkrovu. *Bratislava, Alfa, 155 s.*

Článok v časopise: Vrba, P., 1989: Strižné zóny v metapelitoch. *Miner. Slov., 21, 135 – 142.*

Zborník: Návesný, D., 1987: Vysokodraselné ryolity. *In: Romanov, V. (ed.): Stratiformné ložiská gemerika. Špec. publ. Košice, Slov. geol. spol., 203 – 215.*

Manuskript: Radvanský, F., Slivka, B., Viktor, J. & Srnka, T., 1985: Žilné ložiská jedľoveckého príkrovu gemerika. Záverečná správa z úlohy SGR--geofyzika. *Manuskript. Spišská Nová Ves, archív Št. Geol. Úst. D. Štúra, 28 s.*

3. Pri článku viac ako dvoch autorov sa v texte cituje iba prvý autor s dodatkom et al., ale v zozname literatúry sa uvádzajú všetci.

Instructions to authors

Publication ethics, being obligatory for publishing in the journal Mineralia Slovaca: *www.geology.sk/mineralia item* ***Publication ethics***

1. Geoscientific journal Mineralia Slovaca publishes scientometrically valuable original peer-reviewed scientific articles with a high citation potential. In the introduction of each article the author(s) must clearly declare, which innovative data the paper brings for the development of geosciences. The retrieval studies are published only exceptionally.

2. The articles for publishing (manuscripts) must be sent to Editorial Office by post (two printed copies and CD with editable files), or by e-mail (editable files plus complete preview version in PDF format).

3. Simultaneously with the article the Editorial Office must receive the author´s proclamation that no part of the manuscript was already published and figures and tables are original as well. Copied illustrations from other publications must contain a copyright.

4. The extent of the manuscript for publishing is limited to 25 manuscript pages (MS Word, 12 points Times New Roman, line spacing 1.5) including figures, tables, explanations and references. In the case of contribution with a high scientific value, the longer manuscripts for publishing are exceptionally permitted.

5. Articles are published in English, with Slovak summary at their end. In a case of foreign authors not able to submit the article summary in Slovak, the Editorial Office translates their English summary to Slovak version.

Text

1. Abstract briefly summarizing the article is limited to 200 words, no references are allowed. The maximum number of key words is 6. Text of the article has to contain the introduction, characterization (state) of investigated problem, applied methodology, presented new data, discussion, conclusion and references. The obtained data must be distinctly separated from interpretations. All applied figures and tables must be referred in the text.

2. The hierarchy of headings in the manuscript must be clearly indicated.

3. The references in the text prefer parentheses, e.g. (Dubčák, 1987; Hrubý et al., 1988). The form “according to Dubčák (1987)” should be used only exceptionally.

4. Position of figures and tables must be indicated in the manuscript. Editable text of manuscript sent to editorial office must be without figures and tables, though the preview PDF has to contain them in a correct position.

5. Greek letter in the text must be identified at the left margin of the text (e.g. sigma). The text should strictly distinguish the dash from hyphen. Symbols, mathematic signs, names of fossils, etc., which should be printed in italics, must be underlined in the manuscript.

Figures and tables

1. The high quality figures and tables can be published either in **maximum width of column (81 mm) or page (170 mm).** The optimum size of letters and numbers in the camera-ready figure is 2 mm. All texts in figures and tables, as well as descriptions and notes to figures and tables must be in English. **Maximum dimension of figures and tables in the journal is 170 x 230 mm. Larger (fanfolded)** illustrations are published only exceptionally.

2. For figures drawing the editorial office recommends the vector graphics editors (Corel Draw, Adobe Illustrator, etc.). The very thin lines (hair lines), the pre-defined software or raster fillings of polygons (e.g. in Corel Draw) are not allowed. The filling must consist from separately set objects.

3. Each illustration including photographs must contain graphic (metric) scale, eventually the dimensions of visualized objects have to be stated in the describing text to figure. Maps and profiles must contain also the azimuth orientation, their detail explanations are stated at the first figure. Grouped figures, e.g. photographs and diagrams, are compiled as one figure with separate parts designated by letters (a, b, c, etc.).

4. The photographs sent as JPG of TIF files are required for having minimum 600 DPI resolution. Publishing of colour illustrations can be charged by a fee.

References

1. Minimum 50 % of referred works must represent contemporary publications after 2000. The references in alphanumeric order encompass only literature cited in the article.

2. Examples of referring:

Book: Gazda, L. & Čech, M., 1988: Paleozoic of the Medzev nappe. *Bratislava, Alfa, 155 p.*

Article in journal: Vrba, P., 1989: Shear zones in the metapelite complexes. *Miner. Slov., 21, 135–142.*

Anniversary volume: Návesný, D., 1987: High-potassium rhyolites. *In: Romanov, V. (ed.): Stratiform deposits of Gemericum. Spec. publ. Košice, Slov. geol. soc., 203–215.*

Manuscript: Radvanský, F., Slivka, B., Viktor, J. & Srnka, T., 1985: Vein deposits of the Jedľovec nappe of Gemericum. Final report from the project SGR-geophysics. *Manuscript. Spišská Nová Ves, Archive Št. Geol. Úst. D. Štúra, 28 p.*

3. The article with more than two authors is referred by the name of the first author with the amendment et al., but the list of references contains names of all authors.

Ďalšie informácie / Further information: mineralia.slovaca@geology.sk; zoltan.nemeth@geology.sk

OBSAH – CONTENT

PÔVODNÉ ČLÁNKY – ORIGINAL PAPERS

Indexed / Abstracted / Accessed by SCOPUS, WEB OF SCIENCE and EBSCO
Indexované / abstraktované / sprístupňované databázami SCOPUS, WEB OF SCIENCE a EBSCO

www.geology.sk/mineralia